IPP-Report

Max-Planck-Institut für Plasmaphysik

Niklas Höpfl

Modification and characterization of ASDEX Upgrade's room-temperature solid-state pellet injector for the use on COMPASS

IPP 2019-07
April 2019

Max-Planck-Institut für Plasmaphysik

Modification and characterization of ASDEX Upgrade's room-temperature solid-state pellet injector for the use on COMPASS

Bachelor Thesis

Niklas Höpfl

Engineering Physics

Munich University of Applied Sciences

Munich, March 2019

Max-Planck-Institut für Plasmaphysik

HOCHSCHULE FÜR ANGEWANDTE WISSENSCHAFTEN MÜNCHEN

Bachelorarbeit

Modification and characterization of ASDEX Upgrade's room-temperature solid-state pellet injector for the use on COMPASS

Modifikation und Charakterisierung von ASDEX Upgrade's Raumtemperatur-Festkörper-Pelletinjektor für die Verwendung an COMPASS

Verfasser: Niklas Höpfl
Matrikelnummer: 66848914

Ausgabedatum: 14.11.2018
Abgabedatum: 14.03.2019

Hochschule für angewandte Wissenschaften München
Fakultät für angewandte Naturwissenschaften und Mechatronik
Studiengang Physikalische Technik

Erstkorrektor: Prof. Dr.-Ing. Datong Wu
Zweitkorrektor: Prof. Dr. rer. nat. Alfred Kersch
Betreuer am Institut: Dr. Peter T. Lang

Angefertigt am Max-Planck-Institut für Plasmaphysik
Abteilung Tokamak-Szenario-Entwicklung
Boltzmannstraße 2
D-85748 Garching

Erklärung

Hiermit erkläre ich gemäß der Rahmenprüfungsordnung der Hochschule München, dass ich die vorliegende Arbeit mit dem Titel *„Modification and characterization of ASDEX Upgrade's room-temperature solid-state pellet injector for the use on COMPASS“* selbständig verfasst, noch nicht anderweitig für Prüfungszwecke vorgelegt, keine anderen als die angegebenen Quellen oder Hilfsmittel benutzt, sowie wörtliche und sinngemäße Zitate als solche gekennzeichnet habe.

_____ _____

Ort, Datum Unterschrift

Modification and characterization of ASDEX Upgrade's room-temperature solid-state pellet injector for the use on COMPASS

Abstract

The Max-Planck-Institut für Plasmaphysik (IPP) is one of the world's leading facilities regarding fusion research with its fusion experiment ASDEX Upgrade (AUG) in Garching. An important task in fusion science is the use of pellets, injected into the fusion plasma during a plasma discharge. The room-temperature solid-state pellet injector (RTSP) is a gas gun used to inject such pellets and is capable of accelerating spherical and cylindrical pellets into the fusion plasma with up to 2 Hz using different propellant gases. Following a successful campaign at AUG in 2015, where lithium pellets were injected into the fusion plasma by the RTSP, the injector has now been revised and characterized to be used at the Institute of Plasma Physics of the Czech Academy of Sciences in Prague on the COMPASS fusion experiment. It is planned to carry out investigations on runaway electrons, high-energy particles in fusion experiments, using cylindrical boron nitride (BN) pellets (Ø=1.5 mm, l= 2.0 mm/1.0 mm, m_P= 6.8 mg/3.4 mg). Characterizing the injector in a testbed, 1 mm and 2 mm long BN pellets were accelerated to speeds ranging from $120\frac{m}{s}$ to $720\frac{m}{s}$ using argon (Ar) and helium (He) as propellant gases at pressures between 5 bar and 100 bar. Delivery efficiencies within a prescribed 1° maximum pellet trajectory scattering of more than 91% were achieved. Testbed impact tests on graphite wall component tiles of COMPASS showed damage potential of BN pellets, which has to be taken into account.

Modifikation und Charakterisierung von ASDEX Upgrade's Raumtemperatur-Festkörper-Pelletinjektor für die Verwendung an COMPASS

Kurzfassung

Das Max-Planck-Institut für Plasmaphysik (IPP) ist mit seinem Fusionsexperiment ASDEX Upgrade (AUG) in Garching eines der weltweit führenden Einrichtungen für Fusionsforschung. Ein wichtiger Aspekt der Fusionswissenschaft sind Pellets, die während einer Plasmaentladung in das Fusionsplasma injiziert werden. Der Raumtemperatur-Festkörper-Pelletinjektor (room-temperature solid-state pellet injector, kurz: RTSP) ist eine zum Injizieren solcher Pellets verwendete Gaskanone und in der Lage sphärische und zylindrische Pellets aus unterschiedlichen Materialien unter Verwendung verschiedener Treibgase mit bis zu 2 Hz in das Fusionsplasma zu beschleunigen. Nach einer erfolgreichen Kampagne an AUG, bei der 2015 Lithiumpellets mithilfe des RTSP in das Fusionsplasma injiziert wurden, ist der RTSP nun überarbeitet und charakterisiert worden, um am Institut für Plasmaphysik der tschechischen Akademie der Wissenschaften in Prag an dem Fusionsexperiment COMPASS eingesetzt zu werden. Dort ist geplant, mithilfe von zylindrischen Bornitrid (BN)-Pellets ($Ø = 1.5\ mm, l = 2.0\ mm/1.0\ mm\ , m_P = 6.80\ mg/3.4\ mg$) Untersuchungen zu Runaway-Elektronen, hochenergetische Teilchen in Fusionsexperimenten, durchzuführen. Bei der Charakterisierung des Injektors an einem Teststand wurden 1mm, sowie 2mm lange BN-Pellets mithilfe von Argon (Ar) und Helium (He) bei Treibgasdrücken zwischen 5 bar und 100 bar auf Geschwindigkeiten von $120\frac{m}{s}$ bis $720\frac{m}{s}$ beschleunigt und in das Vakuum-Zielgefäß geschossen. Die Ankunftswahrscheinlichkeit innerhalb eines vorgeschriebenen, maximal 1° großen Bereiches der Flugbahnstreuung war dabei über 91%. Testschüsse auf Wandkomponenten-Graphitkacheln des COMPASS offenbarten ein mögliches Schadenspotential der BN-Pellets, das berücksichtigt werden muss.

Parts of this thesis, including results and figures will be presented in March 2019 at the DPG-spring meeting for plasma physics in Munich with the title:

The ASDEX Upgrade room-temperature solid-state pellet injector adapted for COMPASS

N. Hoepfl[1,2], P.T. Lang[1], B. Ploeckl[1], D. Wu[2], J. Cerovsky[3,4], O. Ficker[3,4], J. Mlynar[3,4], V. Weinzettl[3], ASDEX Upgrade Team[1]

[1] *Max-Planck-Institut für Plasmaphysik, Boltzmannstr. 2, 85748 Garching, Germany*

[2] *Munich University of Applied Sciences, Lothstr. 34, 80335 München, Germany*

[3] *Institute of Plasma Physics of the CAS, Prague, Czech Republic*

[4] *Faculty of Nuclear Sciences and Physical Engineering, Czech Technical University in Prague, Prague, Czech Republic*

Table of Contents

List of Figures

List of Tables

List of Abbreviations

Abbreviation	Explanation
Ar	Argon
ASDEX	Axially Symmetric Divertor Experiment
AUG	ASDEX Upgrade
BN	Boron Nitride
C	Carbon
D	Deuterium
H	Hydrogen
He	Helium
IPP	Institute for Plasma Physics / Institut für Plasmaphysik
LB	Light Barrier
Li	Lithium
RE	Runaway Electron
RTSP	Room-Temperature Solid-State Pellet Injector
T	Tritium
Tokamak	Toroidal Chamber with Magnetic coils

1 Introduction

With an ongoing growth in world population, an advancing industrialization and a higher standard of living worldwide, the energy consumption rises likewise. Especially with the fast economic growth in primarily Non-OECD countries like China and India, it will be eminently challenging to cover the worldwide demand for energy (see Fig. 1.1). According to forecasts by the U.S. Energy Information Administration (EIA), China and India alone will account for half of the global energy growth through 2035. [1]

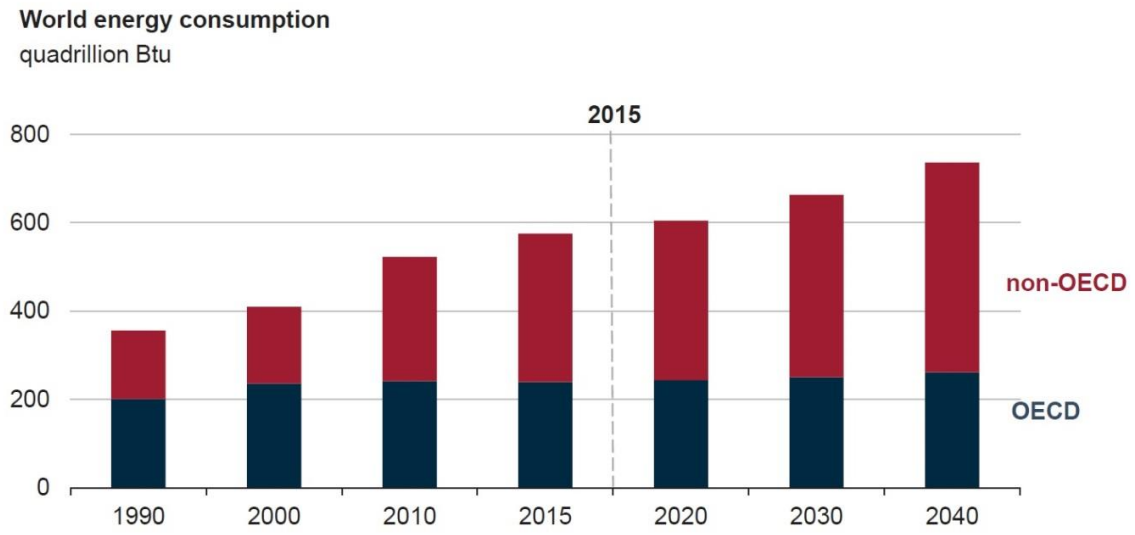

Figure 1.1: EIA world energy consumption projection (BTu: British Thermal unit; 1 BTu ≈ 1055 J) [2]

Solving this issue alone is going to be a major task, but it will prove to be much more difficult, as a simultaneous transition of energy sources must take place. The world energy economy is still carbon-based, with the energy carriers oil, gas, and coal accounting for over 80% of the global primary energy consumption [3]. This poses a problem, as these fossil fuels are limited, and the burning and

utilization leads to increasing levels of SO_x, NO_x, carbon, and other pollutants in the atmosphere. A transition to non-carbon-based energy is inevitable but would necessarily involve almost unprecedented commitments and actions by government and industry throughout the world. Although the proportion of renewable energy sources saw a significantly increase over the recent years, negative aspects like geographical limitations and a strong volatility show, that renewables in its current state do not offer a solution to the energy crisis. [4] [5]

Another possibility to serve as a source of energy is nuclear energy, which is based on the use of nuclear reactions. A well-established form of nuclear energy is nuclear fission, which is used since the 1960s as a carbon-free way to produce electricity for commercial use [6]. With about 50 new reactors under construction, many countries, first and foremost China, are increasing their nuclear power capacity [7]. However, over the years disastrous events like Chernobyl and Fukushima have had a negative impact on the image of the technology. Moreover, the awareness for long-term effects like the final deposition of nuclear waste have led to public concerns about nuclear fission and subsequently led to the decision of some countries to phase out of nuclear fission at all.

Another carbon-free technology to harness nuclear energy is nuclear fusion. The energy released by fusing atoms is enormous, around four million times the energy of chemical reactions such as the burning of fossil fuels and four times more than a nuclear fission reaction at equal mass. The fusion fuels are also widely available and nearly inexhaustible and since there are no enriched materials involved, an exploitation to make nuclear weapons can be ruled out. Additionally, there are no risks of a nuclear accident, as even the smallest disturbances lead to an immediate stop of the reaction, so chain reactions like a meltdown are impossible. Although radioactivity is involved in fusion reactors as well, the amount and radiotoxicity of the nuclear waste generated in fusion reactors is nowhere near in comparison to the high activity, long-lived nuclear waste resulting from nuclear fission. It is estimated, that the activated components from fusion reactors can be recycled or reused within a 100-year period. [8]

Although it is not commercially available by now, the benefits of nuclear fusion are clear and the main drive behind previous and current fusion research. In the early 1950s scientists began searching for ways of a controlled fusion on earth as a new source of energy. Throughout the years, research

on fusion expanded with more and more research programs worldwide. The Max-Planck-Institutut für Plasmaphysik (IPP) is one of the worldwide leading research facilities, regarding fusion science and fusion technology. With a workforce of around 1100 it is also one of the largest fusion research centers in Europe. IPP is part of the Max-Planck-Society, an independent, non-profit organization supporting fundamental research, and associated to the Helmholtz Association of German Research Centres, the largest scientific organization in Germany. The IPP is also member of the EUROfusion consortium, a large-scale European collaboration on fusion research and operates as their coordinator. The logos of the associations can be seen in Fig. 1.2. [9]

Figure 1.2: Logos of the associations, IPP is part of [9]

IPP is operating two fusion experiments, the tokamak ASDEX Upgrade (AUG) in Garching and the stellarator Wendelstein 7-X (W7-X) at the Greifswald Branch Institute. The research conducted at the IPP covers various topics concerning future fusion power plants, one being pellet technology. Its key task will be refueling the reactor from the outside by injecting small cubes of fusion fuel. Currently pellets are also used to probe the plasma by injecting specific materials during a plasma discharge. Different systems are possible for the injection of pellets. The room-temperature solid-state pellet injector (RTSP) is a gas gun type system and capable of accelerating spherical and cylindrical pellets into the fusion plasma with up to 2 Hz using different propellant gases. Following a successful campaign at AUG in 2015, where lithium pellets were injected into the fusion plasma with the RTSP, the injector is going to be used at the Institute of Plasma Physics of the Czech Academy of Sciences in Prague on the COMPASS fusion experiment. To prepare the injection system for its upcoming application, the operating properties are characterized in a testbed. [10]

2 Structure of the thesis

The first part of the thesis covers the basics of fusion science and research. The fusion experimental tokamaks ASDEX Upgrade and COMPASS are introduced and the phenomenon of runaway electrons is explained (Chapter 3).

The second part gives a technical description of the room-temperature solid-state pellet injector and the testing environment with preparations for the characterization (Chapter 4 and 5).

The next part covers the theory, as well as the procedure of the performed tests. The analysis of the test results is also included in this part (Chapter 6, 7 and 8).

The final part gives a conclusion and prospects the future of the injector on COMPASS (Chapter 9 and 10).

3 Theoretical principles

3.1 Plasma

Plasma is often referred to as the fourth state of matter. As heat is added into a system, the state of matter changes from solid to liquid and further from liquid to gaseous, caused by atoms becoming more energetic and bonds between adjacent particles close together being loosened and finally broken. If heat keeps getting added, the atoms start decomposing into their substituents, usually negatively charged electrons and positively charged nuclei. This state is called plasma. The name plasma originates from Ancient Greek and described a 'moldable substance'. The use of this word on this given state of matter is attributed to American chemist Irving Langmuir, when he tried to describe a 'region containing balanced charges of ions and electrons' in 1928 [11]. Since free moving positive and negative charges are more or less numerous a component of the plasma (the amount determines the degree of ionization), it produces electric and magnetic fields. By moving in random directions, on average, an electrically neutral medium is given. But its constituents can be influenced by external electric and magnetic fields as well. This property of plasma is exploited in fusion devices by using magnetic coils. [12] [13]

3.2 Nuclear fusion

Nuclei are made up of protons and neutrons. When comparing the mass of the nuclei with the sum of masses of its constituents on its own, a difference can be observed. This is caused by the binding energy holding the nucleus together. This is called mass defect and goes back to Albert Einstein's equation 3.1 in his work on special relativity, describing the equivalence of mass and energy [14].

$$E = m \cdot c^2 \tag{3.1}$$

In connection with mass increase or defect, the equation is often used in terms of the change in energy and mass (see equation 3.2). Considering the tremendous value of c^2 (eq. 3.3) even small changes in mass can lead to a huge change in energy.

$$\Delta E = \Delta m \cdot c^2 \tag{3.2}$$

$$c^2 = \left(299\,792\,458\ \frac{m}{s}\right)^2 = 8.987551787 \cdot 10^{16}\ \frac{m^2}{s^2}\ [15] \tag{3.3}$$

Fig. 3.1 shows the binding energy per nucleon for stable nuclei, weighed by the mass number. As nuclear energy is released when transmutations lead to an increase in the binding energy and the curve peaks with iron, nuclei heavier than iron release energy by fissioning and lighter nuclei by fusing. The steep slope for light nuclei fusing compared with the gentle slope for the fission of heavy nuclei shows the much bigger energy yield from nuclear fusion, especially with low mass nuclei. [16]

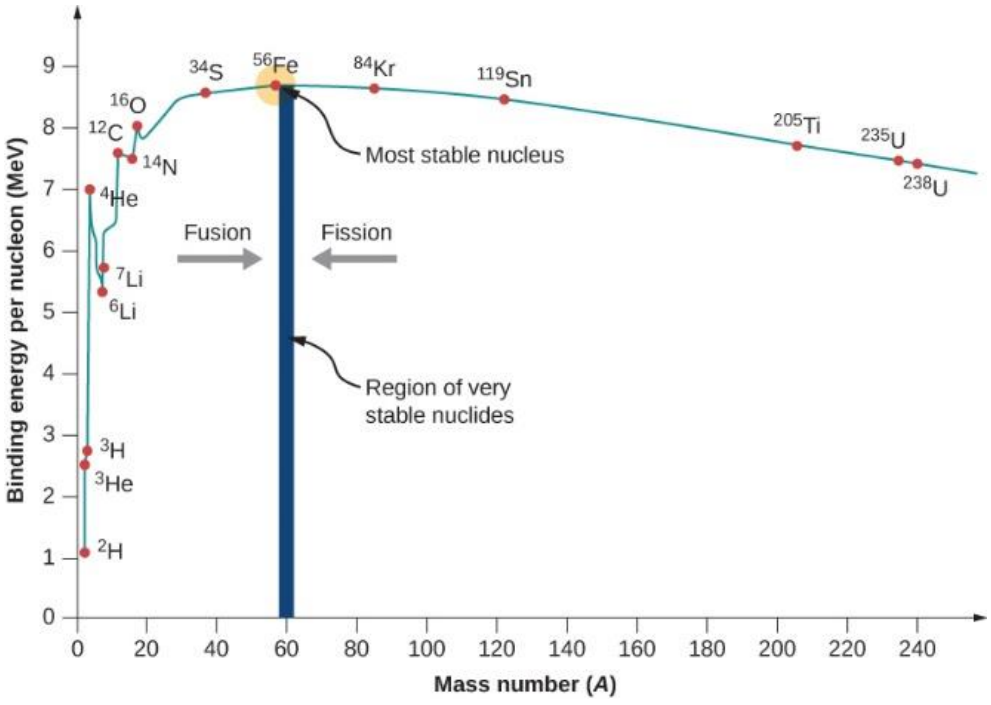

Figure 3.1: Binding energy per nucleon as a function of mass number [16]

The model for fusion on earth has always been the sun. Every second, in its core 600 million tons of hydrogen (H) fuse to 596 million tons of helium (He), with the consequential mass defect being turned into energy [17]. While stellar nucleosynthesis mostly relies on extremely slow proton-proton chain reactions or the carbon-nitrogen-oxygen cycle, fusion on earth will be based on the two hydrogen isotopes deuterium (D) and tritium (T), shown in the reaction equation 3.4. Compared to other possible reactions, the D-T reaction is the most convenient reaction to achieve. It has a large net yield of energy (17.6 MeV), combined with the highest collision cross section and occurs at the lowest temperature. Furthermore, both fusion fuels are available in very large quantities. Deuterium can be obtained from seawater and tritium will be bred on the inner walls of the fusion reactor, called blanket, using a side reaction with lithium. [18]

$$^{2}D + {}^{3}T \rightarrow {}^{4}He\ (3.5\ MeV) + n^{0}\ (14.1\ MeV) \tag{3.4}$$

3.3 Lawson criterion

To overcome the repulsive Coulomb force acting between the nuclei, they need to have enough energy to approach sufficiently close, so the short-range attractive nuclear force becomes dominant. This is done by adding heat. For net power to be produced from the fusion reaction, fusion power must exceed external heating power. This is called the scientific breakeven and expressed by a fusion gain factor Q (ratio of fusion power to external heating power) bigger than one. With increasing utilization of fusion power for self-heating, Q rises to the point where the fusion power is enough to sustain the thermonuclear temperature entirely on its own without the need of external power at all. This state of a self-sustaining nuclear fusion would have an infinite fusion gain factor and is called “ignited”. The fusion reaction contains three plasma parameters. The plasma temperature T, plasma density n, and the energy confinement time τ_E, a measure for the thermal insulation, describing the time it would take for the thermal energy to be lost to the environment. By rearranging the equation describing the power balance, a set minimum value for the product of the three parameters (“triple-product”) can be calculated. This minimum is necessary for an ignition and is called the Lawson criterion. [19] [20]

For the D-T-reaction (eq. 3.4) the value minimizes at temperatures around 14 keV leading to a triple-product of:

$$n \cdot T \cdot \tau_E > 3 \cdot 10^{21} \frac{keV \cdot s}{m^3} \tag{3.5}$$

Figure 3.2 shows the advancements made during the last decades. Although the triple product was improved substantially, no reactor surpassed the Lawson criterion for the D-T reaction yet. The closest to an ignited plasma was achieved on the JET tokamak with the triple-product being short only by a factor of 5 [20].

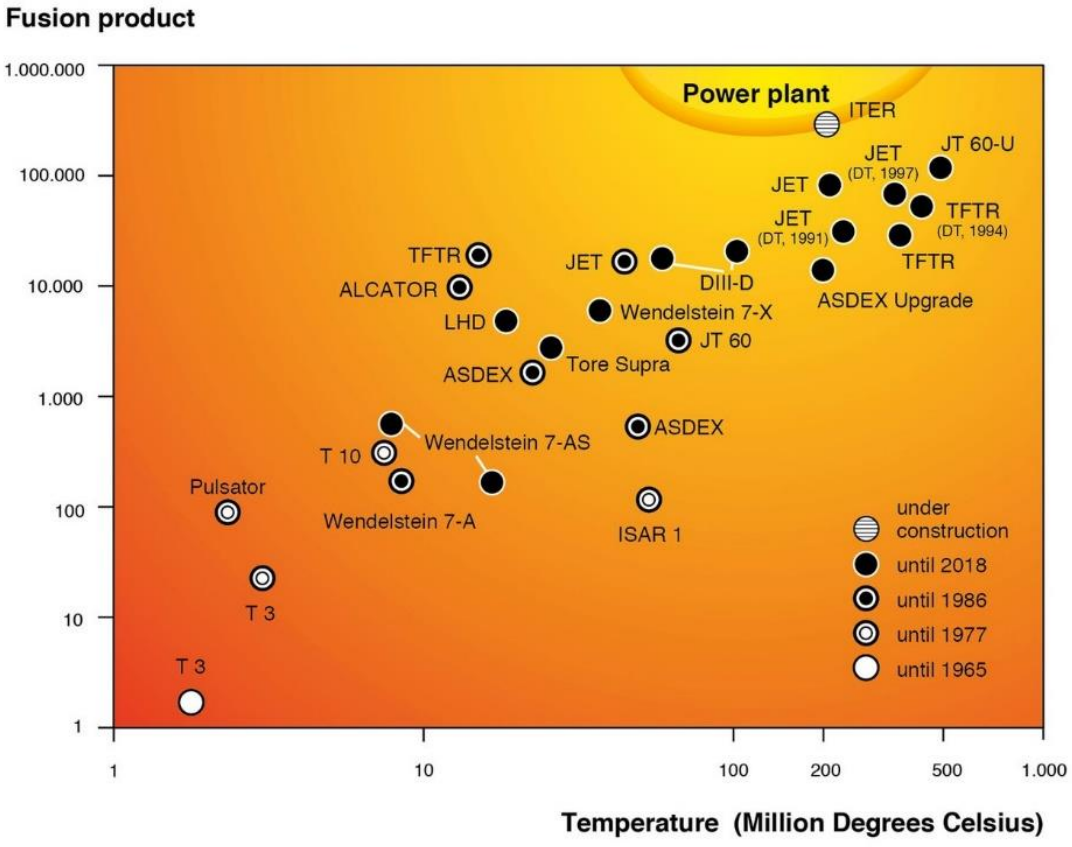

Figure 3.2: Triple product and temperatures of different fusion reactors [20]

3.4 Magnetic confinement

There are different methods to implement fusion. Magnetic confinement being one of the two major approaches beside inertial confinement. As the name suggests, magnets are employed to confine the hot plasma in a specific volume, in order to not damage the wall and cool the plasma. The electromagnetic properties of the charged plasma particles are utilized to restrain the motion across the magnetic field lines of force, while they can still move freely along them. Lorentz forces acting perpendicular to the magnetic field lines, force the particles on a gyrating movement along the field lines. Different configuration concepts were researched and developed in magnetic confinement fusion. The tokamak (Toroidal Chamber with Magnetic coils) concept proved to be the most successful “confinement cage” to trap the particles. The magnetic coil configuration of a tokamak can be seen in Fig. 3.3. The toroidal arrangement of ring-like coils leads to a self-contained toroidal field. As an electric field caused by charge separation of electrons and ions would lead to a loss of the plasma to the wall in a purely toroidal field, an additional poloidal field is needed. This is implemented by inducing a toroidal current through the plasma. Most tokamaks use inner poloidal transformer coils placed in the center of the torus for this. An indefinite spiral movement around the inner magnetic field line forming closed so-called “magnetic flux surfaces”, is the consequence. This configuration however would experience an expanding, outwards directed force. To prevent this, outer poloidal field coils provide an additional vertical magnetic field. This results in helical field lines in radial equilibrium. Other toroidal concepts, the major one being the stellarator, miss the poloidal coils. The complex, adjusted arrangement of the non-axisymmetric toroidal coils take over this task by producing the poloidal magnetic field. [21] [22]

The transformer coils used in most tokamaks to induce the plasma current are the reason, why it is currently not possible to run a tokamak in continuous mode. After an increasing current is generated in the primary winding and consequently a current is driven in the plasma, it needs to be discharged and the current restarted. To achieve steady state operation in tokamaks is part of current research. [23]

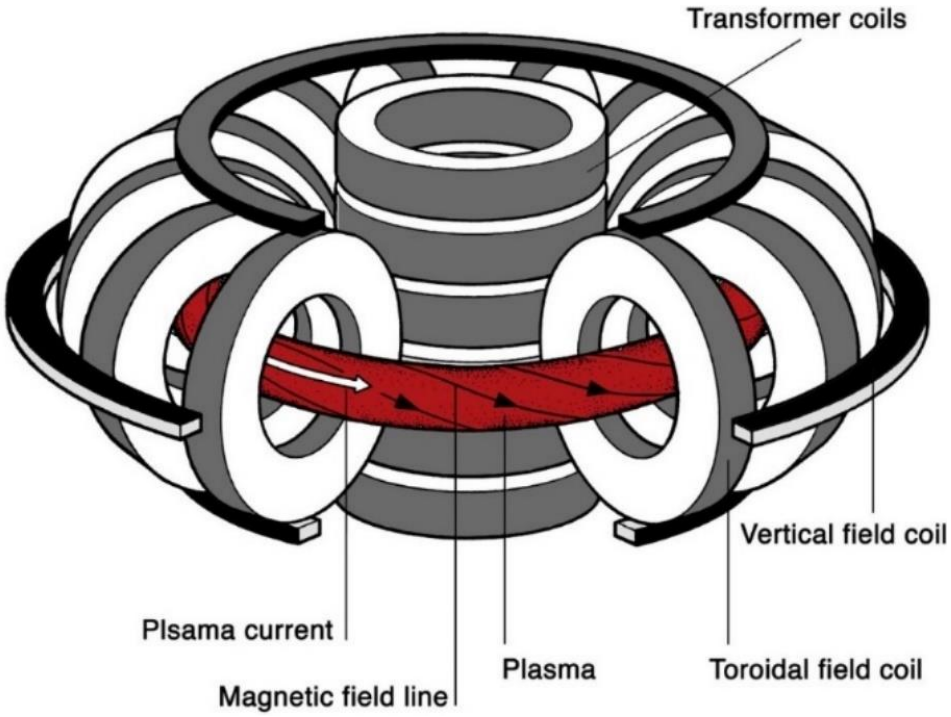

Figure 3.3: Magnetic confinement of a tokamak [23]

3.5 Fusion experiements

With an ongoing expansion in the fields of magnetic confinement fusion research over the last decades, there are currently 20 tokamak-type and 12 stellarator-type fusion experiments in operation worldwide [24]. More projects are planned or under construction, with the biggest milestones being ITER (International Thermonuclear Experimental Reactor), an international collaboration of many countries to build the world's largest experimental tokamak (Start of construction: 2013; planned first plasma: 2025) and DEMO (DEMOnstration Power Station), a planned tokamak fusion reactor, that affords all the functions of a power plant and demonstrates the feasibility for commercial use of fusion power (planned start of construction: approx. 2031). To prepare the physics base for advanced fusion projects like ITER and DEMO, essential plasma properties are intensively investigated on smaller scale fusion experiments like ASDEX Upgrade and COMPASS. [25]

3.5.1 ASDEX Upgrade

ASDEX, the predecessor to ASDEX Upgrade was the first tokamak with divertor configuration. A divertor is a special magnetic assembly of additional coils to deflect fusion ash (Helium-4) and impurities during operation resulting in better thermal insulation. Hence, the name ASDEX (Axially Symmetric Divertor Experiment) was chosen. When ASDEX was shut down in 1990 the new, advanced tokamak ASDEX Upgrade began operation. Throughout the years ASDEX and ASDEX Upgrade have done pioneering work and made innovative, important contributions on different key areas of fusion research. For instance, the development and advancements of the divertor, the first and first completely tungsten coating and the discovery of the high confinement regime, a state of significantly enhanced energy confinement, called H-mode. [26]

Figure 3.4 shows a photograph of ASDEX Upgrade in the torus hall in Garching:

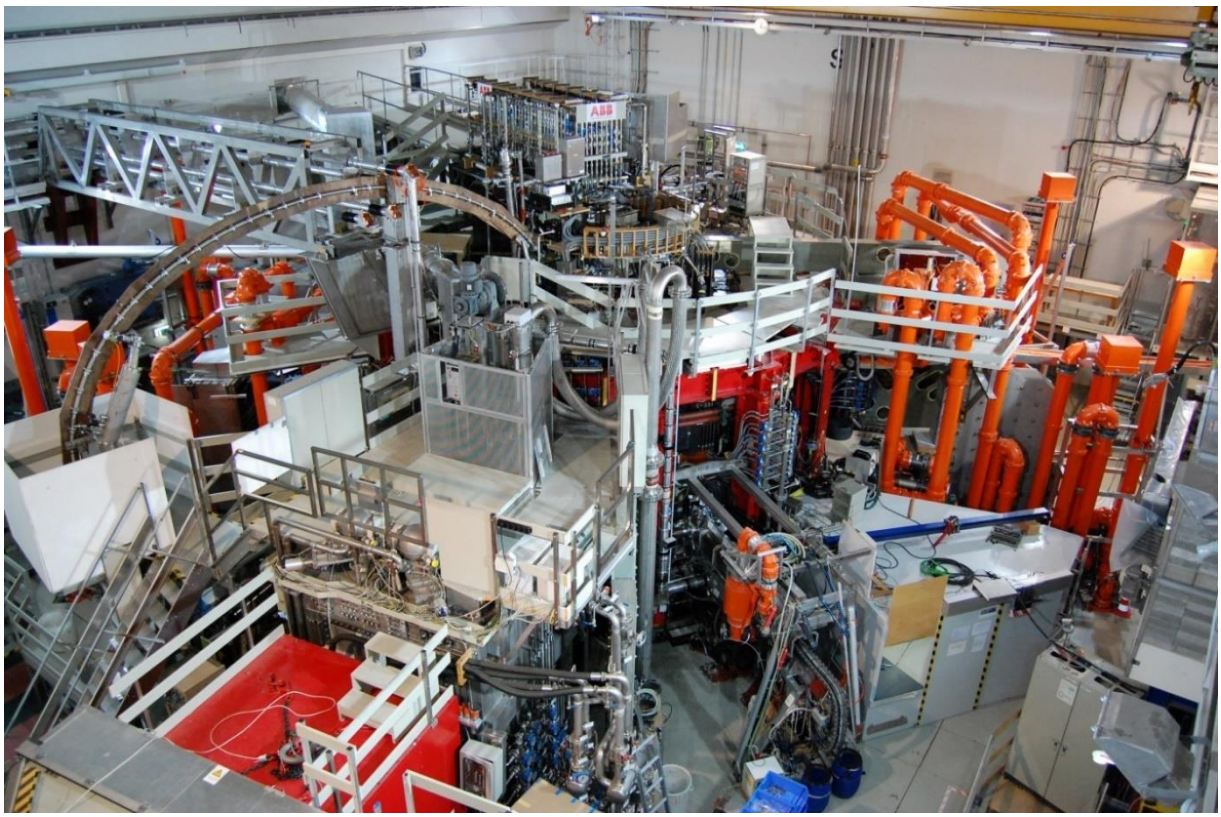

Figure 3.4: Photograph of ASDEX Upgrade in the torus hall [27]

Current research focuses on different topics, among others, plasma stability, numerical descriptions of the plasma behavior and ongoing studies on the divertor. AUG has a special role in fusion power research. With its power-plant-like geometry it is closer to the ITER geometry than any other tokamak. Furthermore, it has a powerful flexible plasma heating realized by different heating systems and a full tungsten vessel wall. Thus, experimentation is primarily performed under power-plant-like conditions, with plasma properties like plasma density, plasma pressure and wall load matching the conditions of a future power plant. Although the goal is to realize a reaction with the fusion fuels deuterium and tritium, the current research dispenses with the use of radioactive tritium. The model plasma of ordinary hydrogen and deuterium is similar in its properties and allows experiments in like circumstances, with fusion reactions occurring in the model plasma. [28]

Figure 3.5 shows a 3D model of the torus and its framework without attachments and diagnostics. Table 3.1 lists the main technical properties:

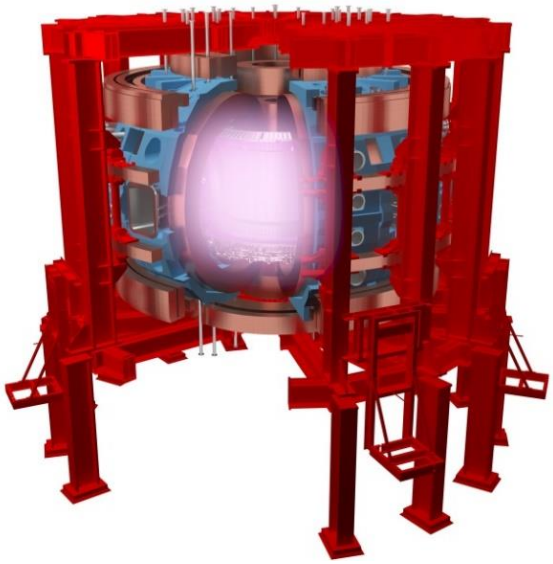

Figure 3.5: 3D-model of ASDEX Upgrade [61]

Technical data:	
Total height of the device	9 metres
Major plasma radius	1.6 metres
Minor plasma radii	0.5 / 0.8 metres
Magnetic field	3.9 tesla
Plasma current	2 megaamperes
Pulse length	10 seconds
Plasma heating	27 megawatts
Plasma volume	13 cubic metres
Plasma quantity	3 milligrams
Plasma mixture	hydrogen, deuterium
Plasma density	$2 \cdot 10^{20}$ particles per m^3
Plasma temperature	100 million degrees

Table 3.1:Technical data of ASDEX Upgrade, data from [29]

3.5.2 COMPASS

The COMPASS (COMPact ASSembly) tokamak was built during the 1980s in the British Culham Science Centre. The first plasma discharge was performed in 1989. After British scientists started alternative research, it was offered to the Institute of Plasma Physics of the Czech Academy of Sciences in Prague 2004, where it commenced operation in 2008. The widespread research covers plasmas with temperatures from relatively low to very hot, different densities, pulsed plasma systems and laser plasmas, among others. Beside AUG and JET it is the only operational tokamak in Europe with ITER-like configuration and capability of a H-mode regime. [30]

A photograph of the COMPASS tokamak can be seen in Fig. 3.6. Some main parameters are shown in Table 3.2 and the graphic in Fig. 3.7 compares the size of COMPASS to AUG, JET and ITER.

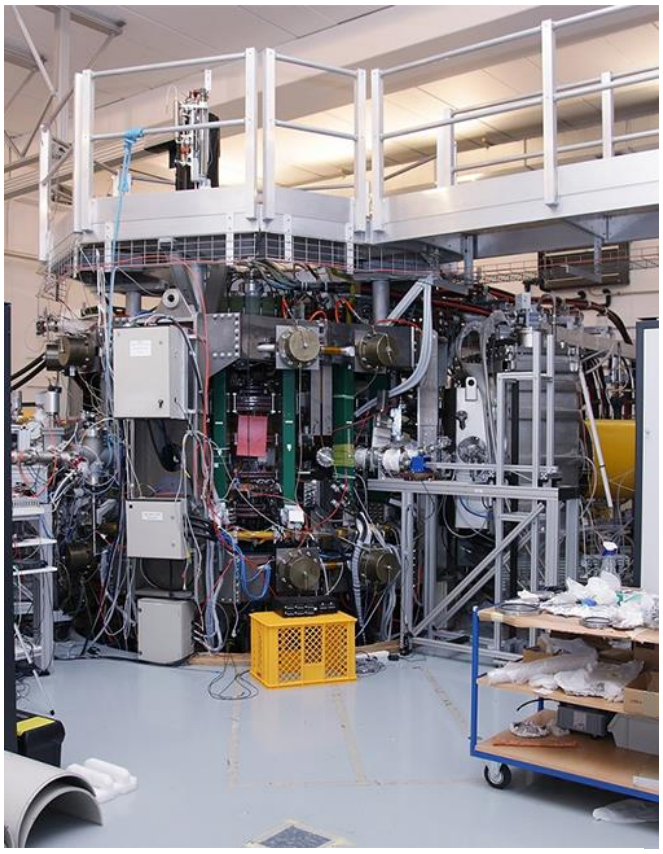

Figure 3.6: Photograph of the COMPASS tokamak [30]

Parameters	**Values**
Major radius R	0.56 m
Minor radius a	0.23 m
Plasma current I_P (max)	400 kA
Magnetic field B_T	0.9 - 2.1 T
Vacuum pressure	$1 \cdot 10^{-6}$ Pa
Elongation	1.8
Plasma shape	D, SND, elliptical, circular
Pulse length	~ 1 s
Beam heating P_{NBI} 40 keV	2 · 0.4 MW

Table 3.2: Main parameters of the COMPASS tokamak, data from [30]

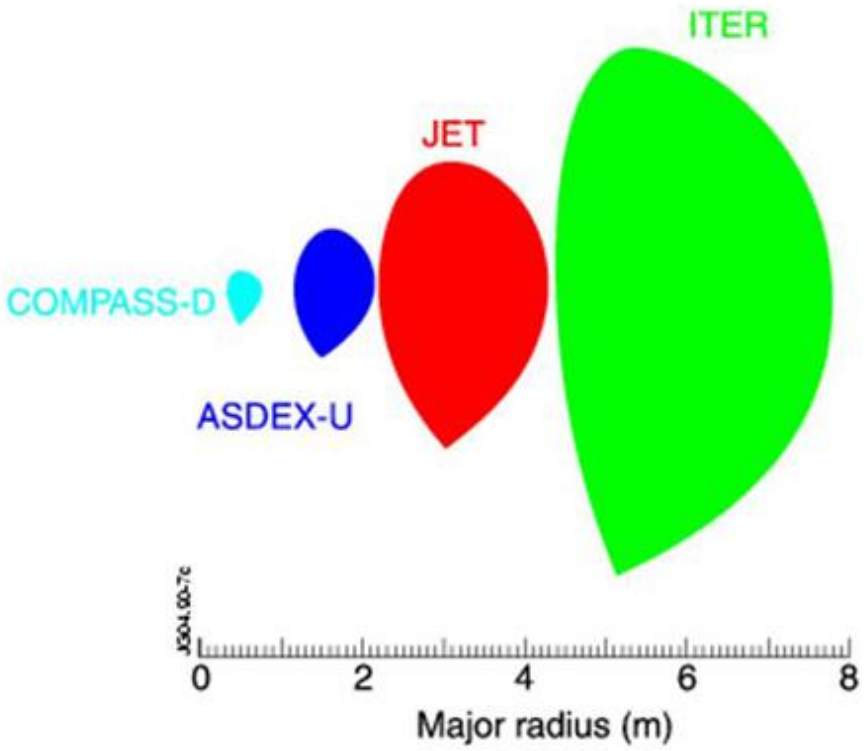

Figure 3.7: Size comparison of COMPASS to AUG, JET and ITER [30]

Currently scientists of the Institute of Plasma Physics of the Czech Academy of Sciences are also working on a new upcoming project, the COMPASS Upgrade. This advanced tokamak will help to expand the field of research, improve performance and address some key gaps with relevance for upcoming reactors like ITER and DEMO. The start of operation is planned for 2022. With a major radius of 0.84 m and a minor radius of 0.28 it is slightly bigger than the current COMPASS. [31]

3.6 Runaway electrons

Runaway electrons (REs) are electrons accelerating to relativistic energies. As electrons are charged particles, they experience an accelerating force in the presence of an electric field. Collisions with background electrons and ions have a decelerating effect on the electrons. In opposition to the behavior of increased friction exerted by the air on objects as the velocity increases, the drag force of background particles on the electron decreases at large velocities. If the force on the electrons by the electric field can overcome the drag force, electrons experience an acceleration to relativistic velocities and therefore “run away”. Beside natural occurrences in lightning bolts and astrophysical events, they can be generated in tokamaks, due to the closed magnetic flux surfaces providing enough path length for the large mean free path of runaways. There are three main mechanisms that can give rise to REs in tokamaks. Primary generation is due to the toroidal electric field overcoming the drag force. Secondary generation, also called avalanche mechanism, describes the transfer of energy from a runaway electron to a thermal electron through collision, knocking the thermal electron into the runaway state. Thirdly, a generation through transfer of energy from energetic particles (α, β) or gamma rays is possible.

Mainly disruptions, events where the energy stored in the plasma is rapidly deposited to the vessel wall due to a loss of confinement, exert enough force to generate REs. The avalanche mechanism can then increase the number of runaways exponentially, leading to runaway beams with currents of up to several megaamperes in a large tokamak [32]. This poses a huge threat for future fusion reactors, as they can damage the first wall of the tokamak. To avoid damages, disruption and runaway electron mitigation systems need to be developed. Studies in this field include the injection of impurity gases or pellets into the plasma, to generate or mitigate runaway electrons. This in an essential part of tokamak research. [33] [34]

4 The room-temperature solid-state pellet injector

4.1 History of the RTSP

The room-temperature solid-state pellet injector (RTSP) is a pellet launching system developed and built in the year 1996 at the Max-Planck-Institut für Plasmaphysik in Garching with the intention to test an injector system for lithium. Since at that time there was no initial use for the system on ASDEX Upgrade given, it was stored for future investigations. In the year 2001 it was characterized and tested again for a possible application with lithium pellets. After another 10 years of storage it was modified and characterized for the use of other pellet materials, such as aluminum, steel and copper. In 2014 the RTSP was modified back to lithium pellets, to install the RTSP on AUG to inject lithium. After deep lithium injections into the plasma on other tokamaks yielded promising results by improving several key plasma parameters, the decision was made to perform similar experiments on AUG. After the injector was characterized and tested in a testing environment, it was installed on AUG in 2015 and launched a total of 79 shots into the fusion plasma [35]. A picture of a lithium pellet ablating in the plasma can be seen in Fig. 4.1. [36] [37]

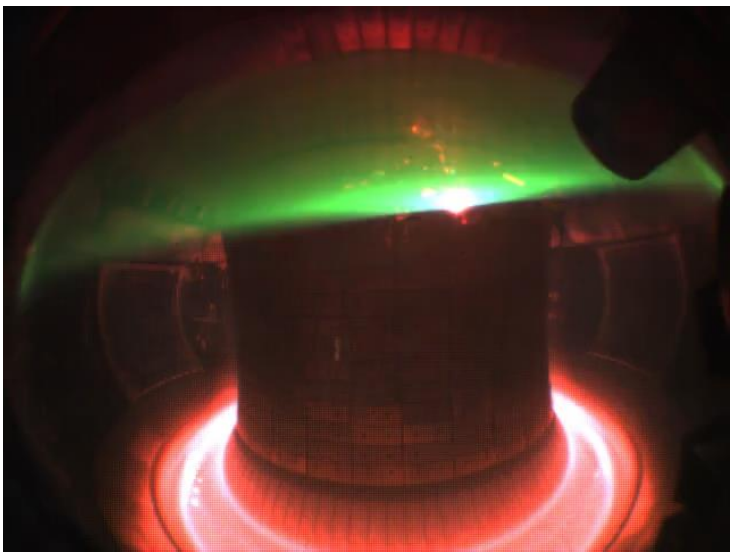

Figure 4.1: Picture of lithium injection on AUG [38]

The findings of this campaign were, opposing to the results on other fusion experiments, that plasma parameters were not improved by deep plasma injections of lithium. However, small improvements by wall conditioning effects, due to an ablation of lithium on the plasma facing wall-components, were observed [39]. This led to further investigations for a possible applicability as a wall conditioning machine, which followed in the years 2016 and 2017. Therefore, boron nitride was chosen as a pellet material and tested in a testbed, if a feasible utilization of such pellets could replace the procedure of conditioning the torus walls with diborane gas. This work was carried out by R. Hoepfl and covered in his bachelor's thesis [40]. His results were summarized and presented by the author of this thesis on an IPP intern Edge Physics Forum discussion, where the scientific management decided, that the RTSP will not be installed on AUG again and a future usage of the injector in the institute is not planned. Upon a request by the Institute of Plasma Physics of the Czech Academy of Sciences in Prague, to use the injector in their facility on the COMPASS tokamak for planned runaway electron studies, it was agreed on, that the RTSP injector will be modified and characterized in the existing testbed at IPP Garching to prepare the injector for COMPASS and subsequently provide it to the institute in Prague.

4.2 Working principle and technical design

4.2.1 Design of the system

Most parts of the room-temperature solid-state pellet injector are made of a special alloy called V2A steel (short name: X5CrNi18-10, material no: 1.4301), it is non-ferromagnetic to prevent magnetic forces acting on the injector. Overall the entire RTSP, as it is seen in Fig. 4.2, has a weight of approximately 20 kg without the bracket. With a length of 55 cm, width of 28 cm and height of 21 cm it is an overall quite compact pellet system.

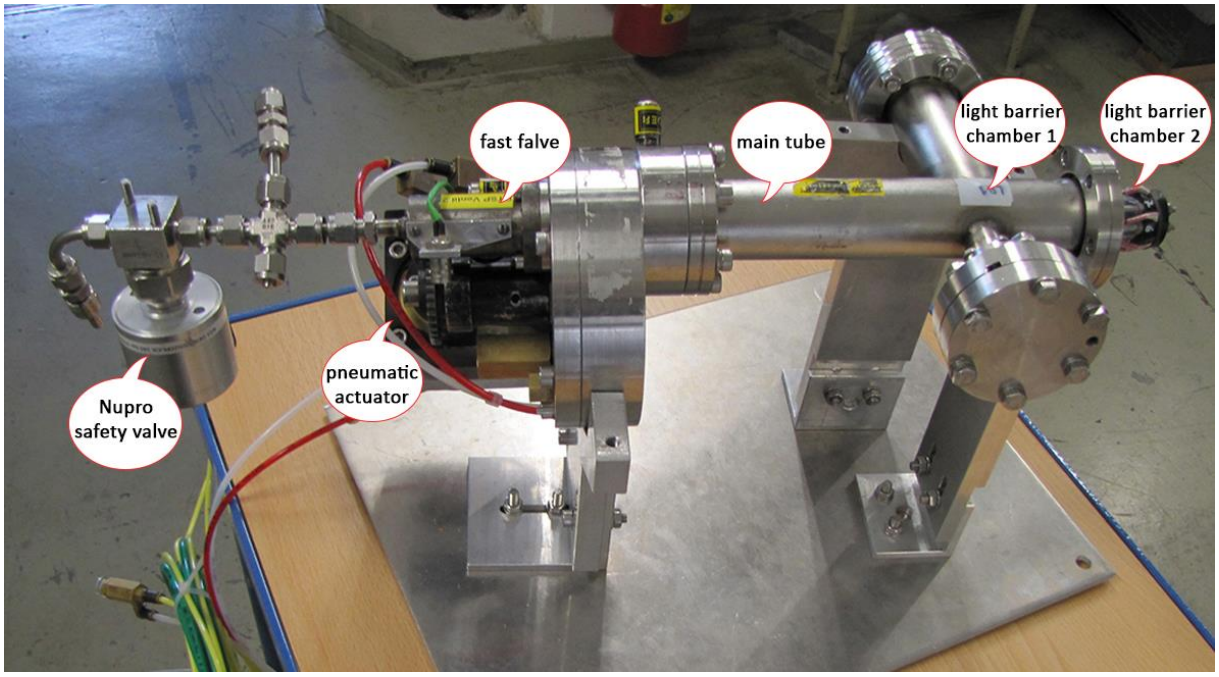

Figure 4.2: Photograph of the room-temperature solid-state pellet injector

The main parts for the injection system are shown in Fig. 4.3 and consist of the fast valve, the chambers of the pellet magazine and the acceleration barrel, all aligning on the trajectory axis of the pellet. The main body includes the pellet magazine within, as well as the connected fast valve, the pneumatic system and a loading port on the backside. The latter allows reloading the magazine with soft materials, like lithium, through additional extrusion nozzles.

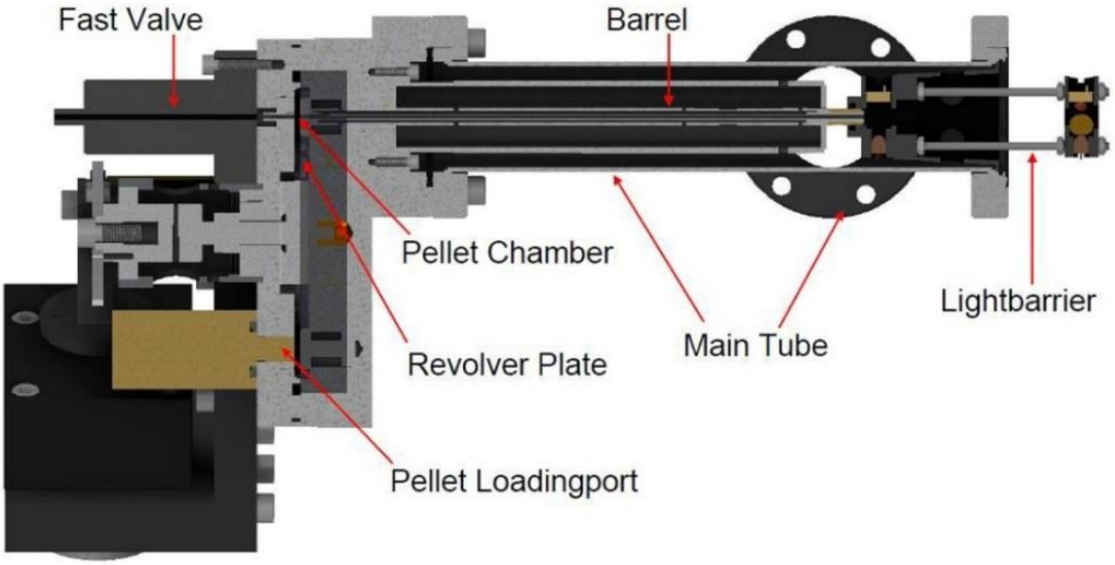

Figure 4.3: Lateral cut of the injector [41]

The acceleration barrel ($Ø = 1.5\ mm, l = 160\ mm$) and the light barrier in parts are surrounded by the main tube, which front end serves as the connecting flange to vacuum components (see Fig. 4.4). As for the application on fusion experiments it must withstand and maintain ultra-high vacuums, so the connection of the main tube to the main body and all the other connection parts are compact and airtight. On both sides of the main tube additional tubes are protruding. On one end of these tubes the connecting for the light barrier is located, on the other side an additional back-up flange gives the option for future diagnostic or vacuum extensions. [41] [42]

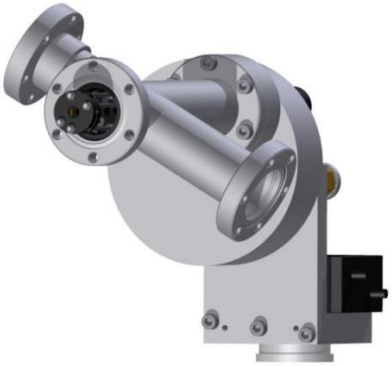

Figure 4.4: 3D-model of the RTSP - front view [43]

4.2.2 Gas injection system and pneumatics

The RTSP uses two different gas systems, which are partly interconnected, as you can see on the pneumatic schematic in the appendix E.1. The first one is the system for propellant gas injection, a schematic overview can be seen in Fig. 4.5. A 200 bar propellant gas bottle feeds the fast valve through an intermediary bellows sealed valve (Swagelok Nupro SS-HBS6-C). The pressure can be adjusted by a pressure regulator with manometer on the gas bottle (5-150bar). By flipping a switch on the pneumatic circuit twice, the Nupro valve opens and closes again trapping only a certain amount of the propellant in a reservoir between the Nupro and the fast valve. This way the propellant gas flux is reduced by a factor of two and it serves as a precaution in case of a malfunction of the fast valve, to prevent an uncontrolled influx of propellant gas. The fast valve itself is a non-commercial solenoid valve. It is connected via BNO-cable to an electronic control unit. A capacitor in the unit is loaded with 120 V. When triggering the control unit, the electrical current generates a magnetic field in the valve's solenoid, which operates the opening mechanism in the fast valve. The time it takes to reach open position is 0.2 ms, remaining open for a total of 2 ms. This way the propellant gas trapped in the reservoir is expanding very fast and the consequential gas pulse accelerates the pellet from the pellet chamber along the barrel. The fast valve sets the upper limit of the operable propellant gas pressure with 150 bar, though the recent years 100 bar was the limit, due to safety concerns. After leaving the barrel the pellet is injected in the target vessel in free flight, as the additional use of a guiding tube would reduce the transfer efficiency drastically [44]. [42] [41]

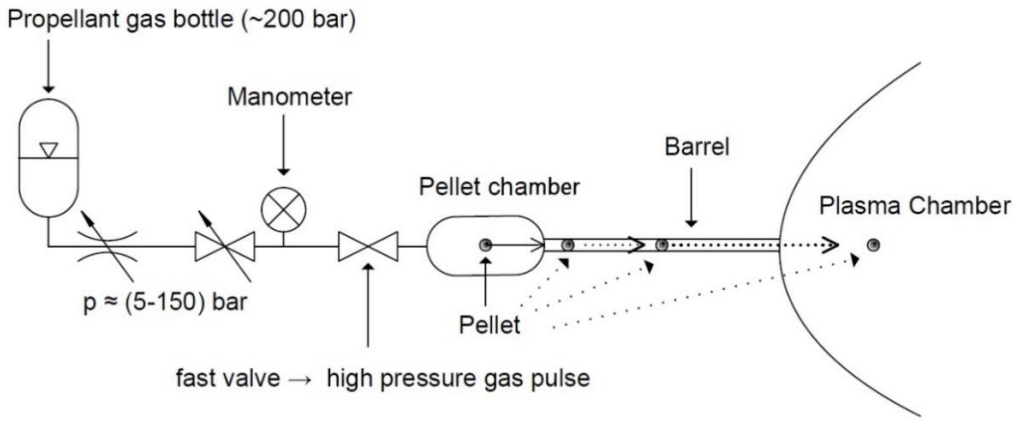

Figure 4.5: Schematic of the propellant gas injection [43]

The second gas system contains several pneumatic hoses, couplings and switches driving the opening mechanism of the Nupro safety valve for gas inlet to the reservoir on the one hand, and the pneumatic actuator for the magazine rotation on the other. The entire pneumatic system runs on 6 bars fed by a compressed air line. In Fig. 4.6 the pneumatic actuator system for magazine rotation can be seen. When pressurized through pushing a pressure switch, the stroke of a pneumatic double-acting cylinder lowers the pushing rod on the piston. When returning into the unpressurized initial position, the pushing rod is thereby pressed against the next tooth of the cogwheel, resulting in a rotation of the cogwheel. The cogwheel has overall 36 teeth. A pawl latches and secures the position. This process, to turn the cogwheel and subsequently the magazine to the next chamber, takes around 0.5 s. Although the fast valve could shoot with slightly higher frequencies, due to this limiting frequency of the pneumatic actuator, the maximum repetition rate of the RTSP is 2 Hz overall. [41] [45]

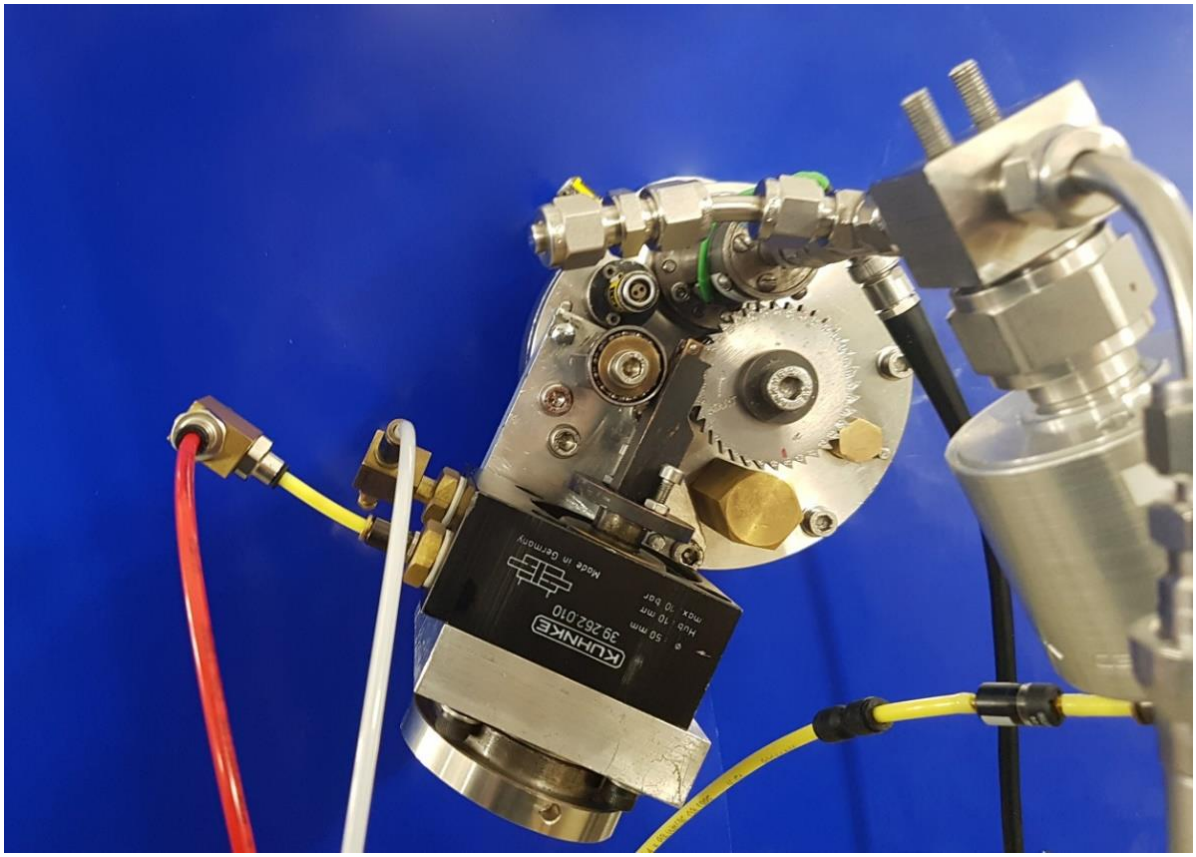

Figure 4.6: Photograph of the pneumatic actuator for magazine rotation

4.2.3 The magazine

For previous investigations different pellet magazines were tested, including magazines having different chamber sizes for pellets with a length of 2 mm and diameters of 0.5 mm and 1.0 mm and even magazine discs made of other materials [41]. The recent years all studies were performed with a V2A alloy steel magazine having 1.5 mm diameter and 2mm long pellet chambers (see Fig. 4.7). The 36 equally spaced chambers can hold cylindrical or spherical pellets with a length of 2 mm and a diameter of 1.5 mm. The shaft of the round magazine plate is joined with the axis of the cogwheel by two pins, resulting in a 10° turn of the magazine when the cogwheel is turned by the pneumatic actuator. To reload the magazine with soft pellets, like lithium, the loadingport on the rear cover of the main body can be used to extrude pellets directly into the chambers. In order to reload it with hard materials, like boron nitride, the main body must be disassembled, and pellets are inserted into the chambers with a tweezer. [35]

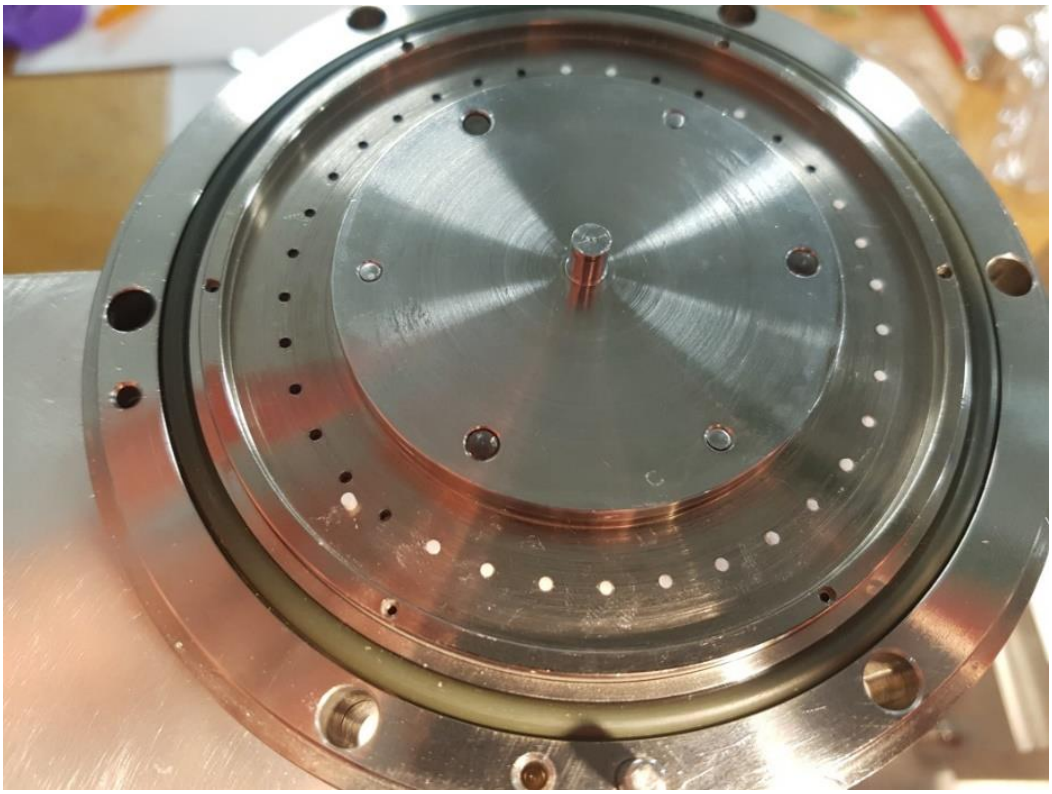

Figure 4.7: Photograph of pellet magazine during refilling process

4.2.4 Pellets

For the most recent study performed by R. Hoepfl, to test the feasibility of using boron nitride pellets with the RTSP for wall conditioning purposes, a large amount of boron nitride material was purchased, most of which was still in the laboratory, sealed in original packaging. The boron nitride is called HeBoSint®P700, was obtained from a company called Henze and delivered in form of 50 mm long rods with a diameter of 1.5 mm. The material itself has a hexagonal crystal structure, a density of around 2.0 g/cm³ and a purity of 99.7 %, major impurity being oxygen. A detailed data sheet of the impurities can be seen in the appendix D.4. The boron nitride rods (Ø= 1.5 mm; l= 50 mm) are processed to pellets usually the size of 2 mm length with maintaining the diameter. These pellets have an average weight of (6.80±0.02) mg and roughly a particle number of $8.45 \cdot 10^{19}$ B and N, each in equal shares. [46]

The production process of BN pellets is shown in Fig. 4.8 and follows the same steps for each pellet:

1. Unfortunately, some of the boron nitride rods do not meet the allowable tolerances in diameter (Ø > 1.5 mm). This was noticed, when some pellets would not fit into the magazine chambers. In order to avoid producing more pellets not fitting, the first step is measuring the rods' diameter using a micrometer screw.
2. Fitting rods are placed in the 2 mm deep bore on the bracket. Using a small saw, the rod is carefully cut at the flat top surface of the bracket. To make sure, that the rod is completely in the bore, it is secured with a finger.
3. To smooth out irregularities on the surface of the pellet, a file is used. The cut surface of the rod is also leveled with the file.
4. By gently knocking the edge of the bracket on the table the finished pellet falls out.
5. With a tweezer the pellets can be picked up and put into a storage box or inserted into the magazine immediately after.

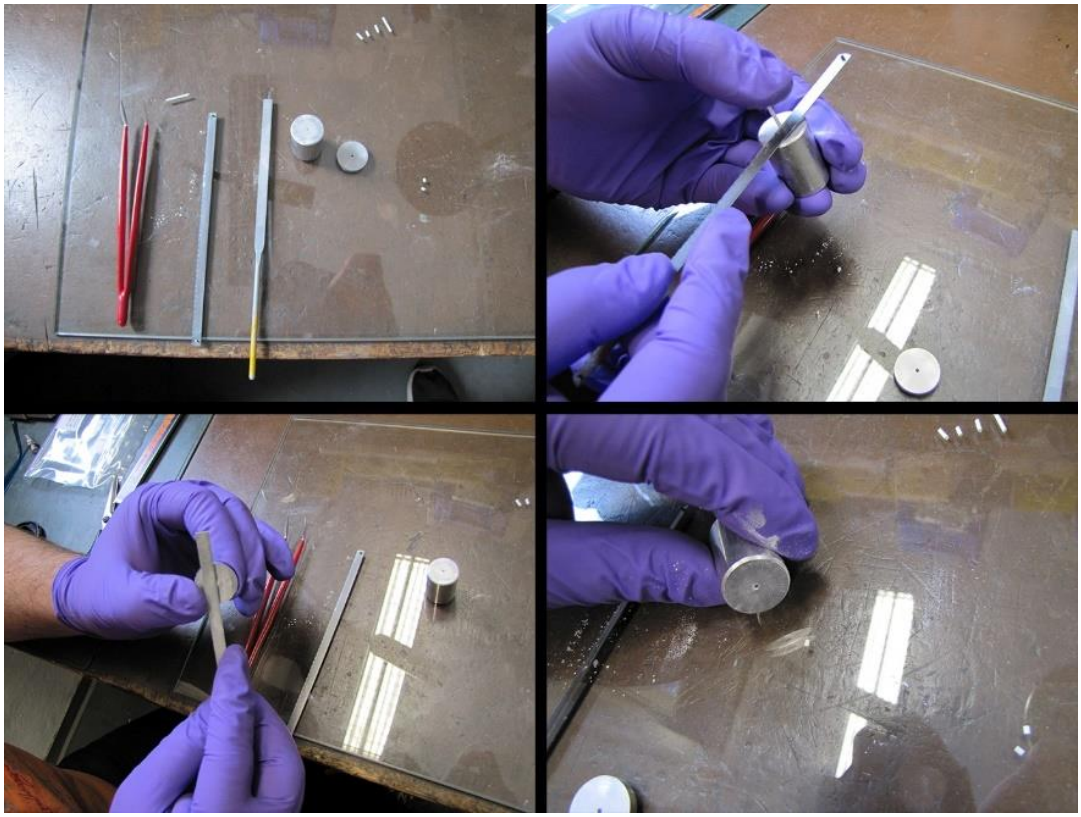

Figure 4.8: Process steps of manufacturing BN pellets

As it could be the case, that 2 mm long pellets are too much material for the planned runaway electron studies on COMPASS, it was tested, if the possibility is given, to produce and shoot 1 mm long pellets too. As the diameter stays the same and the new 1 mm pellets are made from the same material, they consequently have approx. half the weight and particle number as their 2 mm counterparts. To produce these smaller pellets a new bracket with 1 mm deep bore was made. Other than that, the process of producing and inserting them in the magazine stays the same.

The initial plan envisaged carbon pellets to be tested additionally to the boron nitride pellets for the characterization of the RTSP. Unfortunately, the collaborating Czech institute couldn’t provide them in time for the tests.

4.2.5 Light barrier

As a tool for diagnosing pellet velocities a light barrier, made up of two diode chambers, is integrated into the injector (see Fig. 4.9). The first chamber consists of one LED and one photodiode and is located within the front end of the main tube. The second one is protruding on the front of the injector and is equipped with three LEDs and three photodiodes. Both diode chambers are separated 70 mm apart from each other. On the main tube protruding to the left, the port for connecting the light barrier is located. A passing pellet interrupts the incidence of light on the photodiode, leading to a voltage drop. This can be measured by the connected electronic wiring box, which in turn offers signal outputs of the different photodiodes to determine the time difference between the signals of the two light barrier chambers. The time difference between the signals of the two diode chambers can be used to draw conclusions about the pellet velocity at the end of the acceleration barrel, as the distance between the two light barrier arrays is known.

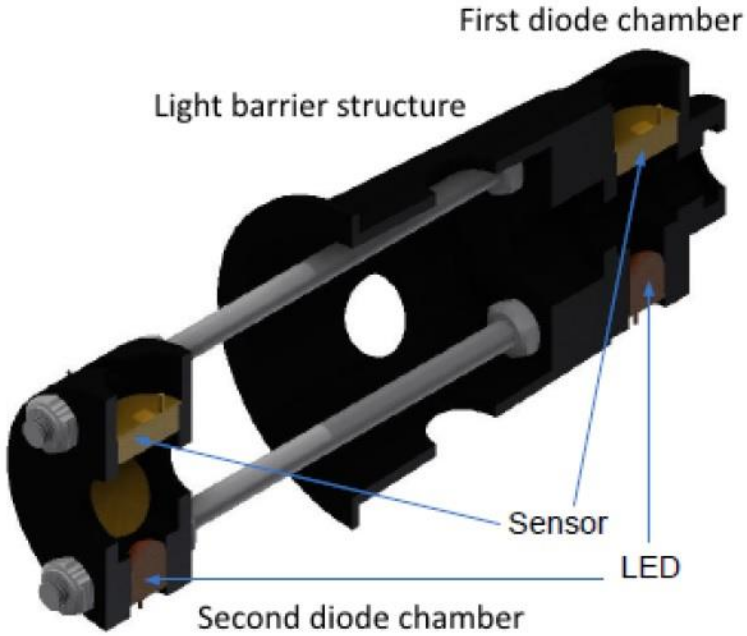

Figure 4.9: 3D model of the light barrier [41]

5 Testbed setup and preparation

5.1 Restarting the injector

Although the last usage of the injector was only a few months earlier, some parts had to be overhauled, because they were not working properly. A steel wire serving as a spring for the pawl on top of the push rod was not strong enough to secure the pawl on the cogwheel and had to be wound anew. Also, the pawl was in a wrong position, causing the fast valve, pellet chamber and entry of acceleration barrel to not be perfectly aligned. To adjust the pawl's position for perfect alignment, an Allen screw located below the piston and two screws with bolts on the upper side of the piston can be adjusted, to change the highest and lowest point of the piston's stroke. A connection valve and some of the hoses as part of the pneumatic system were leaking air and had to be replaced as well. The pneumatic schematic seen in the appendix E.1 describes the new setup. Lastly, during rotation of the magazine, part of the disc was causing friction on the rear cover of the main body. Disassembling, cleaning and reassembling the magazine fixed it and revealed boron nitride powder behind the magazine disc was the cause.

5.2 Overview

Figure 5.1 gives an overview on the testbed setup:

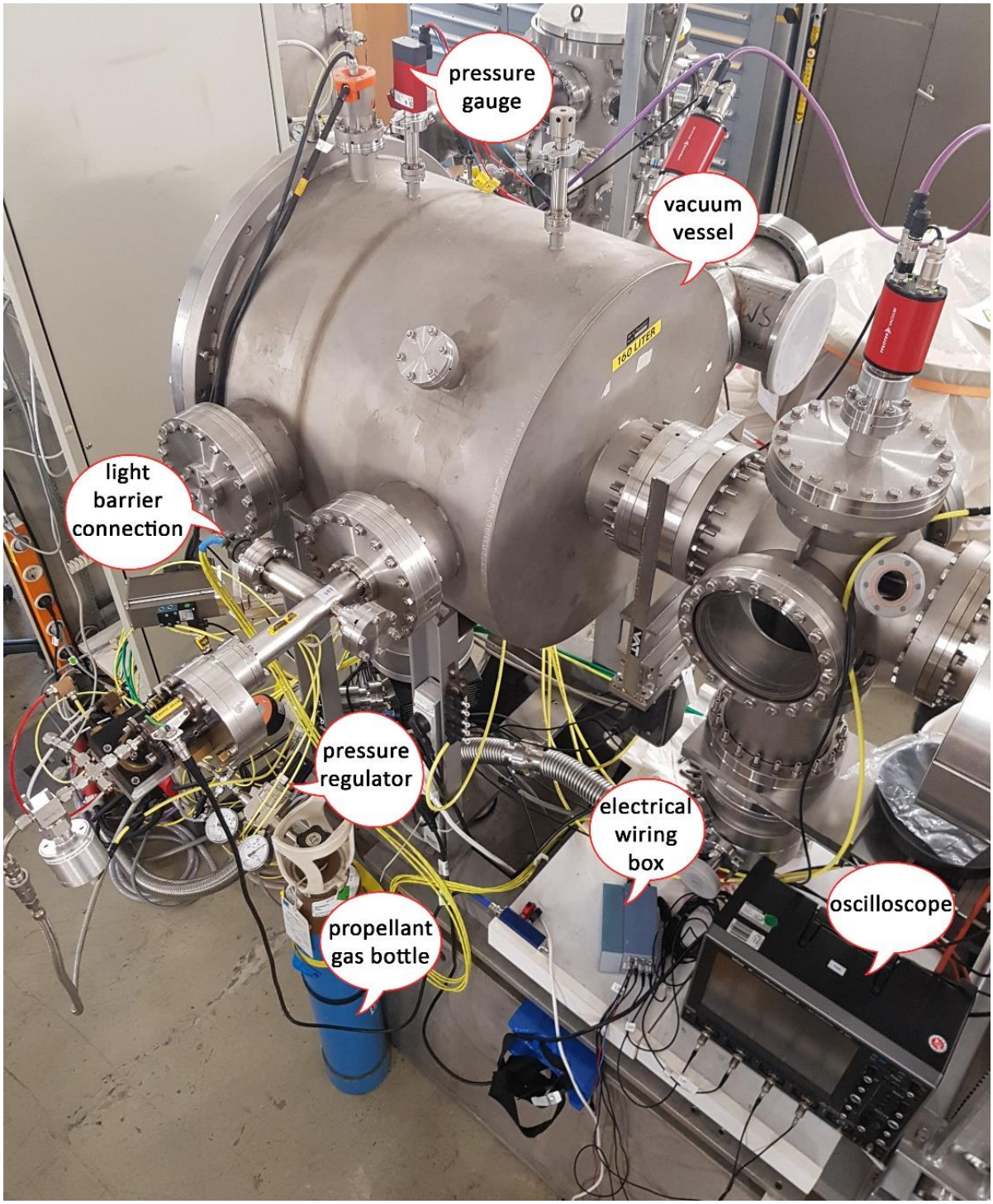

Figure 5.1: Overview on the testbed setup in the laboratory

5.3 Test vessel setup

Main component of the testbed setup in the pellet laboratory is a 160 l vacuum tank, serving as a test vessel to inject pellets. A vacuum gate valve separates the main vessel from the extension parts and stays closed throughout the tests. To achieve a prevacuum of approx. 10^{-1} mbar a Leybold DK200 rotary vane pump is used. When a stable prevacuum is achieved, the turbopump Leybold Turbovac 360 is added by switching it on with the Leybold Turbotronik NT20 controller. Data sheets of both pumps and the turbopump controller can be found in the appendix D.1. After 30 to 45 minutes a high vacuum in the range of 10^{-4} mbar to 10^{-7} mbar is achieved, depending on which additional components are used and how well the RTSP, the test vessel and the components are sealed (a more detailed description of improving the vacuum in the test vessel is described in chapter 7.2). To monitor the pressure inside the vessel, the Pfeiffer MPT 200 pressure gauge on top of the tank is used. The data sheet of the gauge can be seen in the appendix D.2. The pressure gauge is connected to a Siemens Simatic S7 controller. This enables the option to show plots of the pressures on a WinCC user interface on a nearby computer. All angle and gate valves of the testbed vessel are also controlled via the interface to the Simatic controller. For the operation of the RTSP on AUG the injector had to be fully automated. Therefore, it was integrated into the Siemens Simatic as well, enabling the integration to the AUG control environment. This allowed full remote control and monitoring of the RTSP from the control room. An overview of how the RTSP is integrated to the Simatic system can be seen in the appendix E.4. For the characterization the RTSP does not have to be automated, therefore it is controlled manually in the testbed.

As it was planned to use additional components for the angular scatter test and the tile shooting, an additional 4-way cross flange (DN 160 CF-F) was added to the test vessel. A photograph of leveling the flange can be seen in Fig. 5.2. The added flange allows the lateral attachment of a slide-in and the attachment of a tile holding structure, while still having the possibility to observe the interior of the vessel by looking through glass flanges on both sides.

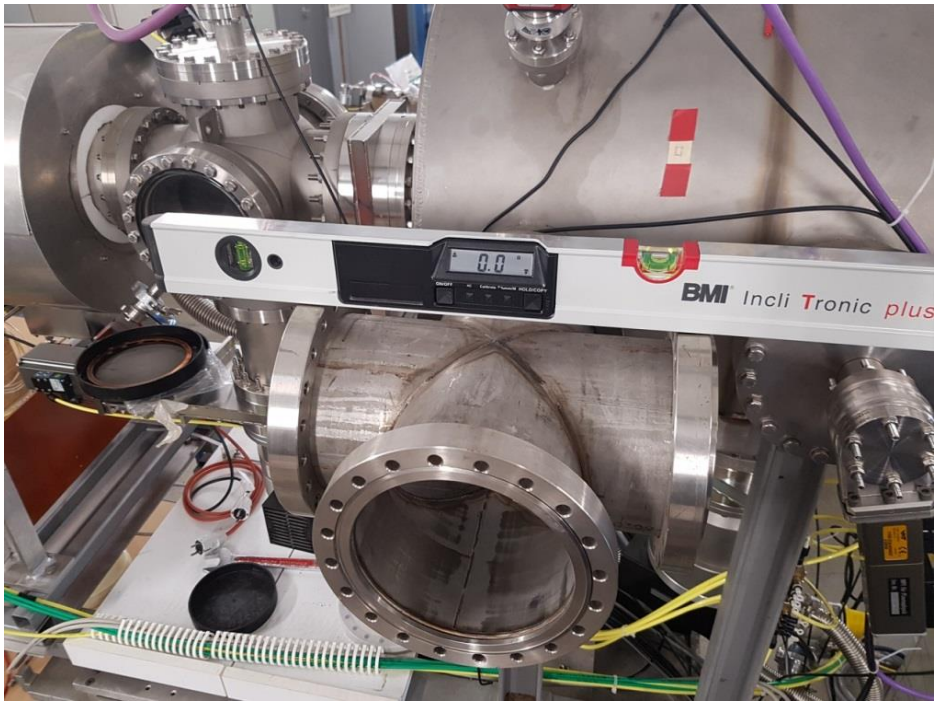

Figure 5.2: Photograph of leveling the additional 4-way Cross flange

5.4 Additional components

5.4.1 Light barrier setup

The setup of the light barriers' electronic wiring box and the oscilloscope can be seen in Fig. 5.3. The wiring box and the light barriers on the injector are connected via an Amphenol connector plug. The pin assignment of the connector plug is shown in the appendix E.3 and the wiring diagrams of the electric wiring box in appendix E.2. The signal outputs of the wiring box are connected to a LeCroy Waverunner 104Xi-A oscilloscope. The four signal outputs of the wiring box are connected to the four channels on the oscilloscope. This way LB1 of the first light barrier chamber and LB2a, b and c of the second, can be displayed. A 15 V supply voltage feeds the wiring box, to run the LEDs and photodiodes.

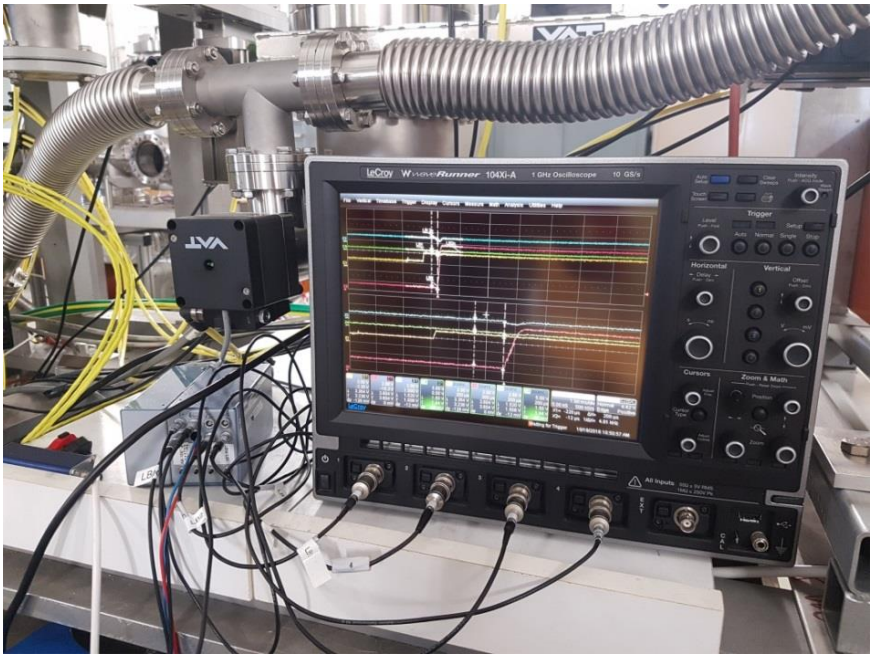

Figure 5.3: Light barrier components - electronic box and oscilloscope

5.4.2 Laser mount

In order to confirm the test vessel's geometry, a measurement with a laser was performed. The scatter angle test presumes a symmetrical test vessel and thereby perfectly parallel flanges. To test, if the flanges on the RTSP side and the opposing target side are truly parallel, a laser cased in a tightly fitting bracket, was flanged on. The suitable mount for the laser pointer was lathed. Pictures of the bracket and the laser measurement can be seen in the appendix C.4. The exact middle of the glass flange on the opposing side was marked previously. As you can see in Fig. 5.4, the laser spot was off-center, indicating, that the flanges are tilted and not perfectly parallel. The middle of the laser dot was off-center by approx. x= 3 mm. The distance between the laser and the glass flange is approx. d= 110 cm. Using the angular function in equation 5.1, this would account for a flange tilt of around 0.156°.

$$\propto = \arctan\left(\frac{x}{d}\right) \tag{5.1}$$

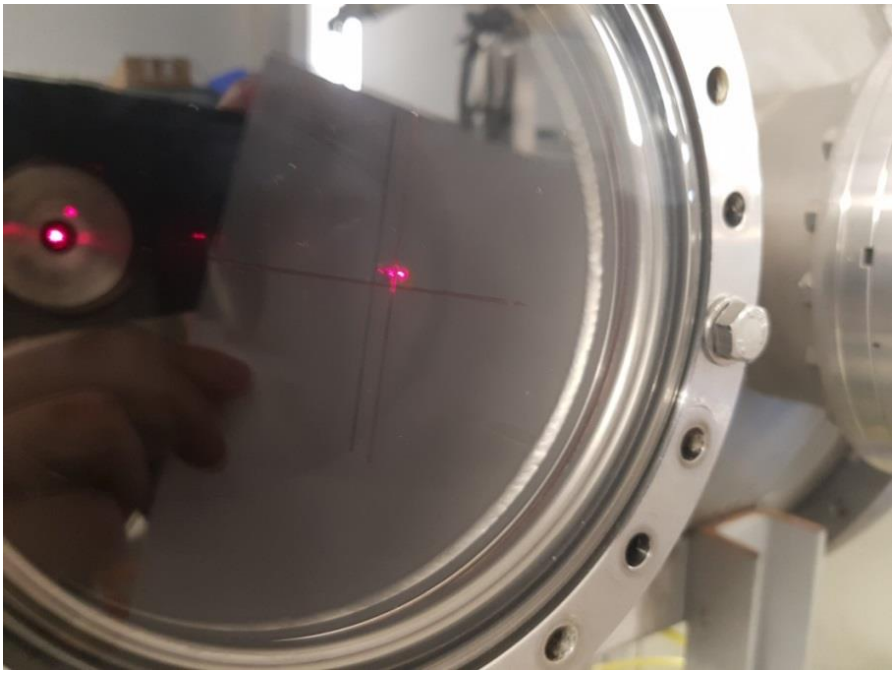

Figure 5.4: Measuring the tilt of flanges using a laser

5.4.3 Paper target slide-in

As target for the scatter angle tests a slide-in flange with a built-in paper roll holder is used (see Fig. 5.5). The paper unrolls, is stretched over the front side of a plane metal frame and furled again on the other side. The advantage of this device is that it is fully operable from outside the vessel, without the need to breach the vacuum, allowing to shoot all 36 pellets in different shot series at different targets. In preparation for the scatter angle test, multiple bullseyes were marked on the paper, indicating the center of each target. The perfect trajectory a pellet should follow without experiencing any deviation is known by looking at the spot, where the laser beam hits the paper. This way, the vertical and horizontal location of the supposed trajectory was marked on the metal frame of the slide-in (see Fig. 5.6). Then, the paper was unrolled and bullseyes on the same vertical height with enough space left between them were made by drawing crosses. The paper was furled up, inserted to the holder and tightened again. By turning the handle on the outside, the paper can be moved. To change to the next target, the handle has to be turned, until the bullseye cross is exactly in one line with the vertical marks on the frame.

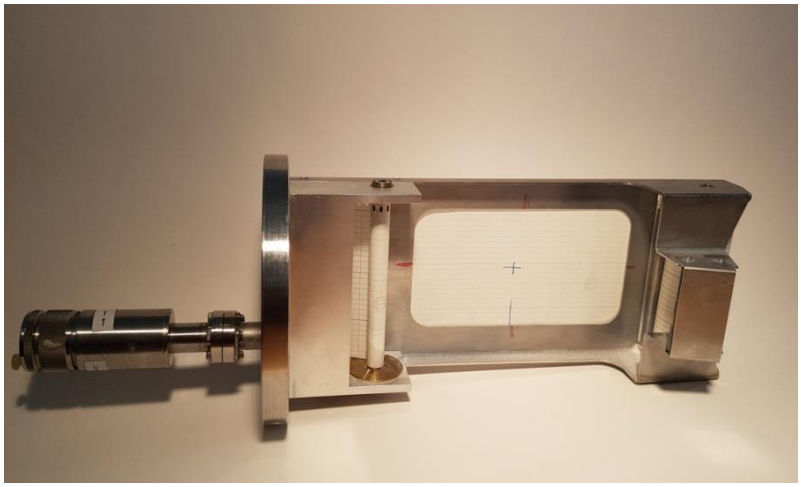

Figure 5.5: Photograph of the paper target slide-in

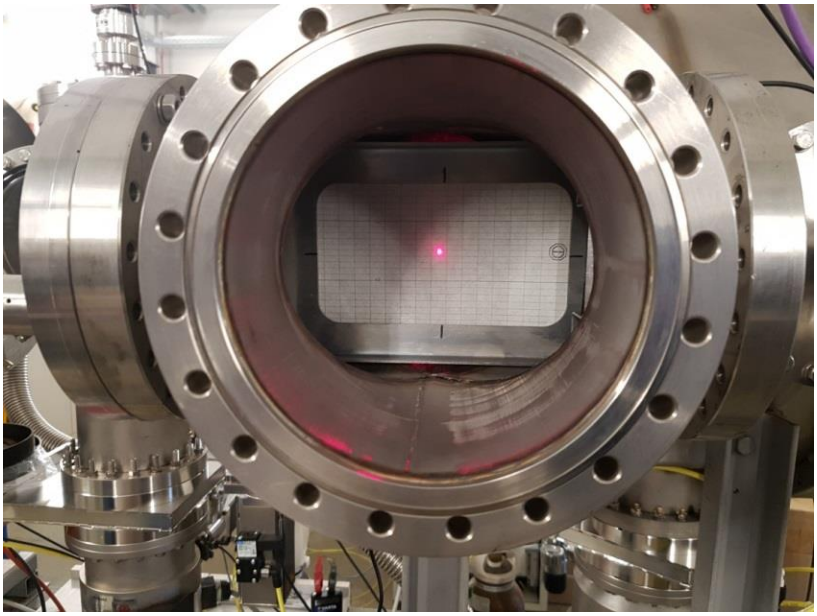

Figure 5.6: Marking the bullseye position by using the laser

5.4.4 Test tile bracket

Two vessel tiles that were withdrawn from service on the COMPASS tokamak could be obtained to perform realistic damage tests. The tiles geometries required a suitable bracket, to secure the tiles safely on their position inside the vessel. Therefore, a blind flange, metal rods as spacer and a clamp

for optical elements were chosen and firmly connected together. Figure 5.7 shows the bracket holding the tile before assembly and figure 5.8 shows the bracket with tile inside the vessel.

Figure 5.7: Bracket with a test tile

Figure 5.8: Bracket with a test tile inside the vessel

5.4.5 Propellant gases

The gases helium (He) and argon (Ar) were chosen as propellants to perform the characterization of the RTSP, as they are envisaged to be used for the studies on COMPASS. Both being noble gases, their inert characteristics are a huge benefit. Studies on disruptions and runaway electrons often involve the injection of impurity gases like argon into the torus anyway. Previous studies performed on COMPASS indicated, that the easiest way to generate post disruptive runaway electrons seems to be the injection of argon gas during the ramp-up-phase of the plasma current, making argon a suitable propellant for planned tests [47]. Helium features a higher speed of sound and is expected to thereby cause high pellet velocities. However, the inclusion of gas must always be well controlled, as larger amounts of gas could hamper the plasma confinement and stability. Thus, it is necessary to know the amount of gas, which is used for pellet injections employing propellant gases. Additional components to reduce the influx of propellant gas into the torus are usually installed.

The main specifications of both gases used in the testbed are listed in Table 5.1, data sheets containing more details and information about the safe handling of these gases can be found in the appendix D.3.

Specifications of propellant gases		
Propellant kind	**Argon (Ar)**	**Helium (He)**
Supplier	Alphagaz™	
Product name	Alphagaz™ 1	Alphagaz™ 1
Purity	99.999%	
Container name	S10	
Content	2.1 m³	1.8 m³
Valve thread	DIN 477, No. 6	
Expiry date	60 months	
Impurities		
H_2O - Moistness	< 2.0 ppm-mol	
O_2 - Oxigen	< 2.0 ppm-mol	
KW -	< 0.2 ppm-mol	
N_2 - Nitrogen	< 5.0 ppm-mol	
CO_2 – Carbon	< 0.2 ppm-mol	-

Table 5.1: Propellant gas specifications

6 Theory of the experimental studies

6.1 Pellet velocity

Velocities are a crucial parameter of pellet experiments. High velocities allow injections deep into the plasma and have the advantage of reducing the delay between trigger and arrival of a pellet. However, increasing velocities comes along with higher gas throughput for a gas gun system like the RTSP. Thus, knowing accurate behavior of the system with regards to pellet velocities is important. To describe the internal ballistics of the RTSP, particularly the acceleration of a pellet in the barrel, a theoretical model is used. C. Muenther described this model in detail in his thesis about the RTSP [48].

When the fast valve is opened, gas expands into the barrel (considered adiabatic). The resulting gas pulse generates a drag force on the pellet overcoming the resistance force and leading to a propulsive force. Equation 6.1 describes the acceleration process [48]:

$$m_P \frac{dv}{dt} = c_w \cdot A_P \cdot \frac{\rho_G(x)}{2} \cdot \left(v_G(x) - v(x)\right)^2 \tag{6.1}$$

Where m_P is the pellet mass, A_P the pellet cross sectional area, v the pellet velocity, c_w the turbulent gas drag coefficient, ρ_G and v_G are the density of the gas and the gas velocity along the flight trajectory. By extending to the total differential:

$$\frac{dv}{dt} = \frac{\partial v}{\partial t} + v \cdot \frac{\partial v}{\partial x} \tag{6.2}$$

And:

$$\frac{\partial v}{\partial t} = 0 \tag{6.3}$$

Equation 6.1 can be expressed as:

$$\frac{v}{\left(v_G(x) - v(x)\right)^2} dv = c_w \cdot A_P \cdot \frac{\rho_G(x)}{2 \cdot m_p} \cdot dx \tag{6.4}$$

Integration for the acceleration process gives:

$$\int_{v^i}^{v^f} \frac{v}{\left(v_G(x) - v(x)\right)^2} dv = \frac{c_w \cdot A_P}{2 \cdot m_P} \int_0^L \rho_G(x)\, dx \tag{6.5}$$

with L being the length of the acceleration barrel and v^i and v^f describing the initial and final pellet velocity. Approximating $v_G(x) = const.$ and $\rho_G(x) = const.$ results in:

$$\ln\left(\frac{v_G - v^f}{v_G - v^i}\right) + \frac{v_G(v^f - v^i)}{(v_G - v^f)(v_G - v^i)} = \frac{c_w \cdot A_P \cdot \rho_G \cdot L}{2 \cdot m_P} \tag{6.6}$$

With the initial velocity in the beginning being $v^i = 0$ and the final velocity at the end of the acceleration process being $v^f = v$ equation 6.6 yields:

$$\ln\left(1-\frac{v}{v_G}\right)+\frac{\frac{v}{v_G}}{1-\frac{v}{v_G}}=\frac{c_w\cdot A_P\cdot\rho_G\cdot L}{2\cdot m_P} \tag{6.7}$$

Equation 6.7 can be solved by iterating on v to obtain the expected pellet velocity, when all other variables are known. For the determination of the gas density ρ_G, the pressure p_0, temperature T_0, molar mass M, heat capacity ratio γ and the Mach number of the propellant are taken into account [49]:

$$p_G=\frac{p_0\cdot M}{R\cdot T_0}\cdot\left(1+\frac{\gamma-1}{2}\cdot Ma^2\right)^{-\frac{1}{\gamma-1}} \tag{6.8}$$

The Mach number is calculated by using the formula for the critical gas velocity v_c, describing an ultimate gas velocity at the end of the acceleration barrel [50]:

$$v_c=c_0\cdot\sqrt{\frac{2}{(\gamma+1)}}=\sqrt{\gamma\cdot\frac{R\cdot T}{M}}\cdot\sqrt{\frac{2}{(\gamma+1)}} \tag{6.9}$$

$$Ma=\frac{v}{c_0}=\sqrt{\frac{2}{(\gamma+1)}} \tag{6.10}$$

The drag coefficient c_w differs for 1 mm and 2 mm pellets. The values for the coefficients were determined by fitting a curve to data points obtained from literature [51]. Fig. 6.1 shows the connection between the ratio of length to diameter and the drag coefficient for cylindrical shaped objects in a gas flow. Fig. 6.2 shows the fit and the approximated drag coefficients for the 2 mm pellet ($c_w=0.88$) and the 1 mm pellet ($c_w=0.97$).

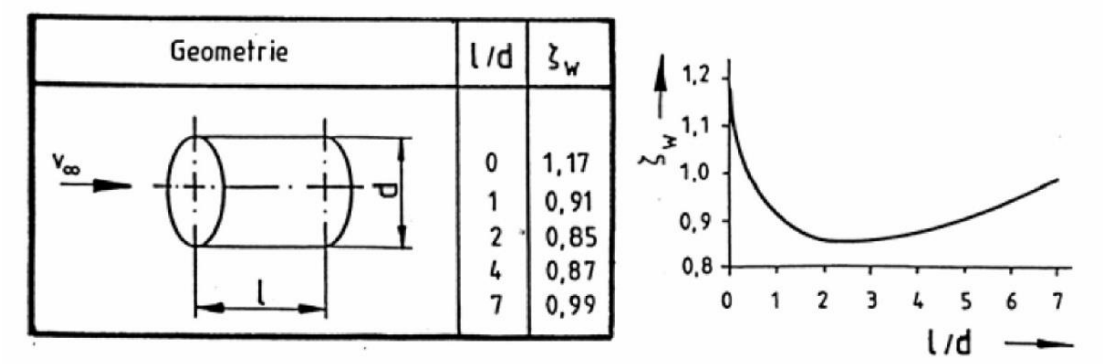

Figure 6.1: The course of drag coefficient depending on the ratio l/d [51]

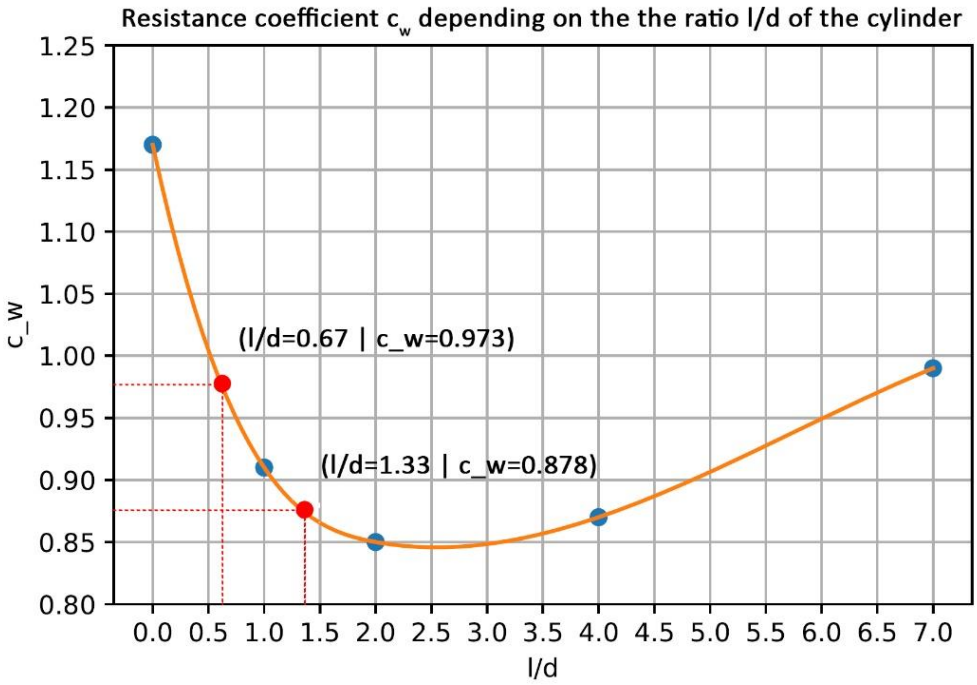

Figure 6.2: Determining of the drag coefficient for 1 mm and 2 mm pellets

Now equation 6.7 was solved by iteration and the expected pellet speeds, according to the time it takes the pellet for passing through the barrel, determined. The graphs in Fig. 6.3 and 6.4 show the pellet velocities at the end of the acceleration barrel predicted by the gas drag model for argon and helium, 1 and 2 mm pellets, each for 5, 50 and 100 bar pressure:

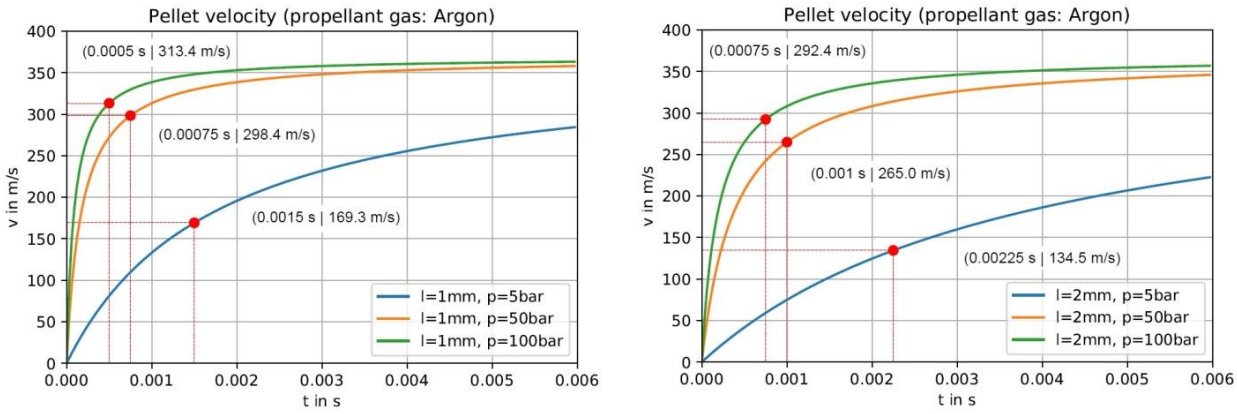

Figure 6.3: Course of pellet velocities for pressures at 5, 50 and 100 bar with argon (model)

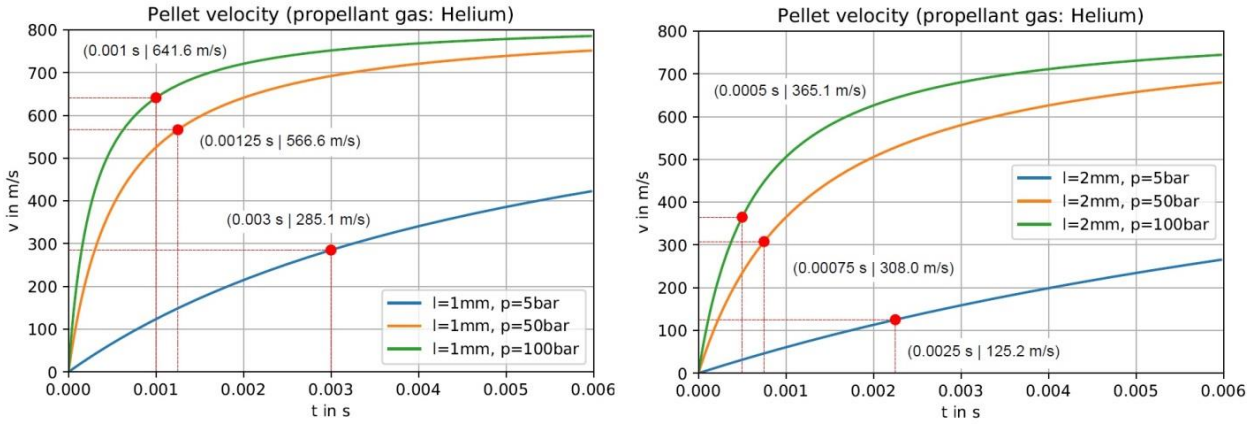

Figure 6.4: Course of pellet velocities for pressures at 5, 50 and 100 bar with helium (model)

The model predicts increasing velocities with rising propellant gas pressure. It also indicates, that the 1 mm sized pellets should be faster than their 2 mm counterparts and that pellets, that are shot employing helium gas can reach almost twice the speed of pellets that are shot with argon.

To determine pellet velocities in the testbed, the time it takes the pellets to travel the known distance between the two light barrier arrays is analyzed:

$$v = \frac{Distance\ between\ light\ barrier\ arrays}{Time\ difference\ between\ light\ barrier\ signals} = \frac{x_{LB}}{\Delta t} = \frac{70mm}{\Delta t} \tag{6.11}$$

Fig. 6.5 shows the procedure of reading off the value of time difference between LB1 and LB2 with the help of the cursor function on the oscilloscope. The light barriers detect a passing pellet. The consequential electric signals are registered by the oscilloscope. One of the signals serves as a trigger and appears at time $t = 0$. The difference in time to the second signal earlier or later represents the time it took the pellet to cover the distance of 70 mm between the two light barriers.

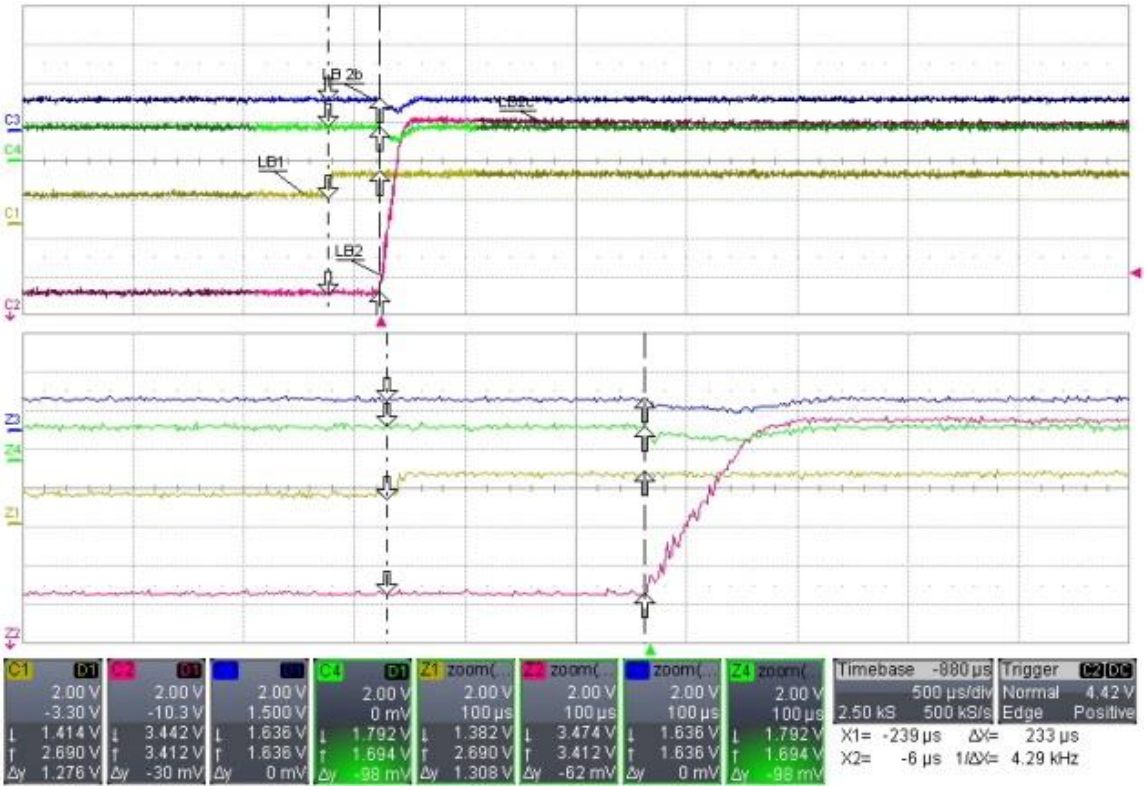

Figure 6.5: Measuring time difference of signals with the cursor

To evaluate the test results, the average velocity of each shot series representing a different pressure is determined. Therefore, the arithmetic mean value of a series is calculated:

$$\bar{v} = \frac{1}{n}\sum_{i=1}^{n} v_i \tag{6.12}$$

The statistical dispersion of pellet velocities for each pressure is taken as the standard deviation of the pellet velocities, assuming a normal distribution:

$$s = \sqrt{\frac{1}{n-1}\sum_{i=1}^{n}(v_i - \bar{v})^2} \tag{6.13}$$

6.2 Angular scatter

The injector cannot be installed directly on a fusion experiment. A certain distance between the RTSP and the torus must be maintained, to allow the installation of additional components. For instance, expansion vessels for the reduction of gas influx into the torus or a shielding tube to prevent damage to diagnostics and plasma facing components. The installation of such components proved to be very difficult for the campaign on AUG, as space close to the torus is limited [52]. Moreover, with increasing distance between RTSP and torus, the acceptable angular scatter for pellets is restricted. Pellets with bigger scatter, will hit the shielding tube and get destroyed, resulting in a lower transfer efficiency. Therefore, the accuracy and precision of the RTSP is tested in an angular scatter measurement. Fig. 6.6 shows a figurative scatter cone for pellets within the test vessel. Due to small differences in pellet properties, the gas pulse not spreading evenly at the exit of the barrel, and other influencing factors for describing the transitional ballistics, a perfect stable trajectory is not given, and statistical dispersion occurs when repeating shots. The end of the acceleration barrel is where pellets can start to experience a deviation from their trajectory, therefore this location is the point of reference for determining the flight distance.

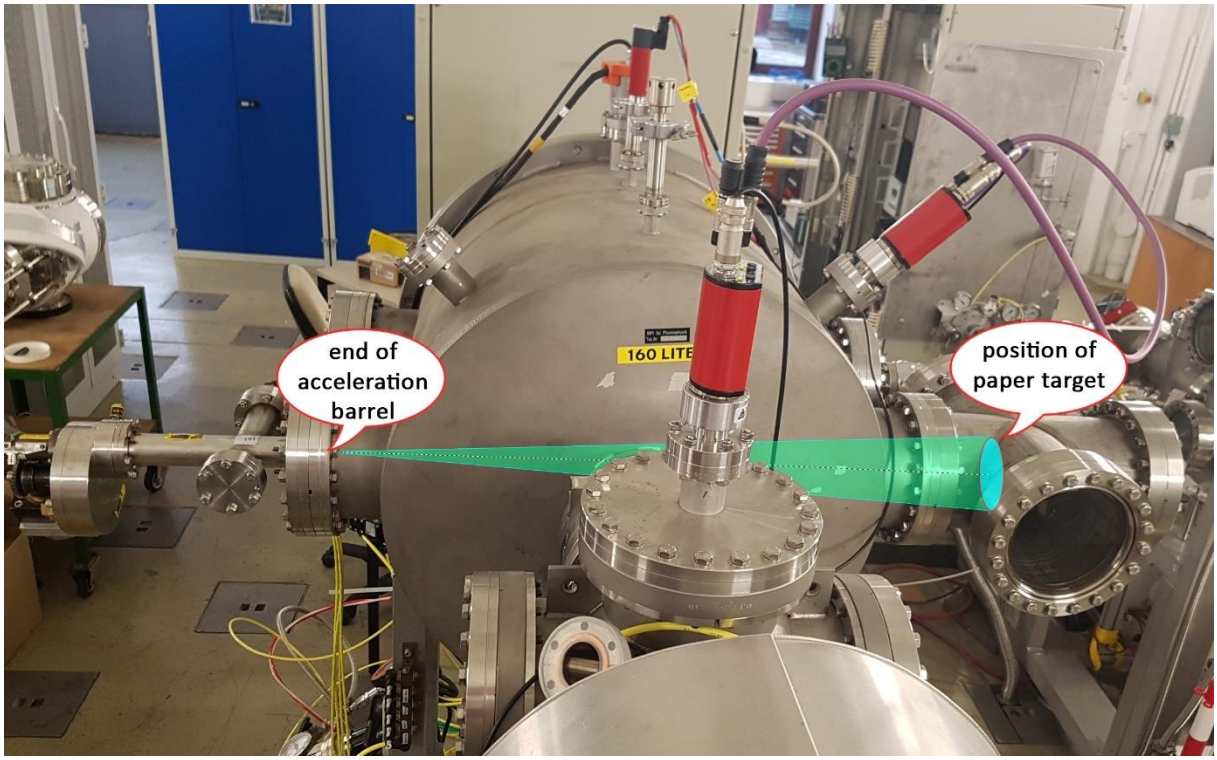

Figure 6.6: Scattering cone within the test vessel

The angular scatter of each pellet is calculated by taking the pellets' dispersion length x on the paper and the flight distance d between the end of the acceleration barrel and the paper target into account:

$$\propto = \arctan\left(\frac{dispersion\ length}{flight\ distance}\right) = \arctan\left(\frac{x}{d}\right) = \arctan\left(\frac{x}{970\ \mathrm{mm}}\right) \tag{6.14}$$

To determine the dispersion length on the paper after the shots, the target is divided into a x and y axis with the bullseye being the point of origin. The x and y values of the impact holes were measured with a standard ruler and noted. A photograph of the procedure measuring impact dispersion lengths can be seen in the appendix C.3, Fig. 11.3. With the Pythagorean theorem the x

and y values were calculated to the dispersion length. With all dispersion lengths measured, the scatter angles are determined and subsequently the mean scatter angle and standard deviation for each pressure calculated:

$$\bar{\alpha} = \frac{1}{n}\sum_{i=1}^{n} \alpha_i \tag{6.15}$$

$$s = \sqrt{\frac{1}{n-1}\sum_{i=1}^{n} (\alpha_i - \bar{\alpha})^2} \tag{6.16}$$

6.3 Propellant gas throughput

The gas pulse, that is used to accelerate the pellets, also enters the test vessel. Whereas an inlet of gas into the test vessel poses no problem, larger quantities of gas could lead to the termination of plasma in the torus. To quantify the influx rates of propellant gas in the test bed, the pressure gauge is used by measuring the pressure inside the tank during a shot. The values are plotted in a graph on the WinCC user interface on a nearby computer. Figure 6.7 shows graphs of pellet shots with 5, 50 and 100 bar in comparison. With higher pressures, more gas is propelled into the vessel. The consequential expansion of the gas within the vessel leads to a rise in pressure, which is higher, the more gas is added. With more gas introduced, it also takes longer to evacuate the vessel again. This can be clearly seen in the comparison picture. The values of pressure before a shot and the value of the highest peak shortly after, are noted. An integrated zoom function helps to find the precise measure points.

For the evaluation of the gas throughput, the known volume of the test vessel (V=160 l) is taken. However, the 4-way cross flange added additionally to the setup, enlarges this volume, so the overall volume in the testbed is slightly larger than 160 l. Though in comparison to the vessel volume and the accuracy of the measurement, this can be neglected.

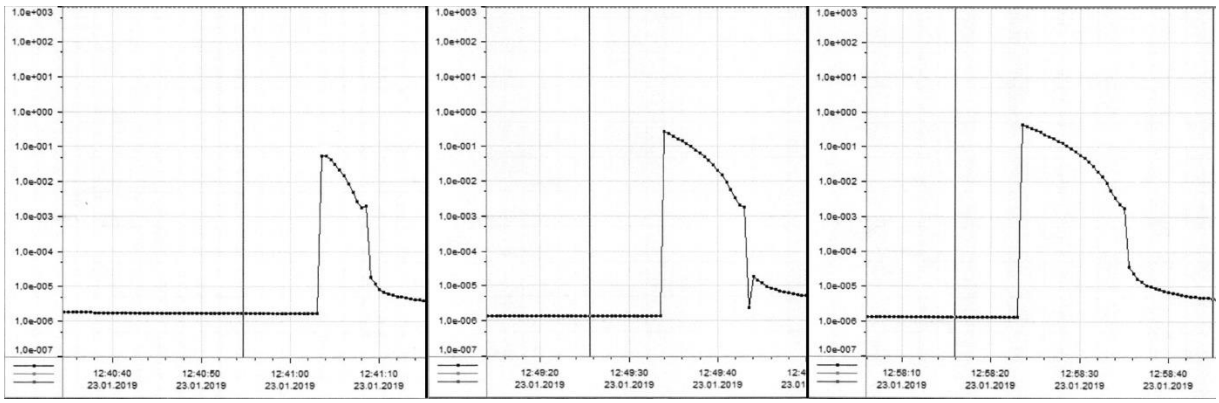

Figure 6.7: Pressure gauge plot of a 5, 50 and 100 bar shot

The amount of gas A is calculated by multiplying the increment of pressure with the volume of the vessel (equation 6.17). Thereafter, mean amount of gas and standard deviation for each pressure representing a shot series are determined (eq. 6.18 and 6.19).

$$\left(P_{Peak} - P_{before}\right)\,[mbar] \cdot Volume\,[l] = Amount\ of\ gas\,[mbar \cdot l] \tag{6.17}$$

$$\bar{A} = \frac{1}{n}\sum_{i=1}^{n} A_i \tag{6.18}$$

$$s = \sqrt{\frac{1}{n-1}\sum_{i=1}^{n}(A_i - \bar{A})^2} \tag{6.19}$$

6.4 Test tile shooting

Two test tiles, that are withdrawn from service on COMPASS, were obtained. They are old, and one tile had minor damages beforehand, nonetheless, they are suited to perform test shots to investigate possible damages of BN pellets to wall components of COMPASS. The old locations in the torus of both tiles can be seen in Fig. 6.8. One tile is from the inner heat shield and the other is a limiter tile.

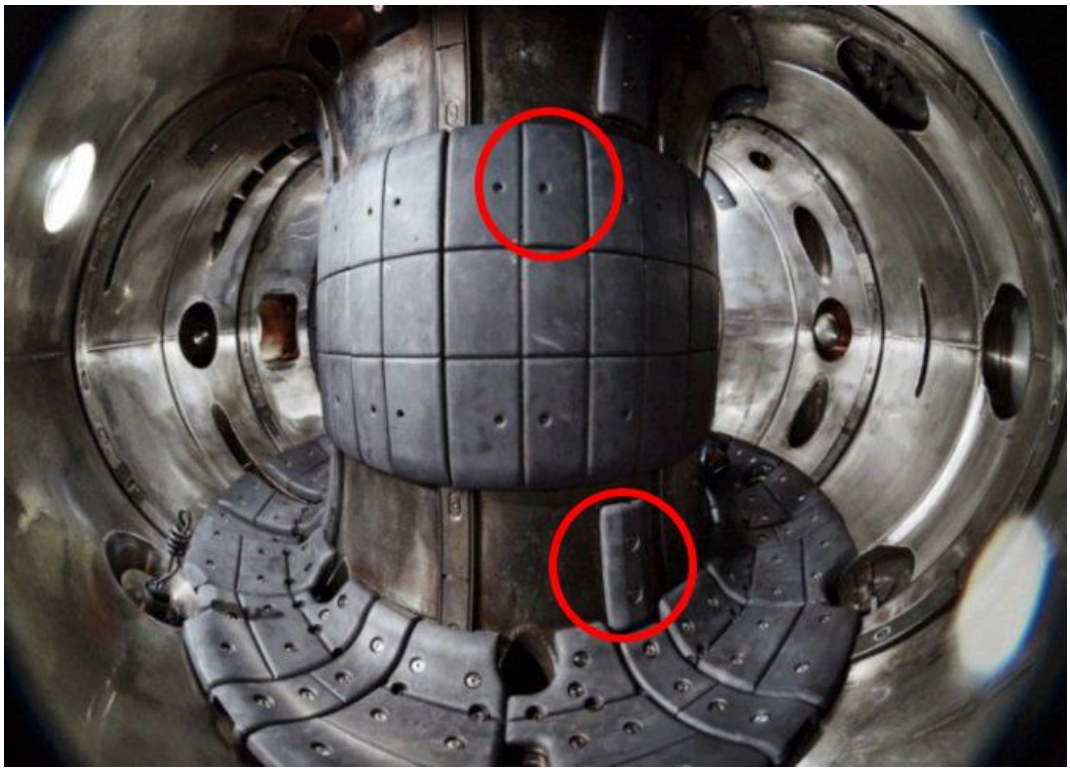

Figure 6.8: Locations of test tiles in COMPASS [30]

For plasma facing components and their materials high requirements are imposed. For instance, they must withstand high heat fluxes, electromagnetic loads and neutron damages. They also have to be resistant to erosion [53]. Thus, there are only a few materials that are suitable for use. COMPASS tiles are made out of graphite and have a density of approx. $\rho = 1.84 \frac{g}{cm^3}$. Previous damage tests were performed by shooting pellets on ASDEX Upgrade's tungsten tiles. Tungsten is a very hard material

with much higher density compared to graphite. Even with maximum achievable pellet velocity at this time ($\sim 340\,\frac{m}{s}$), it was not possible to damage it [54]. To perform the test shots on graphite tiles, they are placed inside the vacuum vessel. The bracket, used to hold the tiles firmly in its position, is described in detail in chapter 5.4.4. By using glass flanges the option to observe possible damage after each shot is given.

The field of study to describe the effects of projectiles on a target is called terminal ballistics and investigates the transfer of energy during the impact. In general, the damage potential of a projectile on a target is determined by its kinetic energy ($E_{kin} = \frac{1}{2} \cdot m \cdot v^2$) and the size of the impact area, where the energy is transferred.

7 Experimental procedure

7.1 Conduct of the experiment

Throughout all tests performed, standard laboratory conditions prevailed in the testing environment. To begin every series of shots, at first pellets must be produced and inserted into the magazine chambers. A detailed description of this procedure is covered in chapter 4.2.4. While the front part with the main tube of the injector can always remain flanged on, the main body, containing the magazine, must be disassembled to refill the magazine. For safety purposes the pellet chamber currently aligned with the fast valve is left empty, to avoid pellets slipping out of the chamber or getting stuck on the entry to the acceleration barrel while reassembling. Now the vacuum pumps can be started (for more details see chapter 5.3). When a sufficient vacuum is achieved, the different

parts of the RTSP can be connected to the additional components. The pneumatic actuator and the 6 bar feed of the Nupro safety valve are connected to the compressed air line. The propellant gas bottle is connected to the gas feed of the Nupro valve with a hose. The fast valve is connected to the trigger control unit with the electric cable. Now the trigger control unit, the power supply for the light barriers and the oscilloscope can be switched on. The main valve of the compressed air line and the main valve of the gas bottle can be opened, and the pressure regulator is adjusted to wanted pressure. To prepare for the first shot, the magazine is rotated to a loaded chamber by pushing the according pneumatic button. To let the propellant past the safety valve the pneumatic switch valve is opened for a few seconds and closed again. Now the RTSP is ready and by triggering the fast valve control unit a pellet is shot. If the shot is successful, the auto-trigger of the oscilloscope should immediately register the signals of the light barriers and show the curves of the signals accordingly.

To collect the measuring data, the two values of pressure P_{before} and P_{Peak} are read off the WinCC interface, as well as the time difference of the light barrier signals off the oscilloscope. These values are noted in the measurement protocol with the shot number and the number of the current pellet chamber. In case any unsuccessful attempts were tried prior to the successful shot, this was noted likewise. When all measurement data is gathered, a short visual inspection of the impact marks on the paper target is performed. Reading off and noting the data gives the pumps enough time, to pull the vacuum to ranges prior to the shot. Now the next shot can be fired. If a complete shot series is finished, the paper on the slide-in is rotated to the next target and the pressure for the next series gets adjusted.

Shot series usually had a sample size of n=7 shots for 2 mm pellets and n=3 shots for 1mm pellets. However, if some pellets had odd behavior, additional shots were performed, or if the remaining pellets in the magazine were not enough for another entire series, the remaining pellets were also shot in the current series.

Pellet shots for the analysis of pellet velocity and gas throughput were performed parallel to the angular scatter measurements with pressures of 5, 10, 20, 30, 40, 50, 60, 80 and 100 bar for 2 mm pellets and 5, 10, 20, 40, 60, 80 and 100 bar for 1 mm pellets for each propellant. The tile shooting

tests were performed using helium as propellant gas with shots on the first tile starting at 5 bar pressure and increasing until permanent damage could be clearly seen for both 2 mm and 1 mm pellets. The second tile was shot with even higher pressures, to test an extreme case scenario. The transfer efficiency was observed throughout all tests.

7.2 Incidents

During the first week of characterizing the injector, the best vacuum achievable was approx. $10^{-4}\ mbar$. Leak detection performed with a detector on parts of the vessel and injector susceptible for leakages, showed that indeed multiple leakages were present. By replacing the rubber gaskets with copper gaskets and adjusting or renewing the sealings of loading port, magazine and main tube flange, the vacuum in the test vessel could be improved to $10^{-7}\ mbar$ for the tile shooting tests. However, when using the paper slide-in, the best achievable vacuum is in the range of approx. $10^{-6}\ mbar$.

While performing a shot series for 1 mm pellets with argon, large amounts of propellant gas advected into the test vessel when the Nupro safety valve was opened. This was due to the valve pin of the solenoid fast valve getting stuck in the opened position as a sign of wear. This was fixed by disassembling the fast valve, removing the valve pin and carefully reaming the bore.

After flying through the paper target, pellets hit the glass flange directly. As the characterization was started with argon, no problems occurred following this approach. However, when the propellant gas was changed to helium, the pellets' velocities were high enough to permanently damage the glass flange. This can be seen in the appendix C.2, Fig. 10.2, Picture 1. After this was noticed, a piece of rubber, stuck to the glass flange, should serve as a damper for the impact of the pellets (appendix C.2, Fig. 10.2, Picture 2). While evacuating for the following shot series, stresses in the glass were too much, it had a crack and had to be replaced (appendix C.2, Fig. 10.2, Picture 3). Afterwards, the replacement flange was covered with the rubber damper for the remaining tests.

8 Evaluation of results

8.1 Transfer efficiency

Transfer efficiency describes the probability of pellets arriving in the test vessel. The assumption was made, that all shots triggered by the electronic control unit count as a shot attempt and if no shot is registered by the light barrier or optical assessment through the glass flange, it consequently counts as a failed shot. Additionally, as the injector is disassembled for reloading the magazine, the chambers are checked for pellets remaining in the magazine to verify the number of failed shots. The transfer efficiency analysis includes all shots; from speed and scatter tests to tile shooting tests and some repeated tests and even test shots not appearing in other analysis. Excluded from this analysis is only the shot series, in which the fast valve had a malfunction and three shot series, where the fast valve, pellet chamber and acceleration barrel got out of alignment and greatly reduced transfer efficiencies were noticed. Table 8.1 shows the transfer efficiency for all shots:

Propellant gas: **Argon** ; Pellet size: **Ø= 1.5 mm, l= 2 mm**									
Pressure	5	10	20	30	40	50	60	80	100
Transfer Efficiency	87.5%	77.7%	100.0%	100.0%	100.0%	87.5%	100.0%	100.0%	100.0%

Propellant gas: **Argon** ; Pellet size: **Ø= 1.5 mm, l= 1 mm**									
Pressure	5	10	20		40		60	80	100
Transfer Efficiency	84.6%	90.9%	87.5%		100.0%		100.0%	87.5%	100.0%

Propellant gas: **Helium** ; Pellet size: **Ø= 1.5 mm, l= 2 mm**									
Pressure	5	10	20		40	50	60	80	100
Transfer Efficiency	77.2%	85.7%	86.6%		100.0%	88.9%	100.0%	93.3%	100.0%

Propellant gas: **Helium** ; Pellet size: **Ø= 1.5 mm, l= 1 mm**									
Pressure	5	10	20		40		60	80	100
Transfer Efficiency	86.7%	87.5%	88.2%		100.0%		100.0%	100.0%	85.7%

Table 8.1: Transfer efficiency

The data suggests that transfer efficiencies are slightly reduced for shots at lower pressures. Propellant gas or the size of pellets seems to have little to no effect on the transfer efficiency. In total 336 shots were attempted, with 307 of them actually arriving in the test vessel. Hence, the overall transfer efficiency is:

$$\frac{307}{336} \approx 91.4\% \tag{8.1}$$

Reasons for pellets not firing could be numerous. The main reason is probably due to the propelling force on the pellets being too small to overcome the friction in the chamber, especially for pellets with diameters close to or over 1.5 mm.

8.2 Pellet velocity results

Figure 8.1 shows the average pellet velocities for 1- and 2-mm sized pellets at different argon pressures. Pellet flight speeds range from $135\frac{m}{s}$ at 5 bar to 306 $\frac{m}{s}$ at 100 bar for 2 mm pellets and from $190\frac{m}{s}$ at 5 bar to $380\frac{m}{s}$ at 100 bar for 1 mm ones. The average deviation of pellet velocities across all pressures is $\sigma = 10\frac{m}{s}$ for 2 mm and $\sigma = 9\frac{m}{s}$ for 1 mm.

With increasing argon pressure, the pellet velocity increases likewise. The steep increase at low pressures with a flattening profile for higher pressures and the fact that 1 mm pellets are faster than 2 mm pellets is consistent with the gas drag model. The experimental speeds for 5, 50 and 100 bar fit well with the theoretic ones from the model. The three values miss the theoretic values with an average relative error of 2.3 % for 2 mm pellets and 12.4 % for 1 mm pellets. The fitting of a logarithmic curve shows the flattening course of the data points for higher pressures.

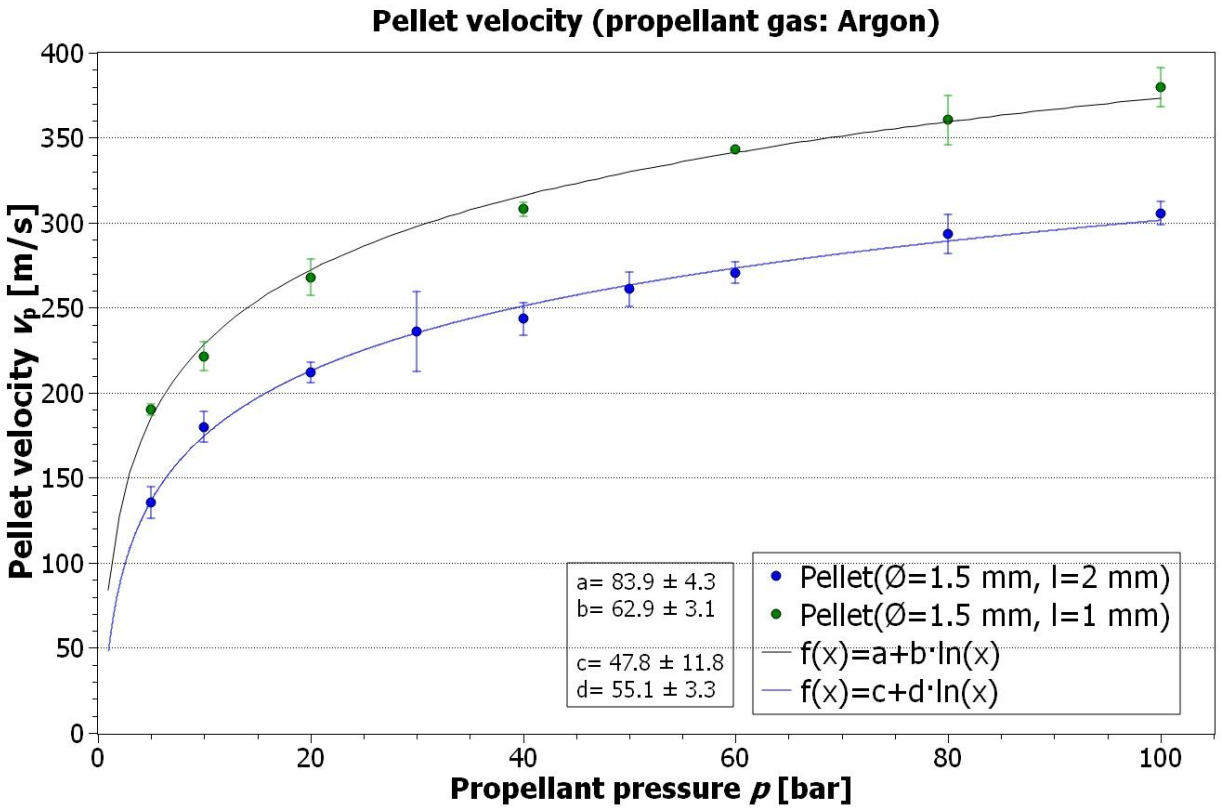

Figure 8.1: Pellet velocity with propellant gas pressure (Argon)

The average pellet velocities for each pressure using helium as propellant are shown in Fig 8.2. The speeds for 2 mm long pellets range from $120\frac{m}{s}$ at 5 bar to $721\frac{m}{s}$ at 100 bar and from $238\frac{m}{s}$ at 5 bar to $685\frac{m}{s}$ at 100 bar for 1 mm. The average deviation of pellet velocities across all pressures is $\sigma = 30\frac{m}{s}$ for 2 mm and $\sigma = 19\frac{m}{s}$ for 1 mm.

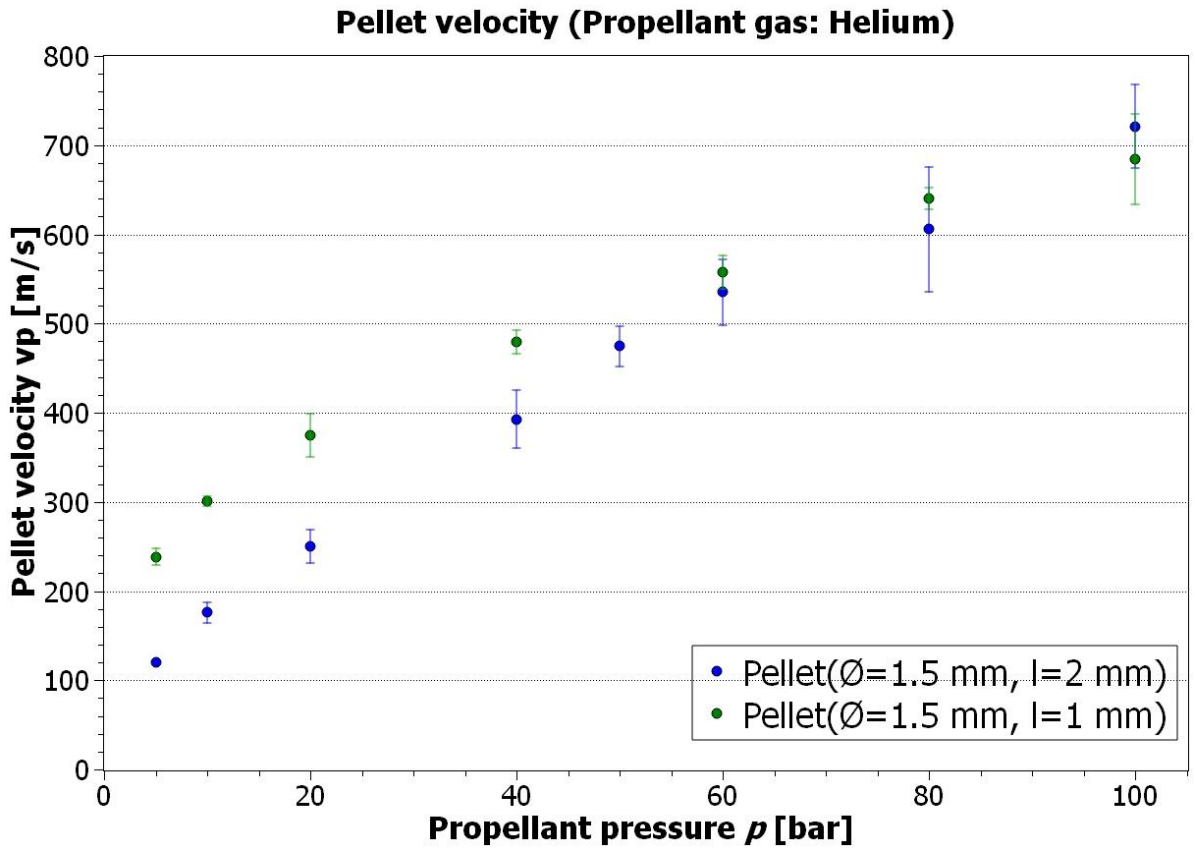

Figure 8.2: Pellet velocity with propellant gas pressure (Helium)

While the 1 mm experimental speeds for 5, 50 and 100 bar fit well again with the theoretic ones from the model (average relative error 10.5 %), the three values for 2 mm miss the theoretic values quite a lot with an average relative error of 29.5 %. A logarithmic curve to gathered pellet velocities would fit bad. Since it was assumed, that the data series for 2 mm does not behave as expected, all shots were repeated. The repeated tests confirmed the initial ones, with all mean velocities being within the limits of the standard deviation of one another. The fact that the course of the data points is not flattening out, is likely due to the high speed of sound of helium (over $1000\frac{m}{s}$). Pressures in the range of 5 - 100 bar are not enough to see said flattening.

Tables of the test results for pellet velocities can be found in the appendix A.1. The measurement uncertainty of determining pellet velocities can be seen in the appendix B.1

8.3 Angular scatter results

Figure 8.3 shows the impact locations of the 244 shots analyzed for their scatter. The amount of impact marks on the picture may be less, as some shots from different shot series had the same impact locations with regards to their x and y position.

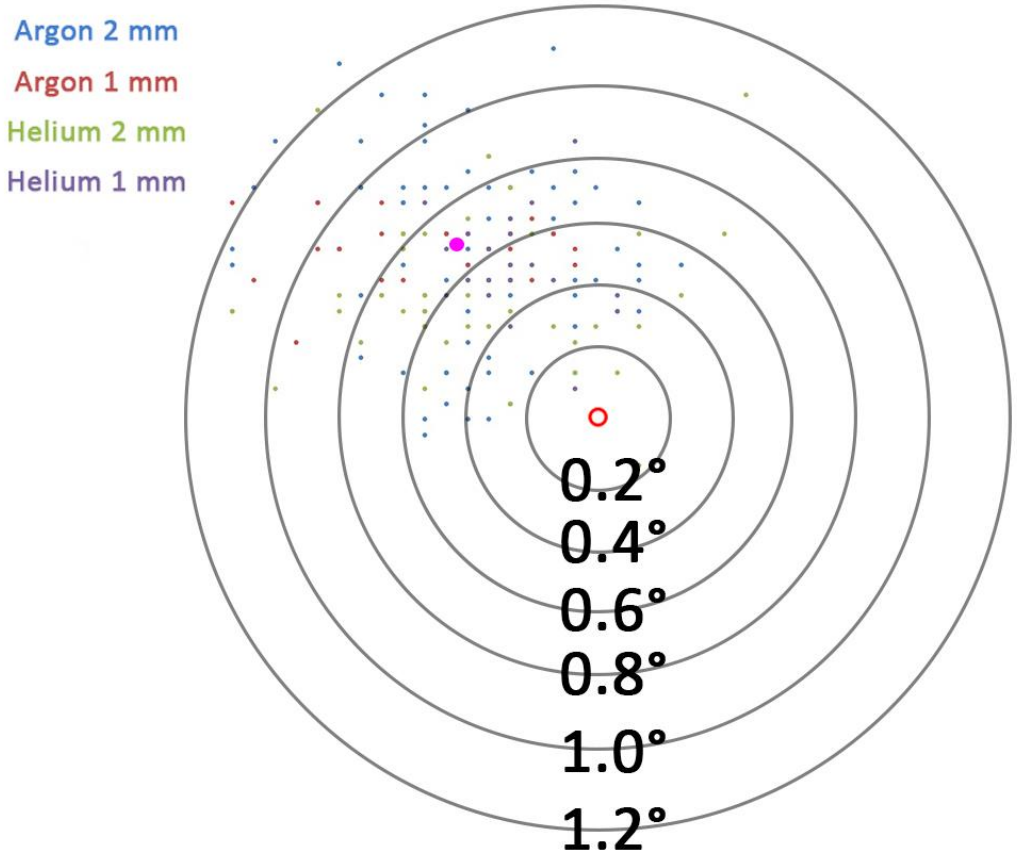

Figure 8.3: Pellet scatter of all shots analyzed

An overall drift to the upper left side can be clearly seen. Almost 90% of all shots were in the upper left quadrant. The bullseye location was determined by the laser. Therefore, the tilt of the flanges on the testbed vessel should already be taken into account. As the trend of the shots and the tilt of the flanges are consistent with regards to their direction, either the tilt of the flanges is stronger than the laser suggested, or the injector was additionally installed not perfectly aligned.

Fig. 8.4 and 8.5 show the mean scatter angles of the different shot series at different pressures for argon and helium gas with the bullseye as the basis point of reference.

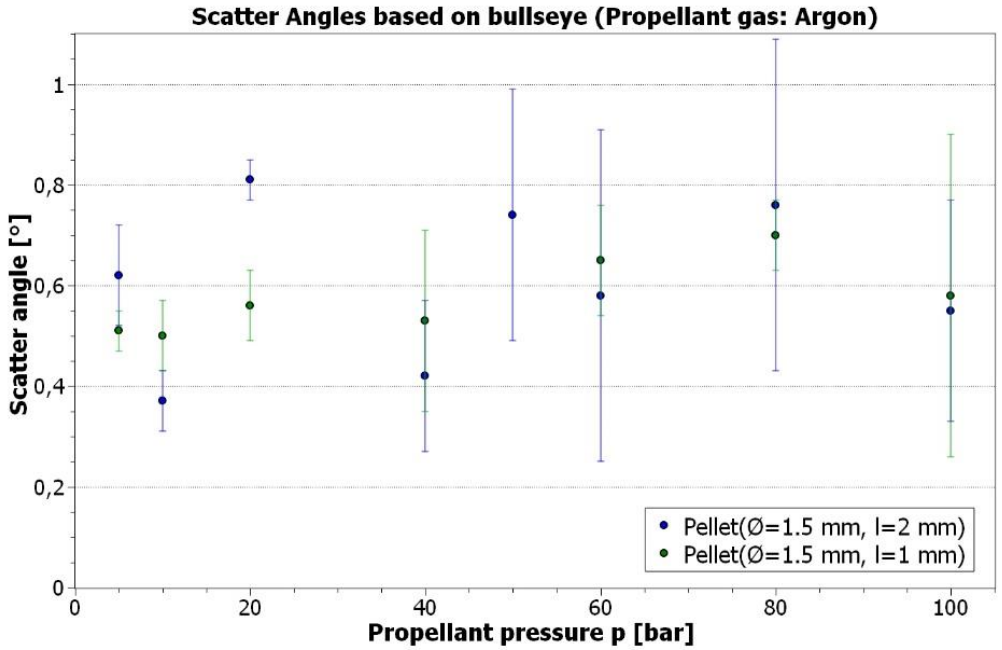

Figure 8.4: Scatter angles based on bullseye (Argon)

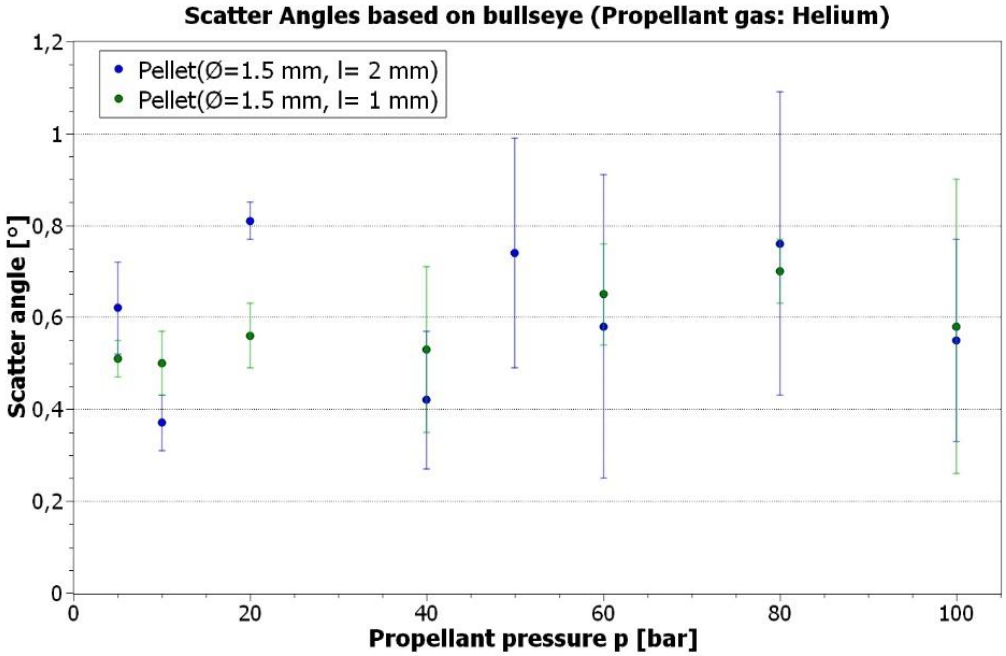

Figure 8.5: Scatter angles based on bullseye (Helium)

To quantify the shooting (in)accuracy of the RTSP, the mean point of impact of all shots is taken by calculating the arithmetic mean of the x and y values:

$$\bar{x} = \frac{1}{n}\sum_{i=1}^{n} x_i \qquad \bar{y} = \frac{1}{n}\sum_{i=1}^{n} y_i \tag{8.2}$$

The mean point of impact is located $\bar{x} = 4.6\,mm$ horizontal to the left and $\bar{y} = 10.3\,mm$ vertical upwards (marked in pink in Fig. 8.3). This equals a distance between bullseye and mean point of impact of approx. 11.3 mm and accounts for an angular deviation of 0.67°. This deviation has a systematic cause, as the mean point of impact should be close to the bullseye. As stated previously, this is probably caused by the injector being installed not perfectly aligned. The setup of the RTSP on COMPASS offers the option to make slight adjustments to the orientation of the connecting flanges. This would allow to compensate or minimize the systematic inaccuracy of the RTSP.

The scatter of the impact holes around the mean point of impact has a statistical origin. In order to focus only on the precision of the RTSP, all x and y values were set depending on the mean point of impact:

$$x_{new,i} = x_i - \bar{x} \qquad y_{new,i} = y_i - \bar{y} \tag{8.3}$$

Figure 8.6 and 8.7 show the mean scatter angles based on the mean point of impact. The shown angles represent a half cone scatter angle. Mean scatter angles for different pressures are mostly kept between 0.30°- 0.50° with 2 mm pellets and 0.10° - 0.30° with 1 mm pellets for both propellants. The average scatter angle for all 2 mm pellets and pressures is 0.40° with an standard deviation of σ=0.19°. In general, 1 mm pellets have smaller angular scatter and therefore a higher precision with an average scatter angle of 0.23° for all pressures (σ=0.12°). Propellant pressure and propellant kind seem to have no significant impact on the scatter angle.

Tables of the test results for angular scatter can be found in the appendix A.2. The measurement uncertainty for determining the angular scatter can be seen in the appendix B.2.

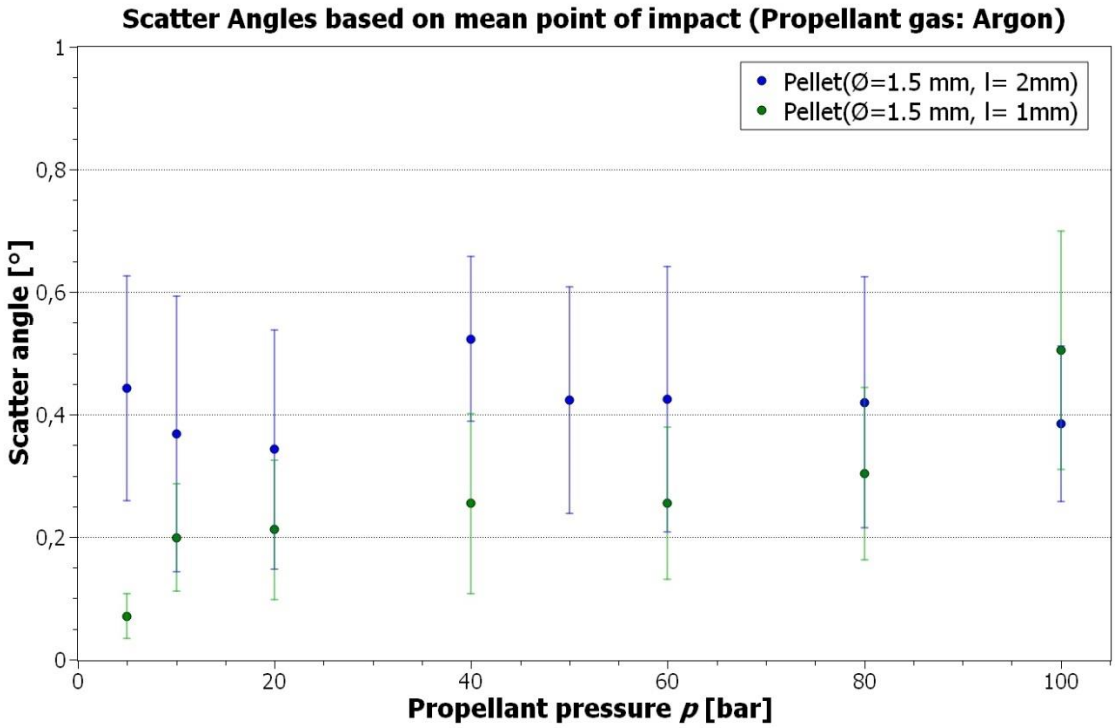

Figure 8.6: Scatter angle based on mean point of impact (Argon)

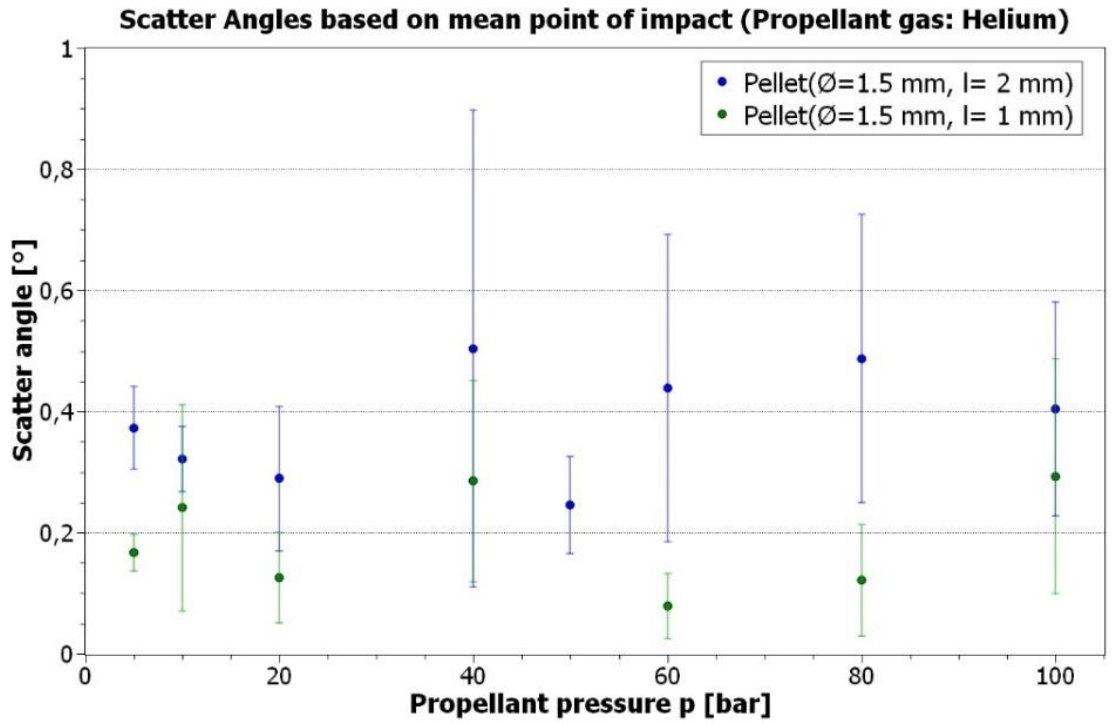

Figure 8.7: Scatter angle based on mean point of impact (Helium)

8.4 Propellant gas throughput results

Figure 8.8 and 8.9 show the propellant gas throughput of argon and helium at different pressures. As expected, the amount of gas A propelled into the vessel increases with the gas pressure. Pellet size seems to have no impact on gas throughput. The average amount of gas $\bar{A}$ reaching the test vessel was between 2.5 mbar · l at 5 bar propellant pressure and 16.7 mbar · l at 100 bar propellant pressure for argon. For helium, the amount of gas ranged between 10 mbar · l and 85 mbar · l for 5 to 100 bar respectively. As stated earlier, the 4-way flange added to the vessel slightly enlarges the volume, so the values are also slightly higher. Because of its characteristics the amount of helium throughput is around one order of magnitude higher in comparison to argon.

According to the ideal gas law this would correspond to about $6.16 \cdot 10^{19}$ argon atoms (5 bar) - $4.11 \cdot 10^{20}$ argon atoms (100 bar) and $2.46 \cdot 10^{20}$ helium atoms (5 bar) – $2.09 \cdot 10^{21}$ helium atoms (100 bar).

This throughput is most likely too high, to use the injector directly on the COMPASS tokamak. The addition of an expansion vessel between the RTSP and the torus helps to reduce the amount of gas. A conceptual design and the acquisition of the vessels and additional vacuum components to implement multiple expansion volumes have already taken place. To investigate the exact gas throughput behavior of the RTSP with the addition of expansion vessels and vacuum pumps, further tests should be performed on site.

Tables of the test results for the propellant gas throughput tests can be found in the appendix A.3.

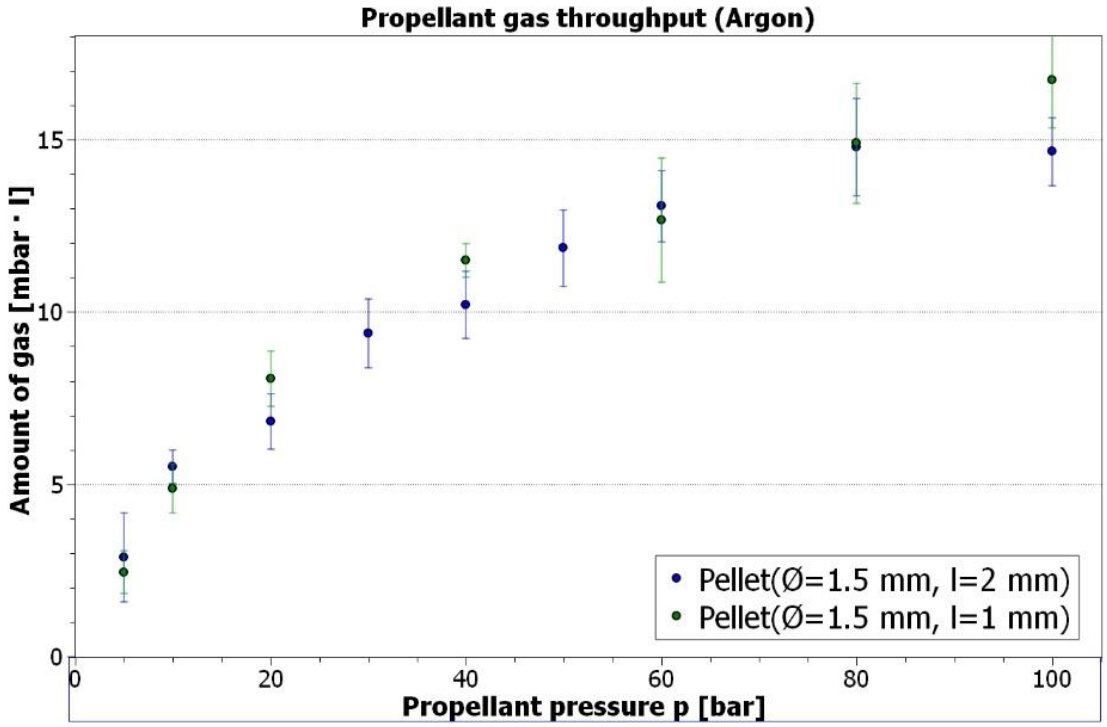

Figure 8.8: Propellant gas throughput (Argon)

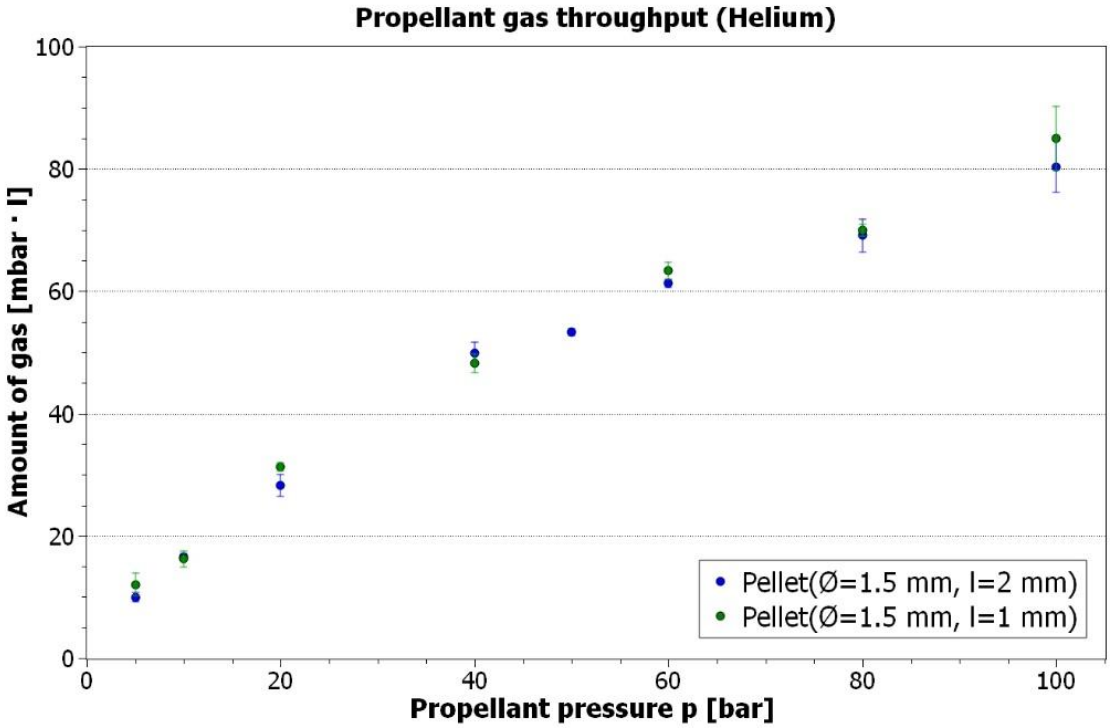

Figure 8.9: Propellant gas throughput (Helium)

8.5 Test tile shooting results

The high damage potential of pellets had already been observed previously, when one of the glass flanges was permanently damaged during the preceding tests (Pictures of the damaged flange can be seen in the appendix C.2).

The damage tests on graphite tiles were started using 2 mm pellets for both tiles. The impact areas for different speeds on the limiter tile can be seen in Fig. 8.10. The red square indicates the place, where the microscopic image 8.11 was taken. Permanent damage on the limiter tile started at speeds of around $340\frac{m}{s}$, though the damage was superficial and could only be seen under the microscope. Clearly visible, deep impact damage began at speeds of around $410\frac{m}{s}$.

Figure 8.12 shows the damage on the inner heat shield tile and 8.13 the magnified image section under the microscope. Visible damage also began with velocities of around $340\frac{m}{s}$, though on a location, where the tile had previously been damaged. Serious visible damage began at speeds of $410\frac{m}{s}$ again. To test an extreme case scenario, a pellet with a velocity of around $480\frac{m}{s}$ was fired. The impact hole is also featured in Fig. 8.13.

The 2 mm long pellets ($m_P \approx 6.8\,mg$) that left permanent damage on the tiles had kinetic energies in ranges between $E_{kin} = 0.39$ J ($340\frac{m}{s}$) and $E_{kin} = 0.78$ J ($480\frac{m}{s}$).

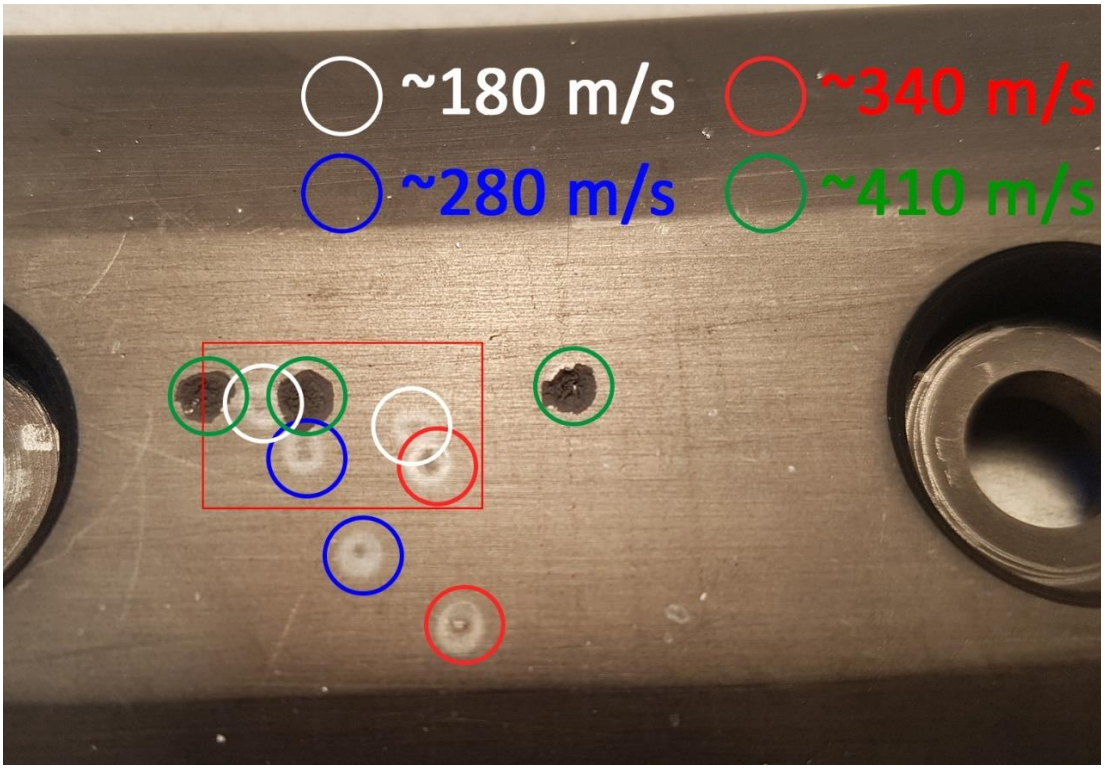

Figure 8.10: Limiter tile - damage at different pressures

Figure 8.11: Microscopic image of the limiter tile

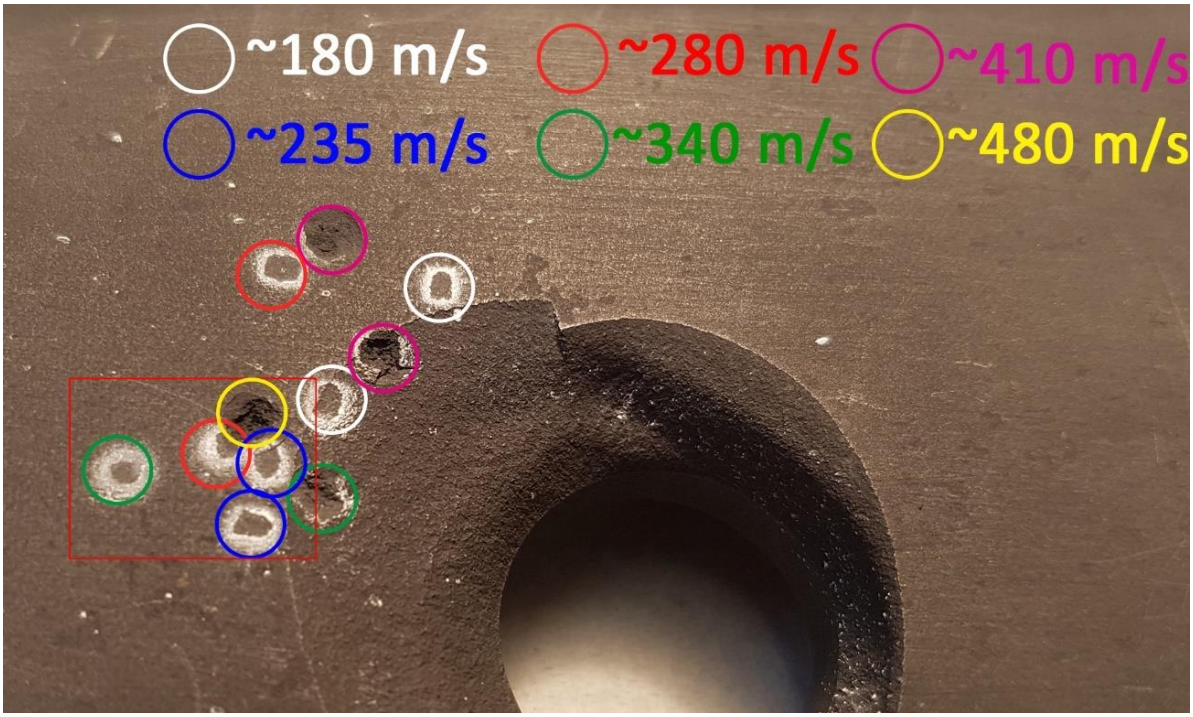

Figure 8.12: Inner heat shield tile - damage at different pressures

Figure 8.13: Microscopic image of the inner heat shield tile

Additional pictures of both tiles after the 2 mm test can be seen in the appendix C.1, Figure 11.1, Picture 3, 4, 5 and 6. The tiles in unscathed condition before the tests are shown in the same Figure on picture 1 and 2.

Tests with 1 mm pellets ($m_P \approx 3.4\,mg$) were performed on both tiles afterwards, with speeds of around $200\frac{m}{s}$, $285\frac{m}{s}$ and $390\frac{m}{s}$. Figure 8.14 shows the impact holes of 1 mm pellets with the inner heat shield tile on the left and the limiter tile on the right. Permanent damage on both tiles began with $285\frac{m}{s}$ ($E_{kin} = 0.14$ J) and increased with $390\frac{m}{s}$ ($E_{kin} = 0.26$ J) . This revealed that although they have less kinetic energy, permanent damage with 1 mm pellets begins at lower speeds and more severe.

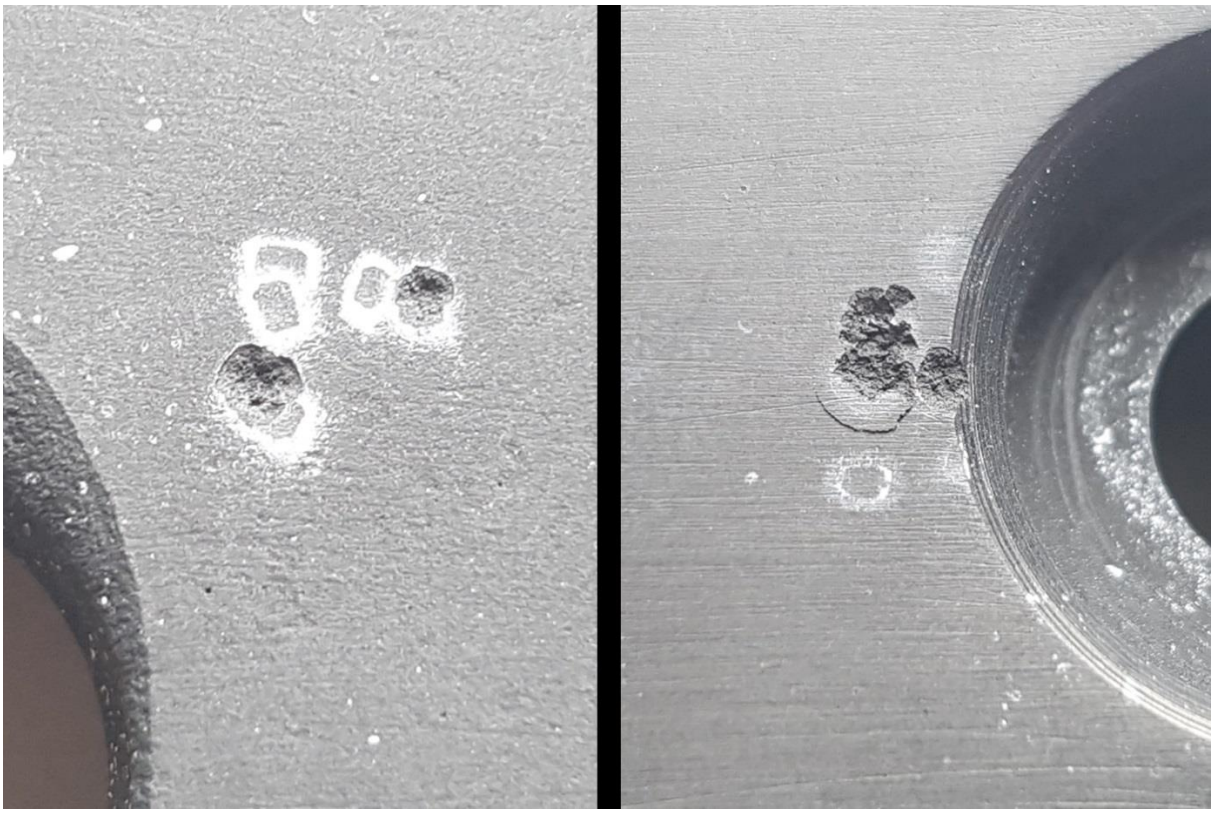

Figure 8.14: Both tiles with 1 mm pellet damage

As the damage of a moving projectile on an object is defined by the energy it transfers to it, the reason for smaller pellets having more damage potential must be due to a smaller impact area. Deeper investigation on the impact behavior of pellets hitting the tiles and paper target, revealed that around 72 % of the times the pellets hit their target lateral. This was done by analyzing 100 clearly distinguishable impact points and counting the amount of frontal and lateral impacts. A photograph demonstrating this can be seen in Figure 8.15.

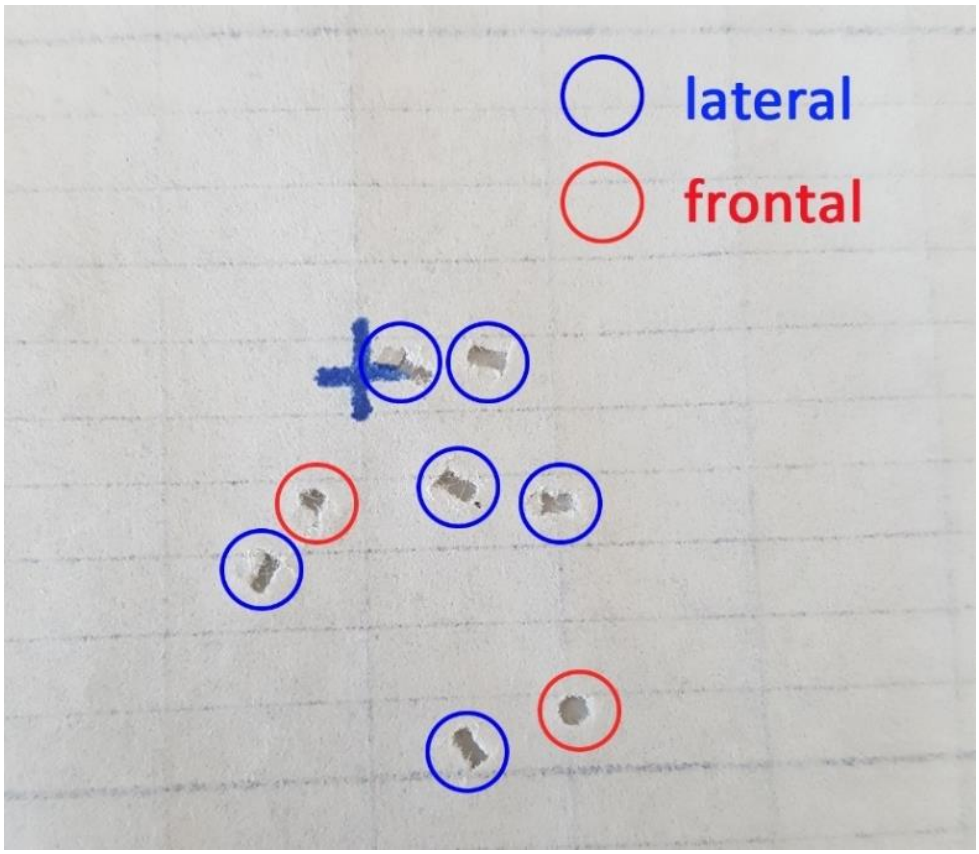

Figure 8.15: Different orientations during impact

Without a spin around the longitudinal axis to stabilize the trajectory, pellets are able to rotate lateral around their center of mass. The associated consequence of almost ¾ of pellets hitting their target sideways, explains the higher damage potential of 1 mm pellets, as the lateral area is smaller for them.

Lastly the amount of eroded material was estimated. The threat imposed by damaged tiles is less about the tiles integrity, but more about the freed particles of wall material, as material removal could impair plasma performance during a discharge. By analyzing the approx. sizes of the clearly visible impact holes under the microscope, the particle numbers were estimated. Figure 8.16 shows the measurement of a hole on the inner heat shield tile (2 mm pellet, $340\,\frac{m}{s}$).

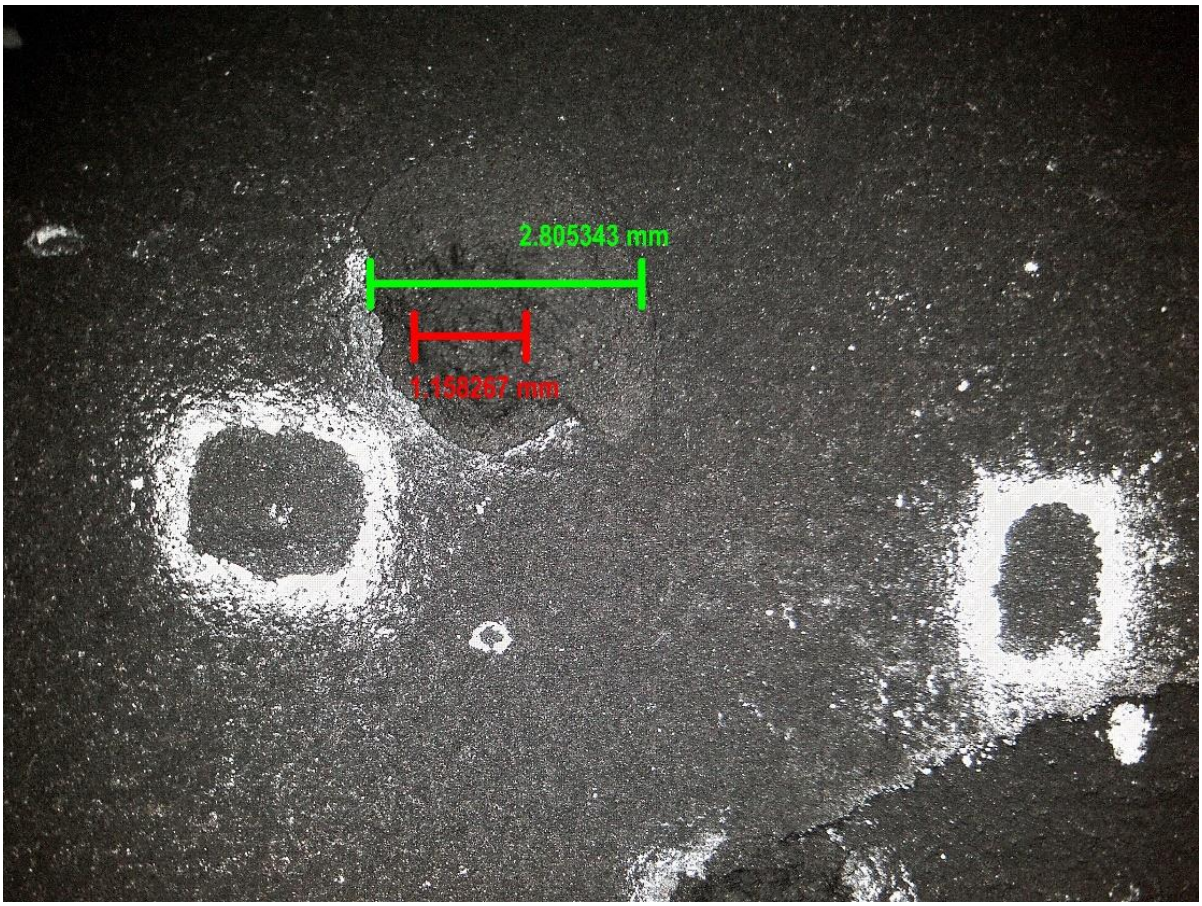

Figure 8.16: Measuring the impact hole size with the microscope tool

With the integrated measurement tool of the microscope, diameters of impact holes were approximated to sizes between $d = 1.14\,mm$ and $d = 2.81\,mm$. With a digital sliding caliper the depth of the impacts were estimated. They ranged from $h = 0.92$ mm to $h = 1.24\,mm$. As an approximation, the shapes of the craters were assumed to be rotational paraboloids. With equation 8.4 the volume of freed material is roughly determined.

$$V = \frac{\pi}{2} \cdot \left(\frac{d}{2}\right)^2 \cdot h \tag{8.4}$$

Volumes range from $V = 0.47\,mm^3$ to $V = 3.84\,mm^3$. With known density of the tiles ($\rho = 1.84\,\frac{g}{cm^3}$), this would account for masses of around 0.86 mg for the smallest and 7.07 mg for the largest hole measured. The freed carbon atoms consequently range between $4.32 \cdot 10^{19}$ and $3.55 \cdot 10^{20}$. A release of impurity particles in this quantity should be avoided as far as possible.

9 Conclusion

To prepare the room-temperature solid-state pellet injector for its upcoming application on the COMPASS tokamak, its properties were characterized in a testbed. In order to create a suitable testing environment, adjustments were made to the test bed and the injector. Using argon and helium as propellants, cylindrical boron nitride pellets were accelerated and tested for their flight behavior. Beside shooting with 2 mm long pellets ($Ø = 1.5\,mm, m_P = 6.8\,mg$), the additional option to produce and shoot smaller pellets with a length of 1 mm ($Ø = 1.5\,mm, m_P = 3.4\,mg$), was proven to be possible.

The results of the tests showed that the injector is capable of reliably shooting both pellet sizes in its full operating range with pressures between 5 and 100 bar, while having an overall transfer efficiency above 91%. Depending on pellet size, as well as propellant kind and pressure, achievable velocities for pellets range from $120\frac{m}{s}$ to $720\frac{m}{s}$. Helium has proven to accelerate pellets to speeds about twice as fast as argon. Propellant gas throughput measurements showed that an amount of 85 mbar · l of propellant gas is too much, and additional expansion vessels are needed for the upcoming installation on COMPASS. Beside a recoverable inaccurate shooting behavior of 0.67° towards the upper left side, the precision of the injector was found to be sufficient, with an average half cone scattering angle of (0.40±0.19)° for 2 mm pellets and (0.23±0.12)° for 1 mm pellets. Propellant kind and pressure seem to have no effects on the precision. To investigate possible damage to wall components, shooting tests on original COMPASS tiles were carried out. Serious damage to the tiles started at pellet velocities of around $410\frac{m}{s}$ with 2 mm pellets and $285\frac{m}{s}$ with 1 mm pellets. Because of a smaller impact area, 1 mm sized pellets pose a bigger threat of eroding wall material, than their 2 mm counterparts.

The fact that 1 mm long pellets reach higher velocities at lower propellant pressures, combined with a higher precision and lower quantity of boron nitride introduced into the torus at once, makes 1 mm sized pellets the more promising choice for studies on COMPASS. However, the high damage potential of especially 1 mm long pellets, must be taken into account.

10 Outlook

The room-temperature solid-state pellet injector was delivered to the Institute of Plasma Physics of the Czech Academy of Sciences in early March. Before the injector is installed on the COMPASS tokamak, additional tests must be performed on site, for instance, testing the behavior with the designed expansion vessels to reduce the gas throughput. As seen on Fig. 10.1, the planned experimental setup on COMPASS foresees an installation of the injector on the port of the neutral beam injection 1, which allows a possible radial or tangential configuration of the injector. Currently it is assumed, that the tangential setup is more likely to be chosen. Potential plasma scenarios include either the generation of runaway electrons by massive gas injections and investigating possible mitigation strategies using pellets, or generating runaways by injecting pellets, thereby cooling the plasma and attempting to mitigate the runaways afterwards by massive gas injections.

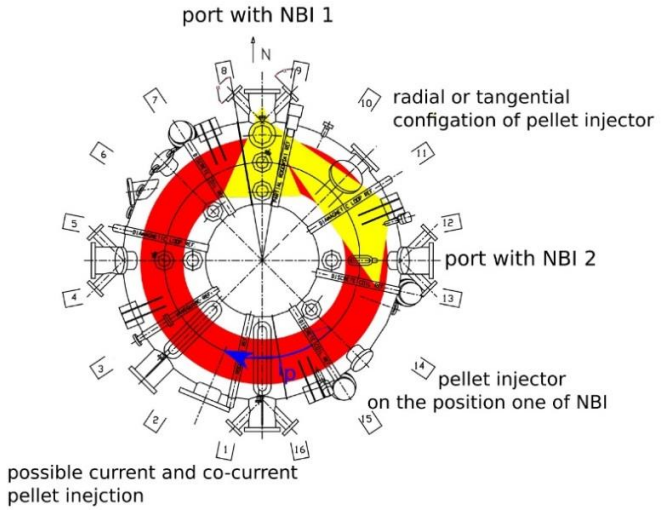

Figure 10.1: Planned experimental setup [55]

For testing further pellet materials in the future, the construction of an on-site test bed is considered. Potential future pellet materials include carbon or powders of metals like tungsten or iron in a substrate. First results of the runaway electron studies are planned for late 2019.

11 Appendix

Appendix A - Tables of test results

A.1 Speed results

A.2 Scatter results

A.3 Gas throughput results

Appendix B - Systematic uncertainties

B.1 Speed uncertainty

B.2 Scatter uncertainty

Appendix C - Additional pictures

C.1 Tile damage test

C.2 Glass flange damage and safety measures

C.3 Scatter angle test

C.4 Laser mount

Appendix D – Data sheets

D.1 Vacuum pumps and controller

D.2 Pressure gauge

D.3 Propellant safety data sheets

D.4 Boron nitride purity and impurities

Appendix E – Drafts

E.1 Pneumatic schematic

E.2 Light barrier electronics

E.3 Light barrier: Pin assignment – Amphenol plug

E.4 Simatic control system

E.5 Injector drafts

Appendix A - Tables of test results

- A.1 Speed results
- A.2 Scatter results
- A.3 Gas throughput results

A.1 Speed results

Propellant gas: **Argon** ; Pellet size: **Ø= 1.5 mm, l= 2 mm**		
Pressure [bar]	**Mean velocity [m/s]**	**Standard deviation [m/s]**
5	135,46	9,43
10	180,03	9,26
20	212,08	6,02
30	236,03	23,47
40	243,47	9,37
50	261,04	9,98
60	270,54	6,23
80	293,29	11,56
100	305,68	6,75

Table 11.1: Test results: Velocity - Argon - 2 mm

Propellant gas: **Argon** ; Pellet size: **Ø= 1.5 mm, l= 1 mm**		
Pressure [bar]	**Mean velocity [m/s]**	**Standard deviation [m/s]**
5	190,08	3,35
10	221,42	8,51
20	267,79	10,67
40	307,96	4,32
60	343,14	1,68
80	360,43	21,23
100	379,88	11,32

Table 11.2: Test results: Velocity - Argon - 1 mm

Propellant gas: Helium ; Pellet size: **Ø= 1.5 mm, l= 2 mm**		
Pressure [bar]	**Mean velocity [m/s]**	**Standard deviation [m/s]**
5	120,02	2,05
10	176,09	11,70
20	250,29	18,51
40	392,77	32,33
50	474,78	22,63
60	535,11	36,84
80	605,65	69,93
100	720,97	46,62

Table 11.3: Test results: Velocity - Helium - 2 mm

Propellant gas: **Helium** ; Pellet size: **Ø= 1.5 mm, l= 1 mm**		
Pressure [bar]	**Mean velocity [m/s]**	**Standard deviation [m/s]**
5	238,08	9,37
10	300,92	5,43
20	374,68	24,21
40	479,69	13,15
60	557,44	18,74
80	640,40	12,29
100	684,65	50,63

Table 11.4: Test results: Velocity - Helium - 1 mm

A.2 Scatter results

Based on mean point of impact:

Propellant gas: **Argon** ; Pellet size: **Ø= 1.5 mm, l= 2 mm**				
Pressure [bar]	**Mean scatter distance [mm]**	**Standard deviation distance [mm]**	**Mean Scatter angle [°]**	**Standard deviation angle [°]**
5	7,50	3,11	0,44	0,18
10	6,24	3,80	0,37	0,22
20	5,81	3,30	0,34	0,20
30	7,24	5,54	0,43	0,33
40	8,86	2,28	0,52	0,13
50	7,17	3,13	0,42	0,18
60	7,20	3,66	0,43	0,22
80	7,10	3,46	0,42	0,20
100	6,51	2,16	0,38	0,13

Table 11.5: Test results: Scatter- mean point impact - Argon - 2 mm

Propellant gas: **Argon** ; Pellet size: **Ø= 1.5 mm, l= 1 mm**				
Pressure [bar]	**Mean scatter distance [mm]**	**Standard deviation distance [mm]**	**Mean Scatter angle [°]**	**Standard deviation angle [°]**
5	1,21	0,62	0,07	0,04
10	3,38	1,49	0,20	0,09
20	3,58	1,93	0,21	0,11
40	4,31	2,49	0,25	0,15
60	4,31	2,11	0,25	0,12
80	5,15	2,38	0,30	0,14
100	8,56	3,29	0,51	0,19

Table 11.6: Test results: Scatter- mean point impact - Argon - 1 mm

Propellant gas: **Helium** ; Pellet size: **Ø= 1.5 mm, l= 2 mm**				
Pressure [bar]	**Mean scatter distance [mm]**	**Standard deviation distance [mm]**	**Mean Scatter angle [°]**	**Standard deviation angle [°]**
5	6,32	1,15	0,37	0,07
10	5,44	0,92	0,32	0,05
20	4,90	2,01	0,29	0,12
40	8,54	6,66	0,50	0,39
50	4,17	1,36	0,25	0,08
60	7,44	4,30	0,44	0,25
80	8,25	4,03	0,49	0,24
100	6,84	2,99	0,40	0,18

Table 11.7: Test results: Scatter- mean point of impact - Helium - 2 mm

Propellant gas: **Helium** ; Pellet size: **Ø= 1.5 mm, l= 1 mm**				
Pressure [bar]	**Mean scatter distance [mm]**	**Standard deviation distance [mm]**	**Mean Scatter angle [°]**	**Standard deviation angle [°]**
5	2,83	0,51	0,17	0,03
10	4,08	2,88	0,24	0,17
20	2,13	1,26	0,13	0,07
40	4,83	2,81	0,29	0,17
60	1,33	0,91	0,08	0,05
80	2,06	1,56	0,12	0,09
100	4,96	3,27	0,29	0,19

Table 11.8: Test results: Scatter- mean point impact - Helium - 1 mm

Based on bullseye:

Propellant gas: **Argon** ; Pellet size: **Ø= 1.5 mm, l= 2 mm**				
Pressure [bar]	**Mean scatter distance [mm]**	**Standard deviation distance [mm]**	**Mean Scatter angle [°]**	**Standard deviation angle [°]**
5	10,26	6,15	0,61	0,36
10	12,43	6,29	0,73	0,37
20	8,37	3,69	0,49	0,22
30	15,00	6,30	0,89	0,37
40	10,61	6,56	0,63	0,39
50	13,15	6,08	0,78	0,36
60	10,19	4,40	0,60	0,26
80	13,04	5,27	0,77	0,31
100	13,47	5,29	0,80	0,31

Table 11.9: Test results: Scatter- bullseye - Argon - 2 mm

Propellant gas: **Argon** ; Pellet size: **Ø= 1.5 mm, l= 1 mm**				
Pressure [bar]	**Mean scatter distance [mm]**	**Standard deviation distance [mm]**	**Mean Scatter angle [°]**	**Standard deviation angle [°]**
5	11,09	0,36	0,65	0,02
10	12,89	2,05	0,76	0,12
20	9,77	0,68	0,58	0,04
40	13,15	1,51	0,78	0,09
60	12,04	1,58	0,71	0,09
80	12,42	4,82	0,73	0,28
100	16,86	2,75	1,00	0,16

Table 11.10: Test results: Scatter- bullseye - Argon - 1 mm

Propellant gas: **Helium** ; Pellet size: **Ø= 1.5 mm, l= 2 mm**				
Pressure [bar]	**Mean scatter distance [mm]**	**Standard deviation distance [mm]**	**Mean Scatter angle [°]**	**Standard deviation angle [°]**
5	10,47	1,62	0,62	0,10
10	6,29	1,05	0,37	0,06
20	13,65	0,64	0,81	0,04
40	7,10	2,52	0,42	0,15
50	12,45	4,23	0,74	0,25
60	9,74	5,61	0,58	0,33
80	12,90	5,52	0,76	0,33
100	9,35	3,77	0,55	0,22

Table 11.11: Test results: Scatter- bullseye - Helium - 2 mm

Propellant gas: **Helium** ; Pellet size: **Ø= 1.5 mm, l= 1 mm**				
Pressure [bar]	**Mean scatter distance [mm]**	**Standard deviation distance [mm]**	**Mean Scatter angle [°]**	**Standard deviation angle [°]**
5	8,68	0,70	0,51	0,04
10	8,44	1,11	0,50	0,07
20	9,51	1,14	0,56	0,07
40	8,92	3,11	0,53	0,18
60	11,04	1,81	0,65	0,11
80	11,78	1,23	0,70	0,07
100	9,85	5,38	0,58	0,32

Table 11.12: Test results: Scatter- bullseye - Helium - 1 mm

A.3 Gas throughput results

Propellant gas: Argon ; Pellet size: Ø= 1.5 mm, l= 2 mm				
Pressure [bar]	Mean delta pressure [mbar]	St. dev. delta pressure [mbar]	Amount of gas [mbar · l]	St. Dev. Amount of gas [mbar · l]
5	1,79E-02	8,05E-03	2,87	1,29
10	3,44E-02	3,08E-03	5,51	0,49
20	4,26E-02	4,97E-03	6,82	0,79
30	5,86E-02	6,22E-03	9,37	1,00
40	6,39E-02	6,09E-03	10,22	0,97
50	7,41E-02	6,93E-03	11,86	1,11
60	8,17E-02	6,51E-03	13,07	1,04
80	9,24E-02	8,80E-03	14,79	1,41
100	9,16E-02	6,12E-03	14,65	0,98

Table 11.13: Test results: Gas throughput - Argon - 2 mm

Propellant gas: Argon ; Pellet size: Ø= 1.5 mm, l= 1 mm				
Pressure [bar]	Mean delta pressure [mbar]	St. dev. delta pressure [mbar]	Amount of gas [mbar · l]	St. Dev. Amount of gas [mbar · l]
5	1,53E-02	3,90E-03	2,45	0,62
10	3,05E-02	4,42E-03	4,87	0,71
20	5,04E-02	5,06E-03	8,06	0,81
40	7,18E-02	2,98E-03	11,49	0,48
60	7,91E-02	1,13E-02	12,66	1,80
80	9,31E-02	1,09E-02	14,90	1,74
100	1,05E-01	8,74E-03	16,74	1,40

Table 11.14: Test results: Gas throughput - Argon - 1 mm

Propellant gas: Helium ; Pellet size: Ø= 1.5 mm, l= 2 mm				
Pressure [bar]	Mean delta pressure [mbar]	St. dev. delta pressure [mbar]	Amount of gas [mbar · l]	St. Dev. Amount of gas [mbar · l]
5	6,21E-02	4,76E-03	9,93	0,76
10	1,04E-01	3,51E-03	16,58	0,56
20	1,77E-01	1,12E-02	28,26	1,78
40	3,11E-01	1,16E-02	49,81	1,86
50	3,33E-01	3,51E-03	53,33	0,56
60	3,83E-01	4,08E-03	61,24	0,65
80	4,32E-01	1,70E-02	69,10	2,73
100	5,02E-01	2,61E-02	80,35	4,17

Table 11.15: Test results: Gas throughput - Helium - 2 mm

Propellant gas: Helium ; Pellet size: Ø= 1.5 mm, l= 1 mm				
Pressure [bar]	**Mean delta pressure [mbar]**	**St. dev. delta pressure [mbar]**	**Amount of gas [mbar · l]**	**St. Dev. Amount of gas [mbar · l]**
5	7,51E-02	1,17E-02	12,02	1,87
10	1,01E-01	8,02E-03	16,19	1,28
20	1,96E-01	4,37E-03	31,28	0,70
40	3,01E-01	9,30E-03	48,20	1,49
60	3,96E-01	8,63E-03	63,40	1,38
80	4,38E-01	6,08E-03	70,02	0,97
100	5,31E-01	3,28E-02	84,94	5,24

Table 11.16: Test results: Gas throughput - Helium - 1 mm

Appendix B - Systematic uncertainties

- B.1 Speed uncertainty
- B.2 Scatter uncertainty

B.1 Speed uncertainty

The pellet velocities were calculated by evaluating the time it takes a pellet to cover a known distance (see equation 6.11). Therefore, the time difference of pellets crossing two light barrier arrays was analyzed. The two arrays are separated $s = 0.070\ m$. This was measured with a standard ruler. The minimum division of 1 mm is taken as measurement inaccuracy. The time delay of the electrical signals in the light barrier and electrical wiring box can be neglected. As maximum time inaccuracy the sampling interval of the oscilloscope is taken. The oscilloscope works in the acquisition mode used with 500 kS/s. The consequential sampling interval is $\Delta t = 2 \cdot 10^{-6}\ m$. As the horizontal scale was zoomed all the way in for working with the cursors, this corresponds to the inaccuracy of the time measurement. The error propagation for determining pellet velocities is shown in equation B.1, the consequential errors for relevant speeds can be seen in Table 11.17.

$$\Delta v = \left|\frac{\partial v}{\partial s}\right| \cdot \Delta s + \left|\frac{\partial v}{\partial t}\right| \cdot \Delta t = \left|\frac{1}{t}\right| \cdot \Delta s + \left|-\frac{s}{t^2}\right| \cdot \Delta t \qquad \text{(B.1)}$$

$$s = 0.070\ m$$

$$\Delta s = 1 \cdot 10^{-3}\ m$$

$$\Delta t = 2 \cdot 10^{-6}\ m$$

velocity [m/s]	time [s]	velocity error [m/s]
200,00	3,50E-04	**4,00**
250,00	2,80E-04	**5,36**
300,00	2,33E-04	**6,86**
350,00	2,00E-04	**8,50**
400,00	1,75E-04	**10,29**
450,00	1,56E-04	**12,21**
500,00	1,40E-04	**14,29**
550,00	1,27E-04	**16,50**
600,00	1,17E-04	**18,86**
650,00	1,08E-04	**21,36**
700,00	1,00E-04	**24,00**
750,00	9,33E-05	**26,79**

Table 11.17: Measurement uncertainty of pellet velocity

B.2 Scatter uncertainty

The angular scatter of pellets was calculated from the distance between impact holes and bullseye on the paper target and the flight distance between the injector and the paper target through equation 6.14. The measurement uncertainty arising thereby is dependent on both these values and their measurement uncertainties. Determining the distance d between the end of the acceleration barrel and the paper target was done with a pocket rule. An uncertainty for this measurement method of 5% was chosen. Analyzing the distance between the impact position and the bullseye position x on the paper target was done with a standard ruler. As some of the pellets tore holes in the paper bigger than their respective size an uncertainty of 10% is chosen for this measuring method. The error propagation for angular scatter is shown in equation B.2, the consequential errors for relevant angles can be seen in Table 11.18.

$$\Delta\alpha = \left|\frac{\partial\alpha}{\partial x}\right| \cdot \Delta x + \left|\frac{\partial\alpha}{\partial d}\right| \cdot \Delta d = \left|\frac{d}{d^2 + x^2}\right| \cdot \Delta x + \left|-\frac{x}{d^2 + x^2}\right| \cdot \Delta d \qquad \text{(B.2)}$$

$$d = 0.97\ m$$

$$\Delta d = 4.85 \cdot 10^{-2}\ m$$

Angle [°]	distance x [m]	Angle error [°]
0,05	8,46E-04	**1,31E-04**
0,10	1,69E-03	**2,62E-04**
0,15	2,54E-03	**3,93E-04**
0,20	3,39E-03	**5,24E-04**
0,25	4,23E-03	**6,54E-04**
0,30	5,08E-03	**7,85E-04**
0,35	5,93E-03	**9,16E-04**
0,40	6,77E-03	**1,05E-03**
0,45	7,62E-03	**1,18E-03**
0,50	8,47E-03	**1,31E-03**
0,55	9,31E-03	**1,44E-03**
0,60	1,02E-02	**1,57E-03**
0,65	1,10E-02	**1,70E-03**
0,70	1,19E-02	**1,83E-03**
0,75	1,27E-02	**1,96E-03**
0,80	1,35E-02	**2,09E-03**
0,85	1,44E-02	**2,22E-03**
0,90	1,52E-02	**2,36E-03**
0,95	1,61E-02	**2,49E-03**
1,00	1,69E-02	**2,62E-03**

Table 11.18: Measurement uncertainty of pellet scatter

Appendix C - Additional pictures

- C.1 Tile damage test
- C.2 Glass flange damage and safety measures
- C.3 Scatter angle test
- C.4 Laser mount

C.1 Tile damage test

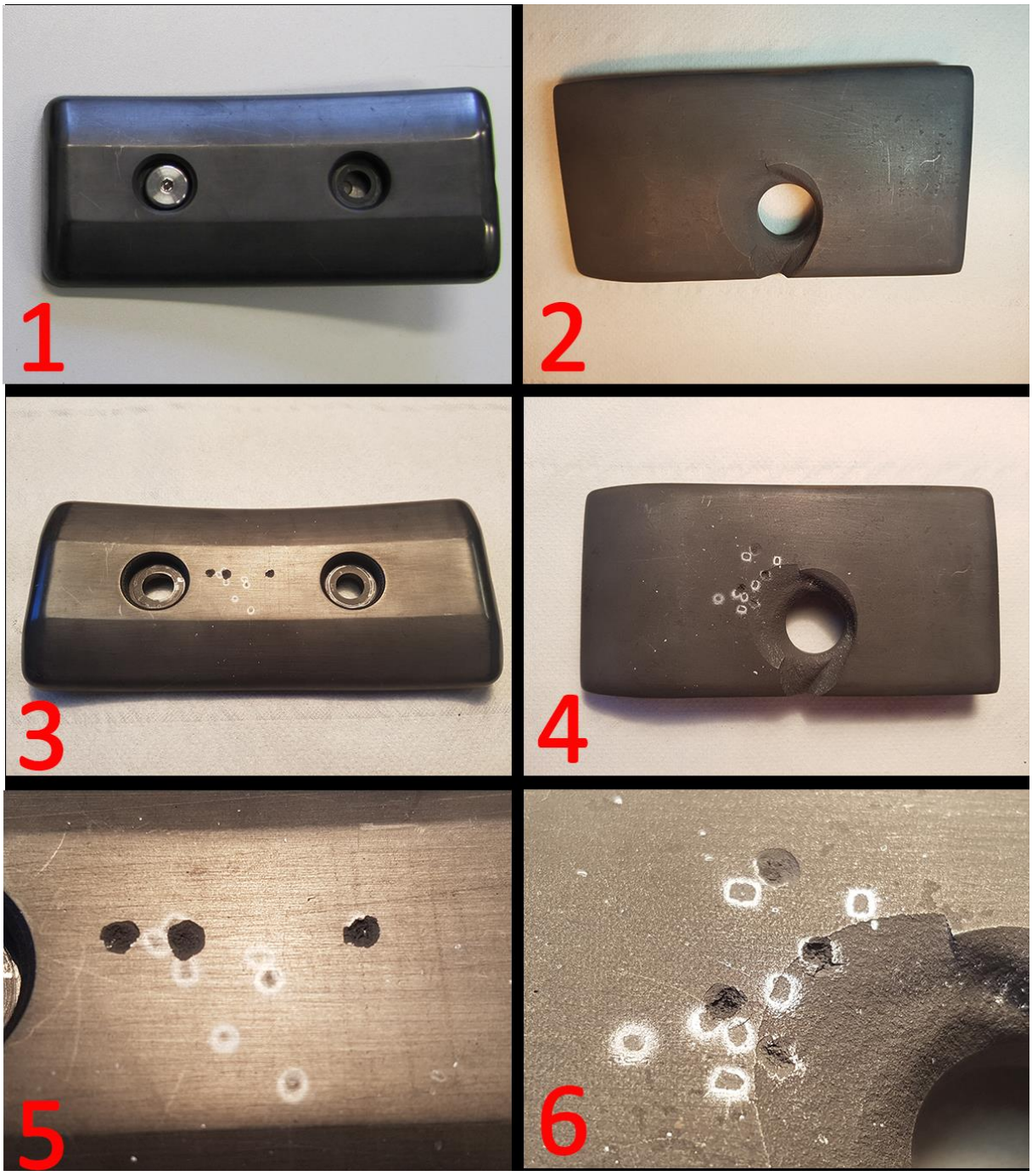

Figure 11.1: Heat shield and limiter tile before and after impact test

C.2 Glass flange damage and safety measures

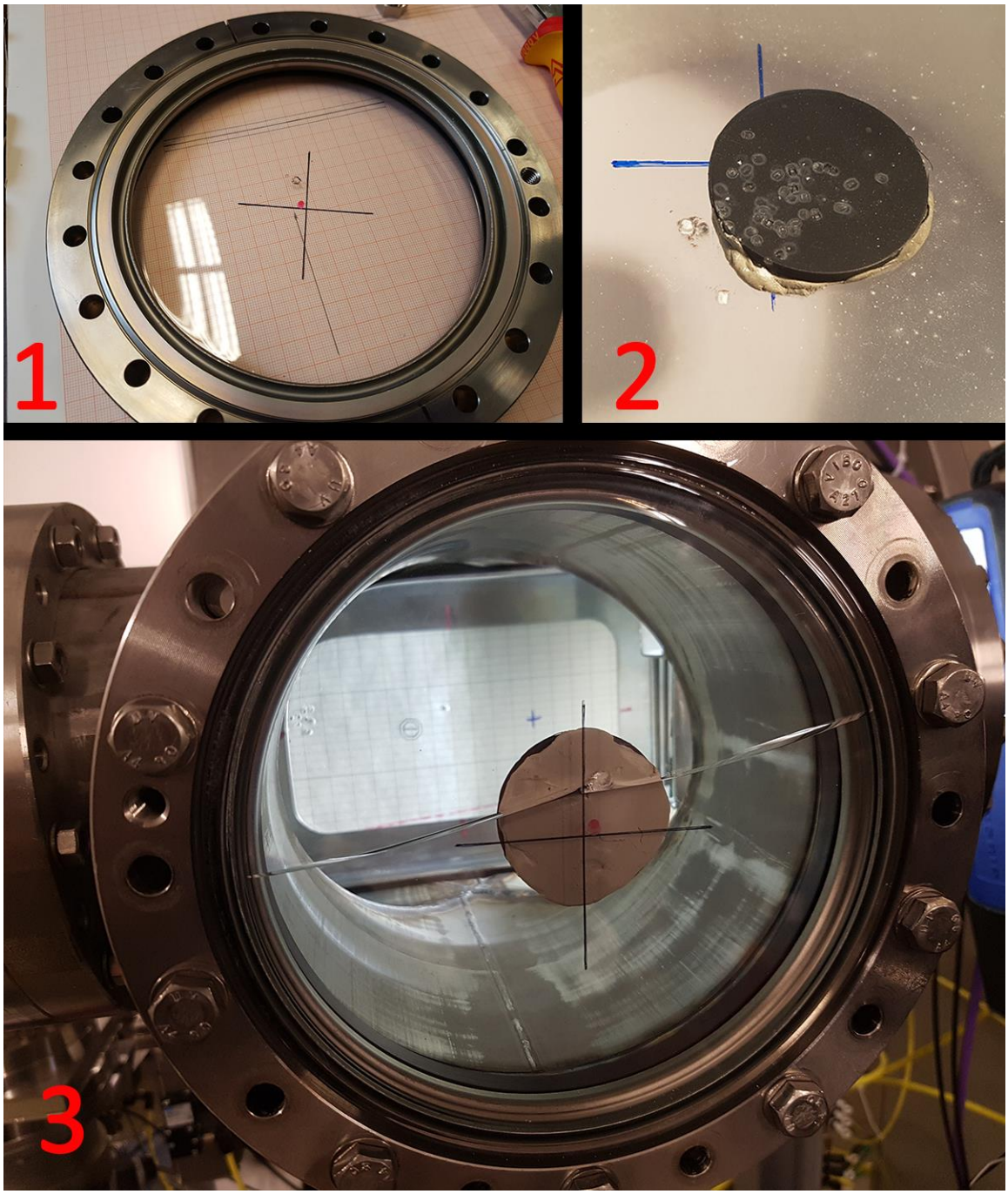

Figure 11.2: Damaged glass flange, safety measurements and broken glass flange

C.3 Scatter angle test

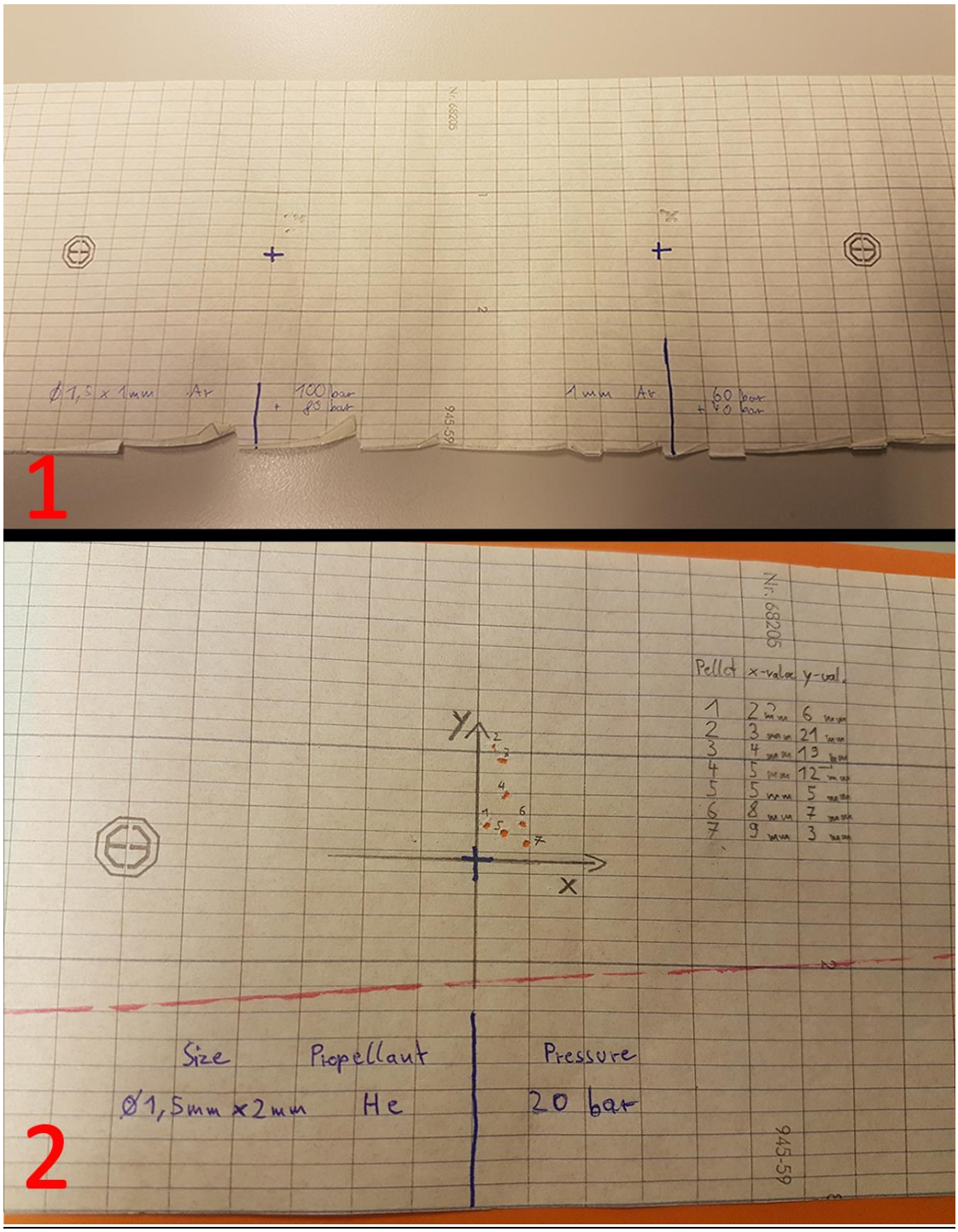

Figure 11.3: Process of angular scatter analysis

C.4 Laser mount

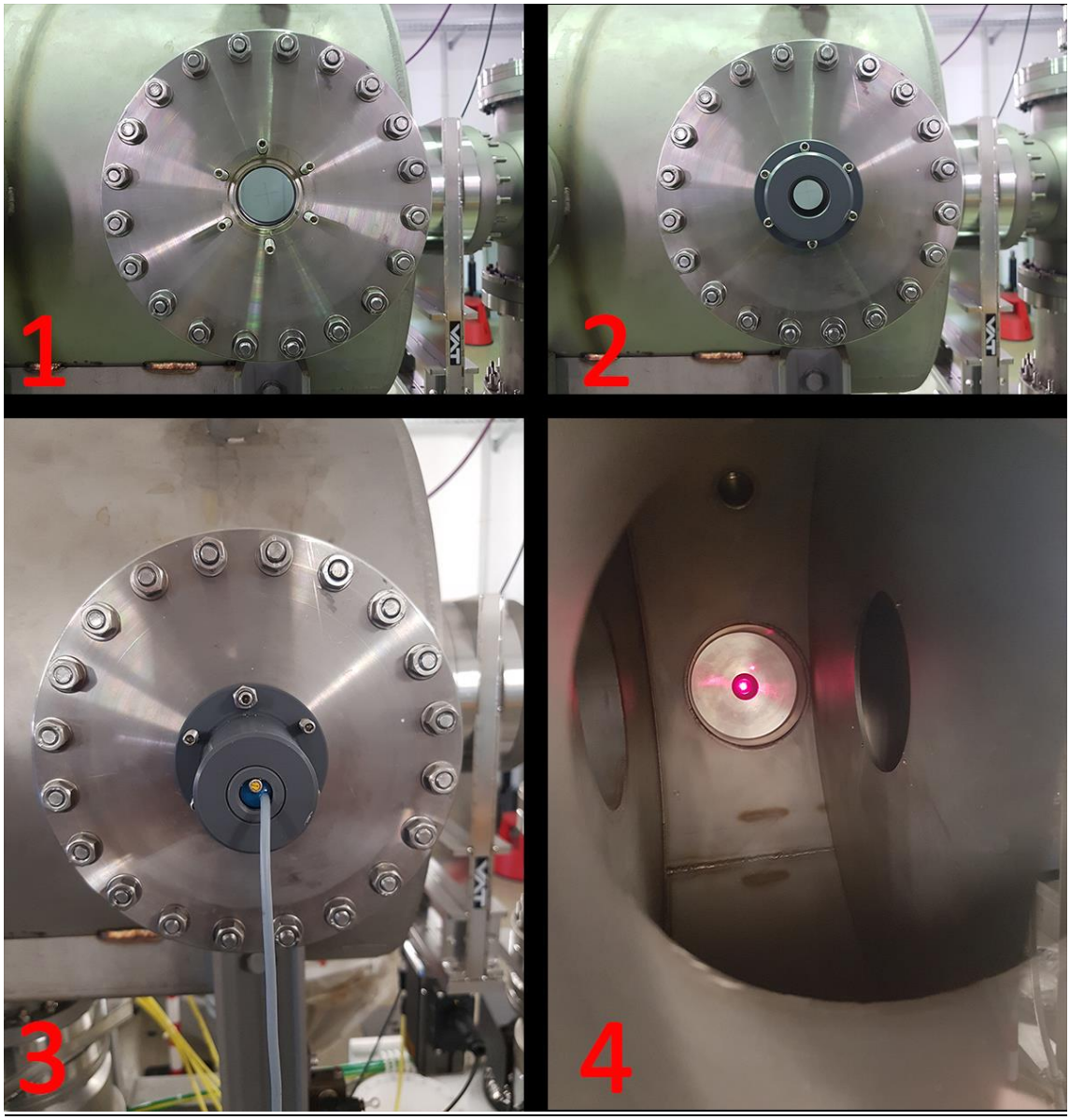

Figure 11.4: Laser mount for test vessel measurement

Appendix D – Data sheets

- D.1 Vacuum pumps and controller
- D.2 Pressure gauges
- D.3 Propellant safety data sheets
- D.4 Boron nitride purity and impurities

D.1 Vacuum pumps and controller

Rotary piston pump DK 200 data sheet [56]:

Description

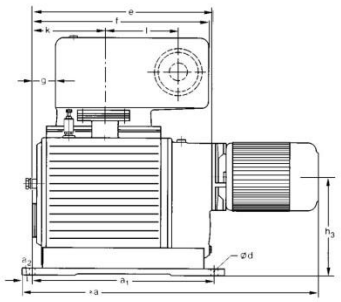

	DN	DN_1	a[1]	a_1	a_2	b	b_1	b_2	b_3	ød
E 250/DK 200	63 ISO-K	63 ISO-K	1190	780	30	340	140	202[2]	52	14

	DN	DN_1	e	f	g	h	h_1	h_2	h_3	k	l
E 250/DK 200	63 ISO-K	63 ISO-K	777	750	65	740	475	636	295	337	290

1) Dimension "a" applies only in connection with the standard type of motor used by us
2) Without adaptor

Fig. 4 Dimensional drawing

1.3 Technical Data and Accessories

Rotary Piston Pump		**E 250**			**DK 200**	
Nominal pumping speed [1]	$m^3 \cdot h^{-1}$	290			225	
Pumping speed [1]	$m^3 \cdot h^{-1}$	250			200	
Ultimate total pressure with gas ballast [1]	mbar	$2{,}5 \cdot 10^{-1}$			$2{,}5 \cdot 10^{-3}$	
Ultimate partial pres. without gas ballast [1]	mbar	$2{,}5 \cdot 10^{-2}$			$1{,}5 \cdot 10^{-4}$	
Water vapour tolerance	mbar	60			26	
Intake port Exhaust port	DN DN	63 ISO-K 63 ISO-K			63 ISO-K 63 ISO-K	
Oil filling, pump chamber	l	8			4	
Oil filling, gear	l	0,4			0,4	
Motor power at 230/380 V	kW	5,5			5,5	
Nominal speed of the motor, 50 Hz	rpm	1500 / 50 Hz	1730 / 60 Hz		1500 / 50 Hz	1730 / 60 Hz
Nominal speed of the pump	rpm	540			540	
Motor protection	IP	54			54	
Weight with motor and oil filling	kg	375			375	
Cat. Nos.		**105 36**	**895 08**	**895 09**	**111 16**	**895 10**

Accessories		**E 250**	**DK 200**
		-- Cat. Nos. --	
Vibration absorbing feet		101 54	101 54
Seal kit		192 63	192 63
Dust separator		178 02	178 02
Molecular filter		178 05	178 05
Dust filter		278 17	278 17
Separator (intake side)		188 45	188 45
Elbow DN 63 ISO-K		268 67	268 67
Drain tap (vacuum tight/oil tight)		190 90	190 90
Separator (exhaust side)		188 45	188 45
Exhaust filter		189 45	189 45
Exhaust filter box		189 47	189 47
SECUVAC valve		283 15	283 15
Oil level regulator		101 37	101 37
Mechanical oil filtering facility		101 31	101 31
Chemical oil filter[2]		101 40	101 40

[1] To DIN 20 400 and subsequent numbers
[2] Active earth insert can only be used in conjunction with the mechanical oil filter Cat. No. 101 31.

Turbopump Leybold Turbovac 360 data [57]:

Pump rate $\left[\frac{l}{s}\right]$	345
Minimum vacuum pressure [mbar]	$< 10^{-10}$
Forevacuum pressure [mbar]	$10^{-2} - 10^{-3}$
Rotation speed [rpm]	45000
Startup time [s]	180
High vacuum port	CF100
Weight [kg]	11
Maximum operating temperature [K]	328

Turbopump controller Leybold Turbotronik NT20 data sheet [58]:

Description

1.2 Standard Specifications

TURBOTRONIK NT 20 table-top electronic frequency converter with housing.

Power linecord
with shock-proof plug (Cat. No. 857 20)
or with US mains plug (Cat. No. 857 21/22),

Miniature fuses: 2 T 8.0 A; 2 T 4.0 A; 2 T 3.15 A; 2 T 1.0 A; 2 T 0.2 A

as well as three mains plugs,

two terminal strips,

one portable socket-outlet and

the Operating Instructions.

1.3 Technical Data

Mains voltage, with selector switch	100/120/220/240 V,+10%/-15%
Mains frequency	50/60 Hz
Power consumption including all connected units	<1000 VA
Power consumption of theTURBOVAC	<400 VA
Power output (motor)	
Nominal voltage	42 V
Link circuit current limitation	
Acceleration (max. 10 min.)	5 A
Continuous operation	3.5 A

TURBOVAC speed ratings

TURBOVAC 150 / 151	50 000 min^{-1}
TURBOVAC 360 / 361	45 000 min^{-1}
TURBOVAC 600	36 000 min^{-1}
TURBOVAC 1000	36 000 min^{-1}
TURBOVAC 1100	30 000 min^{-1}

Control Inputs - digital, floating

each terminal	25 V_{eff} AC max., 60 V DC
	versus protective conductor
	LEYBOTRONIK I compatible
High level; between "+" and "-" terminal	13 V...33 V/max. 10 mA
Low level; between "+" and "-" terminal	0 V...7 V
Pulse duration	>200 ms

for remote control active "START" pump, "STOP" pump, heater On/Off

Control Outputs

Relay	max. 250 V AC, 3 A
	50 V DC, 2 A (resistive load)
for normal operation	operating contact
for acceleration	operating contact
for failure	changeover contact
FOREPUMP Relay point	max. 6 A, 750 VA, 250 V

Supply Outlets VALVE; HEATER, FAN

A relay is used to switch through the mains voltage.
The permissible current for all 3 outlets together is
4.5 A at 100 - 120 V AC
6 A at 220 - 240 V AC

Interface for data output	RS 232/V.24
Connector	25-pin, D-shell, female
Baud rate	9,600

Operating temperature; with sufficient free convection for side profiles	0-45°C (32°F - 113°F)
Storage temperature	-25°C...+70°C (-77°F - +158°F)
Humidity class	F, DIN 40 040

Electrical safety to	IEC 1010/VDE 0411
Interference radiation to VDE 0871	Level B
EMC to IEC 801-2	Severity 2

Dimensions	$^1/_2$19", 3HU*
Weight	7 kg

* Height units - modular spacings high

D.2 Pressure gauge

Data sheet of MPT200 pressure gauge [59]:

Similar Image

MPT 200, DN 40 ISO-KF, RS-485, DeviceNet

- $5 \cdot 10^{-9}$ to 1000 hPa
- Customizable to vacuum application
- DeviceNet Interface

Dimensions

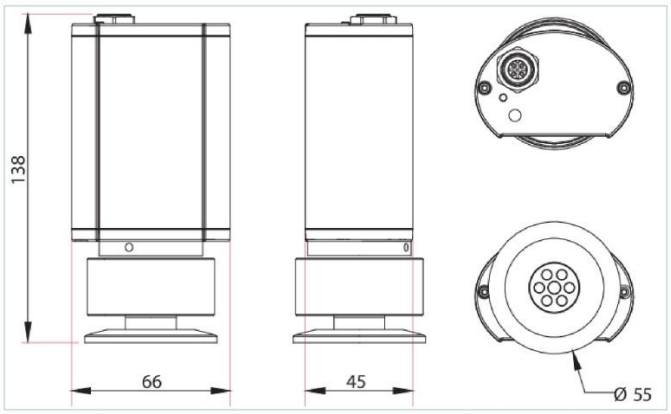

Technical Data	MPT 200, DN 40 ISO-KF, RS-485, DeviceNet
Accuracy: $1 \cdot 10^{-8} – 2 \cdot 10^{-3}$ hPa	25 %
Accuracy: 100 – 1000 hPa	50 %
Accuracy: 10 – 100 hPa	30 %
Accuracy: $2 \cdot 10^{-3}$ – 10 hPa	10 %
Ambient temperature	5-60 °C | 41-140 °F | 278-333 K
Anode	Molybdenum
Bakeout temperature at the flange	180 °C | 356 °F | 453 K
Cold cathode sensor control	Cold Cathode sensor can be switched on and of f via interface
I/O interfaces	RS-485, DeviceNet
Materials in contact with media	Tungsten, stainless steel, nickel, molybdenum, glass
Measurement range	$5 \cdot 10^{-9} – 1 \cdot 10^{3}$ hPa
Measuring cycle	10 ms
Method of measurement	Pirani/Cold Cathode
Nominal diameter	DN 40 ISO-KF
Protection category	IP54
Repeatability: $1 \cdot 10^{-2}$ – 10 hPa	2 %
Repeatability: $1 \cdot 10^{-8} – 1 \cdot 10^{-2}$ hPa	7 %
Seal	Metal
Sensor cable length	100 m
Supply: power consumption	4.5 W
Temperature: Storage	-40-65 °C | -40-149 °F | 233-338 K
Weight	580 g

Order number	
MPT 200 DN	**PT R40 153**

Accessories	
Adapters (electrical)|Adapter Cables	
Connection cable, RS-485, M12/D-sub 9-pole, 3 m	**PT 348 223 -T**
Adapters (electrical)|Adapter Measurement	
Adapter RS-485, M12, 4-pole - D-sub bushing, 9-pole, 0.2 m	**PT 348 133 -T**
Adapters (electrical)|RS-232/485	
Coupling M12 for RS-485	**PM 061 270 -X**
Termination resistor for RS-485	**PT 348 105 -T**
M12 m Plug 4-Pole with Screw Terminals RS-485	**PT 348 106 -T**
Power separator for RS-485	**PT 348 132 -T**
Cables|Connection cables	
Supply Cable DigiLine, M12, 4-pole to TPS, 3 m	**PT 348 163 -T**
Control Devices|Gauge controllers	
DPG 202, Controller and Display Unit for up to 2 Gauges	**PT G12 020**
Control Devices|Power supplies and control displays	
TPS 110, power supply pack for wall/standard rail fitting	**PM 061 340 -T**
TPS 111, power supply pack 3HU 19" rack module	**PM 061 344 -T**
Protection|Inlet filters	
Centering ring, with poral filter, FPM/stainless steel, DN 40 ISO-KF	**PF 117 240 -T**
Software|Display & Data logging	
DokuStar Plus software, 16 channels	**PT 882 501**
Turbopumps	
Y-Connector M12 to RS-485	**P 4723 010**
USB converter to RS-485 interface	**PM 061 207 -T**
Turbopumps/Measurement	
Interface cable, M12 m straight/M12 m straight, 3 m	**PM 061 283 -T**

D.3 Propellant safety data sheet [60]

Propellant: Argon

Air Liquide	SAFETY DATA SHEET	Page : 1/9 Revised edition no : 4.00 Revision date : 2018-05-30 Supersedes : 2015-02-19
ALPHAGAZ™ 1 Argon		003A_01 Country : DE / Language : EN

SECTION 1: Identification of the substance/mixture and of the company/undertaking

1.1. Product identifier

Trade name : ALPHAGAZ™ 1 Argon
SDS no : 003A_01
Chemical description : Argon
CAS-No. : 7440-37-1
EC-No. : 231-147-0
EC Index-No. : ---
Registration-No. : Listed in Annex IV / V REACH, exempted from registration.
Chemical formula : Ar

1.2. Relevant identified uses of the substance or mixture and uses advised against

Relevant identified uses : Industrial and professional. Perform risk assessment prior to use.
Test gas/Calibration gas.
Laboratory use.
Purge gas, diluting gas, inerting gas.
Purging.
Use for manufacture of electronic/photovoltaic components.
Shield gas for welding processes.
Food applications.
Contact supplier for more information on uses.
Uses advised against : Consumer use.

1.3. Details of the supplier of the safety data sheet

Company identification

Supplier
AIR LIQUIDE Deutschland GmbH
Luise-Rainer-Straße 5
40235 Düsseldorf - GERMANY
T +49 (0)211 6699-0 - F +49 (0)211 6699-222
info@airliquide.de

E-Mail address (competent person) : info.SDB@airliquide.de

1.4. Emergency telephone number

Emergency telephone number : +49 (0)2151 398668
Availability
(24 / 7)

SECTION 2: Hazards identification

2.1. Classification of the substance or mixture

Classification according to Regulation (EC) No. 1272/2008 [CLP]

Physical hazards — Gases under pressure : Compressed gas — H280

2.2. Label elements

Labelling according to Regulation (EC) No. 1272/2008 [CLP]

Hazard pictograms (CLP) :

GHS04

Signal word (CLP) : Warning
Hazard statements (CLP) : H280 - Contains gas under pressure; may explode if heated..
Precautionary statements (CLP)
- Storage : P403 - Store in a well-ventilated place..

2.3. Other hazards

: Asphyxiant in high concentrations.

SECTION 3: Composition/information on ingredients

3.1. Substances

Name	Product identifier	Composition [V-%]:	Classification according to Regulation (EC) No. 1272/2008 [CLP]
Argon	(CAS-No.) 7440-37-1 (EC-No.) 231-147-0 (EC Index-No.) --- (Registration-No.) *1	100	Press. Gas (Comp.), H280

Contains no other components or impurities which will influence the classification of the product.

**1: Listed in Annex IV / V REACH, exempted from registration.*

**2: Registration deadline not expired.*

**3: Registration not required: Substance manufactured or imported < 1t/y.*

3.2. Mixtures : Not applicable.

SECTION 4: First aid measures

4.1. Description of first aid measures

- Inhalation : Remove victim to uncontaminated area wearing self contained breathing apparatus. Keep victim warm and rested. Call a doctor. Apply artificial respiration if breathing stopped.
- Skin contact : Adverse effects not expected from this product.
- Eye contact : Adverse effects not expected from this product.
- Ingestion : Ingestion is not considered a potential route of exposure.

4.2. Most important symptoms and effects, both acute and delayed

: In high concentrations may cause asphyxiation. Symptoms may include loss of mobility/consciousness. Victim may not be aware of asphyxiation.

Refer to section 11.

4.3. Indication of any immediate medical attention and special treatment needed

: None.

SECTION 5: Firefighting measures

5.1. Extinguishing media

- Suitable extinguishing media : Water spray or fog.
- Unsuitable extinguishing media : Do not use water jet to extinguish.

5.2. Special hazards arising from the substance or mixture

Specific hazards : Exposure to fire may cause containers to rupture/explode.

Hazardous combustion products : None.

5.3. Advice for firefighters

Specific methods : Use fire control measures appropriate for the surrounding fire. Exposure to fire and heat radiation may cause gas receptacles to rupture. Cool endangered receptacles with water spray jet from a protected position. Prevent water used in emergency cases from entering sewers and drainage systems.

If possible, stop flow of product.

Use water spray or fog to knock down fire fumes if possible.

Move containers away from the fire area if this can be done without risk.

Special protective equipment for fire fighters : In confined space use self-contained breathing apparatus.

Standard protective clothing and equipment (Self Contained Breathing Apparatus) for fire

fighters.

Standard EN 137 - Self-contained open-circuit compressed air breathing apparatus with full face mask.

Standard EN 469 - Protective clothing for firefighters. Standard - EN 659: Protective gloves for firefighters.

SECTION 6: Accidental release measures

6.1. Personal precautions, protective equipment and emergency procedures

: Try to stop release.

Evacuate area.

Wear self-contained breathing apparatus when entering area unless atmosphere is proved to be safe.

Ensure adequate air ventilation.

Prevent from entering sewers, basements and workpits, or any place where its accumulation can be dangerous.

Act in accordance with local emergency plan.

Stay upwind.

Oxygen detectors should be used when asphyxiating gases may be released.

6.2. Environmental precautions

: Try to stop release.

6.3. Methods and material for containment and cleaning up

: Ventilate area.

6.4. Reference to other sections

: See also sections 8 and 13.

SECTION 7: Handling and storage

7.1. Precautions for safe handling

Safe use of the product : The product must be handled in accordance with good industrial hygiene and safety procedures.

Only experienced and properly instructed persons should handle gases under pressure.

Consider pressure relief device(s) in gas installations.

Ensure the complete gas system was (or is regularily) checked for leaks before use.

Do not smoke while handling product.

Use only properly specified equipment which is suitable for this product, its supply pressure and temperature. Contact your gas supplier if in doubt.

Avoid suck back of water, acid and alkalis.

Do not breathe gas.

Avoid release of product into atmosphere.

Safe handling of the gas receptacle : Refer to supplier's container handling instructions.

Do not allow backfeed into the container.

Protect cylinders from physical damage; do not drag, roll, slide or drop.

When moving cylinders, even for short distances, use a cart (trolley, hand truck, etc.) designed to transport cylinders.

Leave valve protection caps in place until the container has been secured against either a wall or bench or placed in a container stand and is ready for use.

If user experiences any difficulty operating cylinder valve discontinue use and contact supplier.

Never attempt to repair or modify container valves or safety relief devices.

Damaged valves should be reported immediately to the supplier.

Keep container valve outlets clean and free from contaminants particularly oil and water.

Replace valve outlet caps or plugs and container caps where supplied as soon as container is disconnected from equipment.

Close container valve after each use and when empty, even if still connected to equipment.

Never attempt to transfer gases from one cylinder/container to another.

Never use direct flame or electrical heating devices to raise the pressure of a container.
Do not remove or deface labels provided by the supplier for the identification of the cylinder contents.
Suck back of water into the container must be prevented.
Open valve slowly to avoid pressure shock.

7.2. Conditions for safe storage, including any incompatibilities

: Observe all regulations and local requirements regarding storage of containers.
Containers should not be stored in conditions likely to encourage corrosion.
Container valve guards or caps should be in place.
Containers should be stored in the vertical position and properly secured to prevent them from falling over.
Stored containers should be periodically checked for general condition and leakage.
Keep container below 50°C in a well ventilated place.
Store containers in location free from fire risk and away from sources of heat and ignition.
Keep away from combustible materials.

7.3. Specific end use(s)

: None.

SECTION 8: Exposure controls/personal protection

8.1. Control parameters

OEL (Occupational Exposure Limits) : No data available.

DNEL (Derived-No Effect Level) : No data available.

PNEC (Predicted No-Effect Concentration) : No data available.

8.2. Exposure controls

8.2.1. Appropriate engineering controls

: Provide adequate general and local exhaust ventilation.
Systems under pressure should be regularily checked for leakages.
Oxygen detectors should be used when asphyxiating gases may be released.
Consider the use of a work permit system e.g. for maintenance activities.

8.2.2. Individual protection measures, e.g. personal protective equipment

: A risk assessment should be conducted and documented in each work area to assess the risks related to the use of the product and to select the PPE that matches the relevant risk. The following recommendations should be considered:
PPE compliant to the recommended EN/ISO standards should be selected.

• Eye/face protection : Wear safety glasses with side shields.
Standard EN 166 - Personal eye-protection - specifications.

• Skin protection

- Hand protection : Wear working gloves when handling gas containers.
Standard EN 388 - Protective gloves against mechanical risk.

- Other : Wear safety shoes while handling containers.
Standard EN ISO 20345 - Personal protective equipment - Safety footwear.

• Respiratory protection : Self contained breathing apparatus (SCBA) or positive pressure airline with mask are to be used in oxygen-deficient atmospheres.
Standard EN 137 - Self-contained open-circuit compressed air breathing apparatus with full face mask.

• Thermal hazards : None in addition to the above sections.

8.2.3. Environmental exposure controls

: None necessary.

Air Liquide	SAFETY DATA SHEET	Page : 5/9 Revised edition no : 4.00 Revision date : 2018-05-30 Supersedes : 2015-02-19
ALPHAGAZ™ 1 Argon		003A_01 Country : DE / Language : EN

SECTION 9: Physical and chemical properties

9.1. Information on basic physical and chemical properties

Appearance		
• Physical state at 20°C / 101.3kPa	:	Gas.
• Colour	:	Colourless.
Odour	:	No odour warning properties.
Odour threshold	:	Odour threshold is subjective and inadequate to warn of overexposure.
Melting point		-189 °C
Boiling point	:	-186 °C
Flash point	:	Not applicable for gases and gas mixtures.
Flammability range	:	Non flammable.
Relative vapour density at 20 °C	:	Not applicable.
Evaporation rate (ether=1)	:	Not applicable for gases and gas mixtures.
Vapour pressure [20°C]	:	Not applicable.
Vapour pressure [50°C]	:	Not applicable.
Relative density, gas (air=1)	:	1.38
Relative density, liquid (water=1)	:	Not applicable.
Solubility in water	:	67.3 mg/l
pH value	:	Not applicable for gases and gas mixtures.
Partition coefficient n-octanol/water [log Kow]	:	Not applicable for inorganic gases.
Decomposition point [°C]	:	Not applicable.
Auto-ignition temperature	:	Non flammable.
Viscosity [20°C]	:	No reliable data available.
Explosive Properties	:	Not applicable.
Oxidising Properties	:	Not applicable.

9.2. Other information

Molar mass	:	40 g/mol
Critical temperature [°C]		-122 °C
Other data	:	Gas/vapour heavier than air. May accumulate in confined spaces, particularly at or below ground level.

SECTION 10: Stability and reactivity

10.1. Reactivity

: No reactivity hazard other than the effects described in sub-sections below.

10.2. Chemical stability

: Stable under normal conditions.

10.3. Possibility of hazardous reactions

: None.

10.4. Conditions to avoid

: Avoid moisture in installation systems.

10.5. Incompatible materials

: None.
For additional information on compatibility refer to ISO 11114.

10.6. Hazardous decomposition products

: None.

Air Liquide	SAFETY DATA SHEET	Page : 6/9 Revised edition no : 4.00 Revision date : 2018-05-30 Supersedes : 2015-02-19
	ALPHAGAZ™ 1 Argon	003A_01 Country : DE / Language : EN

SECTION 11: Toxicological information

11.1. Information on toxicological effects

Acute toxicity	:	No known toxicological effects from this product.
Skin corrosion/irritation	:	No known effects from this product.
Serious eye damage/irritation	:	No known effects from this product.
Respiratory or skin sensitisation	:	No known effects from this product.
Germ cell mutagenicity	:	No known effects from this product.
Carcinogenicity	:	No known effects from this product.
Reproductive toxicity	:	
Toxic for reproduction : Fertility	:	No known effects from this product.
Toxic for reproduction : unborn child	:	No known effects from this product.
STOT-single exposure	:	No known effects from this product.
STOT-repeated exposure	:	No known effects from this product.
Aspiration hazard	:	Not applicable for gases and gas mixtures.

SECTION 12: Ecological information

12.1. Toxicity

Assessment	:	No ecological damage caused by this product.
EC50 48h - Daphnia magna [mg/l]	:	No data available.
EC50 72h - Algae [mg/l]	:	No data available.
LC50 96 h - Fish [mg/l]	:	No data available.

12.2. Persistence and degradability

Assessment	:	No ecological damage caused by this product.

12.3. Bioaccumulative potential

Assessment	:	No data available.

12.4. Mobility in soil

Assessment	:	Because of its high volatility, the product is unlikely to cause ground or water pollution. Partition into soil is unlikely.

12.5. Results of PBT and vPvB assessment

Assessment	:	No data available.

12.6. Other adverse effects

Other adverse effects	:	No known effects from this product.
Effect on the ozone layer	:	None.
Effect on global warming	:	None.

SECTION 13: Disposal considerations

13.1. Waste treatment methods

May be vented to atmosphere in a well ventilated place.
Do not discharge into any place where its accumulation could be dangerous.
Return unused product in original cylinder to supplier.

List of hazardous waste codes (from Commission Decision 2001/118/EC) : 16 05 05 : Gases in pressure containers other than those mentioned in 16 05 04.

13.2. Additional information

: External treatment and disposal of waste should comply with applicable local and/or national regulations.

SECTION 14: Transport information

14.1. UN number

UN-No. : 1006

14.2. UN proper shipping name

Transport by road/rail (ADR/RID) : ARGON, COMPRESSED

Transport by air (ICAO-TI / IATA-DGR) : Argon, compressed

Transport by sea (IMDG) : ARGON, COMPRESSED

14.3. Transport hazard class(es)

Labelling :

2.2 : Non-flammable, non-toxic gases.

Transport by road/rail (ADR/RID)

Class : 2.
Classification code : 1A.
Hazard identification number : 20.
Tunnel Restriction : E - Passage forbidden through tunnels of category E.

Transport by air (ICAO-TI / IATA-DGR)

Class / Div. (Sub. risk(s)) : 2.2

Transport by sea (IMDG)

Class / Div. (Sub. risk(s)) : 2.2
Emergency Schedule (EmS) - Fire : F-C.
Emergency Schedule (EmS) - Spillage : S-V.

14.4. Packing group

Transport by road/rail (ADR/RID) : Not established.
Transport by air (ICAO-TI / IATA-DGR) : Not established.
Transport by sea (IMDG) : Not established.

14.5. Environmental hazards

Transport by road/rail (ADR/RID) : None.
Transport by air (ICAO-TI / IATA-DGR) : None.
Transport by sea (IMDG) : None.

14.6. Special precautions for user

Packing Instruction(s)

Transport by road/rail (ADR/RID) : P200.
Transport by air (ICAO-TI / IATA-DGR)
Passenger and Cargo Aircraft : 200.
Cargo Aircraft only : 200.
Transport by sea (IMDG) : P200.

Special transport precautions : Avoid transport on vehicles where the load space is not separated from the driver's compartment.

Ensure vehicle driver is aware of the potential hazards of the load and knows what to do in the event of an accident or an emergency.

Before transporting product containers:

- Ensure there is adequate ventilation.
- Ensure that containers are firmly secured.
- Ensure cylinder valve is closed and not leaking.
- Ensure valve outlet cap nut or plug (where provided) is correctly fitted.
- Ensure valve protection device (where provided) is correctly fitted.

14.7. Transport in bulk according to Annex II of Marpol and the IBC Code

: Not applicable.

SECTION 15: Regulatory information

15.1. Safety, health and environmental regulations/legislation specific for the substance or mixture

EU-Regulations

Restrictions on use : None.

Seveso Directive : 2012/18/EU (Seveso III) : Not covered.

National regulations

National legislation : Ensure all national/local regulations are observed.

Germany

Water hazard class (WGK) : Water hazard class (WGK) nwg, Non-hazardous to water (Classification according to VwVwS, Annex 1 or 2; ID No. 1348)

Other information, restrictions and prohibition regulations : [German regulations] BetriebssicherheitsV mit TRBSen insbesondere TRBS 3145 / TRGS 725 Ortsbewegliche Druckgasbehälter", TRBS 2141, BGRegel 500 Teil 2.33: "Umgang mit Gasen", GefahrstoffV mit Technischen Regeln Gefährliche Stoffe TRGS insbesondere TRGS 407 "Tätigkeiten mit Gasen - Gefährdungsbeurteilung", TRGS 400, 500, 510, 900."

15.2. Chemical safety assessment

A CSA does not need to be carried out for this product.

SECTION 16: Other information

Indication of changes : Revised safety data sheet in accordance with commission regulation (EU) No 453/2010.

Abbreviations and acronyms : ATE - Acute Toxicity Estimate

CLP - Classification Labelling Packaging Regulation; Regulation (EC) No 1272/2008

REACH - Registration, Evaluation, Authorisation and Restriction of Chemicals Regulation (EC) No 1907/2006

EINECS - European Inventory of Existing Commercial Chemical Substances

CAS# - Chemical Abstract Service number

PPE - Personal Protection Equipment

LC50 - Lethal Concentration to 50 % of a test population

RMM - Risk Management Measures

PBT - Persistent, Bioaccumulative and Toxic

vPvB - Very Persistent and Very Bioaccumulative

STOT- SE : Specific Target Organ Toxicity - Single Exposure

CSA - Chemical Safety Assessment

EN - European Standard

UN - United Nations

ADR - European Agreement concerning the International Carriage of Dangerous Goods by Road

IATA - International Air Transport Association

IMDG code - International Maritime Dangerous Goods

RID - Regulations concerning the International Carriage of Dangerous Goods by Rail

WGK - Water Hazard Class

Training advice : The hazard of asphyxiation is often overlooked and must be stressed during operator training.

Further information : This Safety Data Sheet has been established in accordance with the applicable European Union legislation.

Full text of H- and EUH-statements

Press. Gas (Comp.)	Gases under pressure : Compressed gas
H280	Contains gas under pressure; may explode if heated.

DISCLAIMER OF LIABILITY : Before using this product in any new process or experiment, a thorough material compatibility and safety study should be carried out.

Details given in this document are believed to be correct at the time of going to press.

Whilst proper care has been taken in the preparation of this document, no liability for injury or damage resulting from its use can be accepted.

Propellant: Helium

Air Liquide	SAFETY DATA SHEET	Page : 1/9 Revised edition no : 4.00 Revision date : 2018-07-13 Supersedes : 2015-10-15
ALPHAGAZ™ 1 Helium		061A_01 Country : DE / Language : EN

SECTION 1: Identification of the substance/mixture and of the company/undertaking

1.1. Product identifier

Trade name : ALPHAGAZ™ 1 Helium
SDS no : 061A_01
Chemical description : Helium
CAS-No. : 7440-59-7
EC-No. : 231-168-5
EC Index-No. : ---
Registration-No. : Listed in Annex IV / V REACH, exempted from registration.
Chemical formula : He

1.2. Relevant identified uses of the substance or mixture and uses advised against

Relevant identified uses : Industrial and professional. Perform risk assessment prior to use.
Test gas/Calibration gas.
Laboratory use.
Purge gas, diluting gas, inerting gas.
Purging.
Use for manufacture of electronic/photovoltaic components.
Contact supplier for more information on uses.
Uses advised against : Do not inhale product on purpose because of the risk of asphyxiation.

1.3. Details of the supplier of the safety data sheet

Company identification

Supplier
AIR LIQUIDE Deutschland GmbH
Luise-Rainer-Straße 5
40235 Düsseldorf - GERMANY
T +49 (0)211 6699-0 - F +49 (0)211 6699-222
info@airliquide.de

E-Mail address (competent person) : info.SDB@airliquide.de

1.4. Emergency telephone number

Emergency telephone number : +49 (0)2151 398668
Availability
(24 / 7)

SECTION 2: Hazards identification

2.1. Classification of the substance or mixture

Classification according to Regulation (EC) No. 1272/2008 [CLP]

Physical hazards — Gases under pressure : Compressed gas — H280

2.2. Label elements

Labelling according to Regulation (EC) No. 1272/2008 [CLP]

Hazard pictograms (CLP) :

GHS04

Signal word (CLP) : Warning
Hazard statements (CLP) : H280 - Contains gas under pressure; may explode if heated..
Precautionary statements (CLP)
- Storage : P403 - Store in a well-ventilated place..

Supplemental information : Do not inhale product on purpose because of the risk of asphyxiation.

2.3. Other hazards

: Asphyxiant in high concentrations.

SECTION 3: Composition/information on ingredients

3.1. Substances

Name	Product identifier	Composition [V-%]:	Classification according to Regulation (EC) No. 1272/2008 [CLP]
Helium	(CAS-No.) 7440-59-7 (EC-No.) 231-168-5 (EC Index-No.) --- (Registration-No.) *1	100	Press. Gas (Comp.), H280

Contains no other components or impurities which will influence the classification of the product.

**1: Listed in Annex IV / V REACH, exempted from registration.*

**2: Registration deadline not expired.*

**3: Registration not required: Substance manufactured or imported < 1t/y.*

3.2. Mixtures : Not applicable.

SECTION 4: First aid measures

4.1. Description of first aid measures

- Inhalation : Remove victim to uncontaminated area wearing self contained breathing apparatus. Keep victim warm and rested. Call a doctor. Apply artificial respiration if breathing stopped.
- Skin contact : Adverse effects not expected from this product.
- Eye contact : Adverse effects not expected from this product.
- Ingestion : Ingestion is not considered a potential route of exposure.

4.2. Most important symptoms and effects, both acute and delayed

: In high concentrations may cause asphyxiation. Symptoms may include loss of mobility/consciousness. Victim may not be aware of asphyxiation.

Refer to section 11.

4.3. Indication of any immediate medical attention and special treatment needed

: None.

SECTION 5: Firefighting measures

5.1. Extinguishing media

- Suitable extinguishing media : Water spray or fog.
- Unsuitable extinguishing media : Do not use water jet to extinguish.

5.2. Special hazards arising from the substance or mixture

Specific hazards : Exposure to fire may cause containers to rupture/explode.

Hazardous combustion products : None.

5.3. Advice for firefighters

Specific methods : Use fire control measures appropriate for the surrounding fire. Exposure to fire and heat radiation may cause gas receptacles to rupture. Cool endangered receptacles with water spray jet from a protected position. Prevent water used in emergency cases from entering sewers and drainage systems.

If possible, stop flow of product.

Use water spray or fog to knock down fire fumes if possible.

Move containers away from the fire area if this can be done without risk.

Special protective equipment for fire fighters : In confined space use self-contained breathing apparatus.

Standard protective clothing and equipment (Self Contained Breathing Apparatus) for fire fighters.

Standard EN 137 - Self-contained open-circuit compressed air breathing apparatus with full face mask.

Standard EN 469 - Protective clothing for firefighters. Standard - EN 659: Protective gloves for firefighters.

SECTION 6: Accidental release measures

6.1. Personal precautions, protective equipment and emergency procedures

: Try to stop release.

Evacuate area.

Wear self-contained breathing apparatus when entering area unless atmosphere is proved to be safe.

Ensure adequate air ventilation.

Act in accordance with local emergency plan.

Stay upwind.

Oxygen detectors should be used when asphyxiating gases may be released.

6.2. Environmental precautions

: Try to stop release.

6.3. Methods and material for containment and cleaning up

: Ventilate area.

6.4. Reference to other sections

: See also sections 8 and 13.

SECTION 7: Handling and storage

7.1. Precautions for safe handling

Safe use of the product : The product must be handled in accordance with good industrial hygiene and safety procedures.

Only experienced and properly instructed persons should handle gases under pressure.

Consider pressure relief device(s) in gas installations.

Ensure the complete gas system was (or is regularily) checked for leaks before use.

Do not smoke while handling product.

Use only properly specified equipment which is suitable for this product, its supply pressure and temperature. Contact your gas supplier if in doubt.

Avoid suck back of water, acid and alkalis.

Do not breathe gas.

Avoid release of product into atmosphere.

Safe handling of the gas receptacle : Refer to supplier's container handling instructions.

Do not allow backfeed into the container.

Protect cylinders from physical damage; do not drag, roll, slide or drop.

When moving cylinders, even for short distances, use a cart (trolley, hand truck, etc.) designed to transport cylinders.

Leave valve protection caps in place until the container has been secured against either a wall or bench or placed in a container stand and is ready for use.

If user experiences any difficulty operating cylinder valve discontinue use and contact supplier.

Never attempt to repair or modify container valves or safety relief devices.

Damaged valves should be reported immediately to the supplier.

Keep container valve outlets clean and free from contaminants particularly oil and water.

Replace valve outlet caps or plugs and container caps where supplied as soon as container is disconnected from equipment.

Close container valve after each use and when empty, even if still connected to equipment.

Never attempt to transfer gases from one cylinder/container to another.

Never use direct flame or electrical heating devices to raise the pressure of a container.

Do not remove or deface labels provided by the supplier for the identification of the cylinder contents.

Suck back of water into the container must be prevented.
Open valve slowly to avoid pressure shock.

7.2. Conditions for safe storage, including any incompatibilities

: Observe all regulations and local requirements regarding storage of containers.
Containers should not be stored in conditions likely to encourage corrosion.
Container valve guards or caps should be in place.
Containers should be stored in the vertical position and properly secured to prevent them from falling over.
Stored containers should be periodically checked for general condition and leakage.
Keep container below 50°C in a well ventilated place.
Store containers in location free from fire risk and away from sources of heat and ignition.
Keep away from combustible materials.

7.3. Specific end use(s)

: None.

SECTION 8: Exposure controls/personal protection

8.1. Control parameters

OEL (Occupational Exposure Limits) : No data available.

DNEL (Derived-No Effect Level) : No data available.

PNEC (Predicted No-Effect Concentration) : No data available.

8.2. Exposure controls

8.2.1. Appropriate engineering controls

: Provide adequate general and local exhaust ventilation.
Systems under pressure should be regularily checked for leakages.
Oxygen detectors should be used when asphyxiating gases may be released.
Consider the use of a work permit system e.g. for maintenance activities.

8.2.2. Individual protection measures, e.g. personal protective equipment

: A risk assessment should be conducted and documented in each work area to assess the risks related to the use of the product and to select the PPE that matches the relevant risk. The following recommendations should be considered:
PPE compliant to the recommended EN/ISO standards should be selected.

• Eye/face protection : Wear safety glasses with side shields.
Standard EN 166 - Personal eye-protection - specifications.

• Skin protection

- Hand protection : Wear working gloves when handling gas containers.
Standard EN 388 - Protective gloves against mechanical risk.
- Other : Wear safety shoes while handling containers.
Standard EN ISO 20345 - Personal protective equipment - Safety footwear.

• Respiratory protection : Self contained breathing apparatus (SCBA) or positive pressure airline with mask are to be used in oxygen-deficient atmospheres.
Standard EN 137 - Self-contained open-circuit compressed air breathing apparatus with full face mask.

• Thermal hazards : None in addition to the above sections.

8.2.3. Environmental exposure controls

: None necessary.

Air Liquide	SAFETY DATA SHEET	Page : 5/9 Revised edition no : 4.00 Revision date : 2018-07-13 Supersedes : 2015-10-15
ALPHAGAZ™ 1 Helium		061A_01 Country : DE / Language : EN

SECTION 9: Physical and chemical properties

9.1. Information on basic physical and chemical properties

Appearance		
• Physical state at 20°C / 101.3kPa	:	Gas.
• Colour	:	Colourless.
Odour	:	No odour warning properties.
Odour threshold	:	Odour threshold is subjective and inadequate to warn of overexposure.
Melting point		-272 °C
Boiling point	:	-269 °C
Flash point	:	Not applicable for gases and gas mixtures.
Flammability range	:	Non flammable.
Relative vapour density at 20 °C	:	Not applicable.
Evaporation rate (ether=1)	:	Not applicable for gases and gas mixtures.
Vapour pressure [20°C]	:	Not applicable.
Vapour pressure [50°C]	:	Not applicable.
Relative density, gas (air=1)	:	0.14
Relative density, liquid (water=1)	:	Not applicable.
Solubility in water	:	1.5 mg/l
pH value	:	Not applicable for gases and gas mixtures.
Partition coefficient n-octanol/water [log Kow]	:	Not applicable for inorganic gases.
Decomposition point [°C]	:	Not applicable.
Auto-ignition temperature	:	Non flammable.
Viscosity [20°C]	:	No reliable data available.
Explosive Properties	:	Not applicable.
Oxidising Properties	:	Not applicable.

9.2. Other information

Molar mass	:	4 g/mol
Critical temperature [°C]		-268 °C
Other data	:	No additional information available

SECTION 10: Stability and reactivity

10.1. Reactivity

: No reactivity hazard other than the effects described in sub-sections below.

10.2. Chemical stability

: Stable under normal conditions.

10.3. Possibility of hazardous reactions

: None.

10.4. Conditions to avoid

: Avoid moisture in installation systems.

10.5. Incompatible materials

: None.
For additional information on compatibility refer to ISO 11114.

10.6. Hazardous decomposition products

: None.

SECTION 11: Toxicological information

11.1. Information on toxicological effects

Acute toxicity	:	No known toxicological effects from this product.
Skin corrosion/irritation	:	No known effects from this product.
Serious eye damage/irritation	:	No known effects from this product.
Respiratory or skin sensitisation	:	No known effects from this product.
Germ cell mutagenicity	:	No known effects from this product.
Carcinogenicity	:	No known effects from this product.
Reproductive toxicity	:	
Toxic for reproduction : Fertility	:	No known effects from this product.
Toxic for reproduction : unborn child	:	No known effects from this product.
STOT-single exposure	:	No known effects from this product.
STOT-repeated exposure	:	No known effects from this product.
Aspiration hazard	:	Not applicable for gases and gas mixtures.

SECTION 12: Ecological information

12.1. Toxicity

Assessment	:	No ecological damage caused by this product.
EC50 48h - Daphnia magna [mg/l]	:	No data available.
EC50 72h - Algae [mg/l]	:	No data available.
LC50 96 h - Fish [mg/l]	:	No data available.

12.2. Persistence and degradability

Assessment	:	No ecological damage caused by this product.

12.3. Bioaccumulative potential

Assessment	:	No data available.

12.4. Mobility in soil

Assessment	:	Because of its high volatility, the product is unlikely to cause ground or water pollution. Partition into soil is unlikely.

12.5. Results of PBT and vPvB assessment

Assessment	:	No data available.

12.6. Other adverse effects

Other adverse effects	:	No known effects from this product.
Effect on the ozone layer	:	None.
Effect on global warming	:	None.

SECTION 13: Disposal considerations

13.1. Waste treatment methods

		May be vented to atmosphere in a well ventilated place. Do not discharge into any place where its accumulation could be dangerous. Return unused product in original cylinder to supplier.
List of hazardous waste codes (from Commission Decision 2001/118/EC)	:	16 05 05 : Gases in pressure containers other than those mentioned in 16 05 04.

13.2. Additional information

: External treatment and disposal of waste should comply with applicable local and/or national regulations.

SECTION 14: Transport information

14.1. UN number

UN-No. : 1046

14.2. UN proper shipping name

Transport by road/rail (ADR/RID) : HELIUM, COMPRESSED

Transport by air (ICAO-TI / IATA-DGR) : Helium, compressed

Transport by sea (IMDG) : HELIUM, COMPRESSED

14.3. Transport hazard class(es)

Labelling :

2.2 : Non-flammable, non-toxic gases.

Transport by road/rail (ADR/RID)

Class : 2.

Classification code : 1A.

Hazard identification number : 20.

Tunnel Restriction : E - Passage forbidden through tunnels of category E.

Transport by air (ICAO-TI / IATA-DGR)

Class / Div. (Sub. risk(s)) : 2.2

Transport by sea (IMDG)

Class / Div. (Sub. risk(s)) : 2.2

Emergency Schedule (EmS) - Fire : F-C.

Emergency Schedule (EmS) - Spillage : S-V.

14.4. Packing group

Transport by road/rail (ADR/RID) : Not established.

Transport by air (ICAO-TI / IATA-DGR) : Not established.

Transport by sea (IMDG) : Not established.

14.5. Environmental hazards

Transport by road/rail (ADR/RID) : None.

Transport by air (ICAO-TI / IATA-DGR) : None.

Transport by sea (IMDG) : None.

14.6. Special precautions for user

Packing Instruction(s)

Transport by road/rail (ADR/RID) : P200.

Transport by air (ICAO-TI / IATA-DGR)

Passenger and Cargo Aircraft : 200.

Cargo Aircraft only : 200.

Transport by sea (IMDG) : P200.

Special transport precautions : Avoid transport on vehicles where the load space is not separated from the driver's compartment.

Ensure vehicle driver is aware of the potential hazards of the load and knows what to do in the event of an accident or an emergency.

Before transporting product containers:

- Ensure there is adequate ventilation.
- Ensure that containers are firmly secured.
- Ensure cylinder valve is closed and not leaking.
- Ensure valve outlet cap nut or plug (where provided) is correctly fitted.
- Ensure valve protection device (where provided) is correctly fitted.

14.7. Transport in bulk according to Annex II of Marpol and the IBC Code

: Not applicable.

SECTION 15: Regulatory information

15.1. Safety, health and environmental regulations/legislation specific for the substance or mixture

EU-Regulations

Restrictions on use : None.

Seveso Directive : 2012/18/EU (Seveso III) : Not covered.

National regulations

National legislation : Ensure all national/local regulations are observed.

Germany

Water hazard class (WGK) : Water hazard class (WGK) nwg, Non-hazardous to water

Other information, restrictions and prohibition regulations : [German regulations] BetriebssicherheitsV mit TRBSen insbesondere TRBS 3145 / TRGS 725 Ortsbewegliche Druckgasbehälter", TRBS 2141, BGRegel 500 Teil 2.33: "Umgang mit Gasen", GefahrstoffV mit Technischen Regeln Gefährliche Stoffe TRGS insbesondere TRGS 407 "Tätigkeiten mit Gasen - Gefährdungsbeurteilung", TRGS 400, 500, 510, 900."

15.2. Chemical safety assessment

A CSA does not need to be carried out for this product.

SECTION 16: Other information

Indication of changes : Revised safety data sheet in accordance with commission regulation (EU) No 453/2010.

Abbreviations and acronyms : ATE - Acute Toxicity Estimate

CLP - Classification Labelling Packaging Regulation; Regulation (EC) No 1272/2008

REACH - Registration, Evaluation, Authorisation and Restriction of Chemicals Regulation (EC) No 1907/2006

EINECS - European Inventory of Existing Commercial Chemical Substances

CAS# - Chemical Abstract Service number

PPE - Personal Protection Equipment

LC50 - Lethal Concentration to 50 % of a test population

RMM - Risk Management Measures

PBT - Persistent, Bioaccumulative and Toxic

vPvB - Very Persistent and Very Bioaccumulative

STOT- SE : Specific Target Organ Toxicity - Single Exposure

CSA - Chemical Safety Assessment

EN - European Standard

UN - United Nations

ADR - European Agreement concerning the International Carriage of Dangerous Goods by Road

IATA - International Air Transport Association

IMDG code - International Maritime Dangerous Goods

RID - Regulations concerning the International Carriage of Dangerous Goods by Rail

WGK - Water Hazard Class

Training advice : The hazard of asphyxiation is often overlooked and must be stressed during operator training.

Further information : This Safety Data Sheet has been established in accordance with the applicable European Union legislation.

Full text of H- and EUH-statements

Press. Gas (Comp.)	Gases under pressure : Compressed gas
H280	Contains gas under pressure; may explode if heated.

DISCLAIMER OF LIABILITY : Before using this product in any new process or experiment, a thorough material compatibility and safety study should be carried out.

Details given in this document are believed to be correct at the time of going to press.

Whilst proper care has been taken in the preparation of this document, no liability for injury or damage resulting from its use can be accepted.

D.4 Boron nitride purity and impurities

Chemical analysis of HeBoSint®P700 conducted by company Henze AG

Analysendaten im Vergleich

HeBoSint® P100

HeBoSint® P700

	HeBoSint® P100	HeBoSint® P700 ✓
Emmissionsspektroskopie (alle Werte in ppm*)		
Element		
Al	9	<1
Au	n.b.	<1
Be	n.b.	<1
Ca	220	100
Cr	<2	<1
Cu	n.b.	<1
Fe	16	<1
Ni	<2	<1
Mg	8	<1
Mn	<2	<1
Mo	n.b.	<1
Na	8	<1
Pb	n.b.	<1
Si	41	<1
Sn	n.b.	<1
Ti	<10	<1
V	<1	<1
W	n.b.	<1
Zn	n.b.	<1
Zr	4	<1
Chemische Analyse (alle Werte in %*)		
Boroxid	0.19	0.02
Sauerstoff	0.89	0.22
Bornitrid	98.8	99.7
Kohlenstoff	0.02	n.b.

Appendix E - Drafts

- E.1 Pneumatic schematic
- E.2 Light barrier electronics
- E.3 Light barrier: Pin assignment – Amphenol plug
- E.4 Simatic control system
- E.5 Injector drafts

E.1 Pneumatic schematic

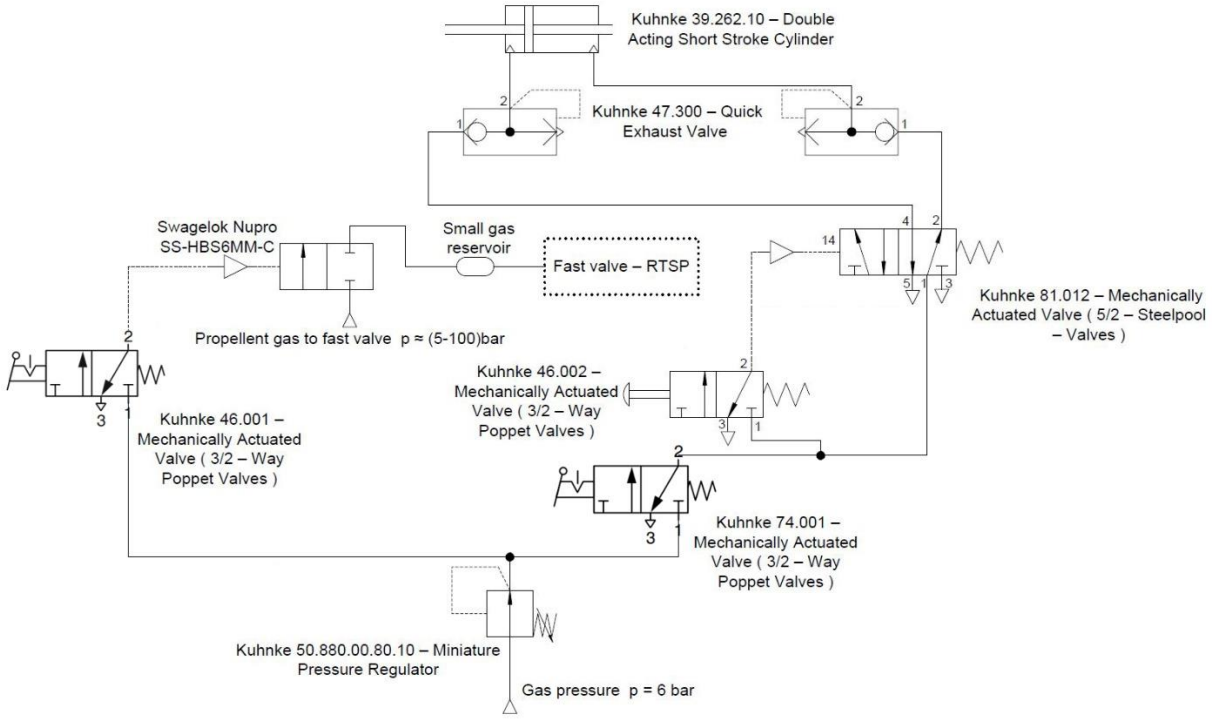

E.2 Light barrier electronics

Pellet Lichtschranke Typ A (v-Messung Li-Kanone)

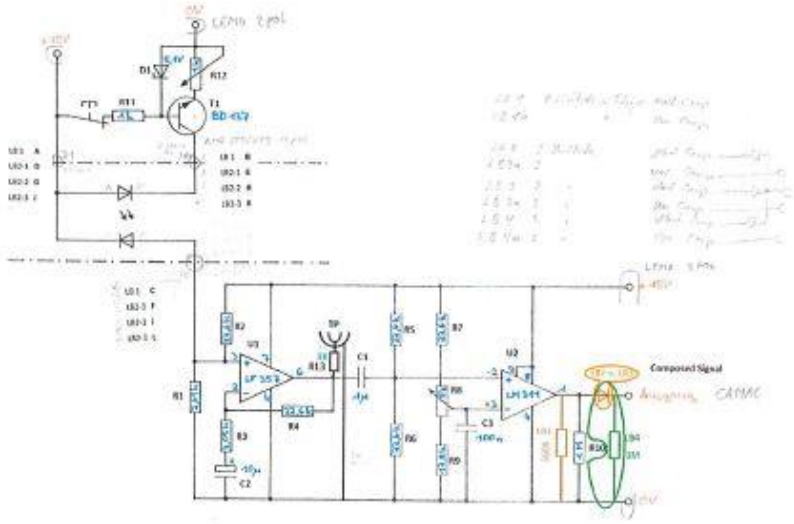

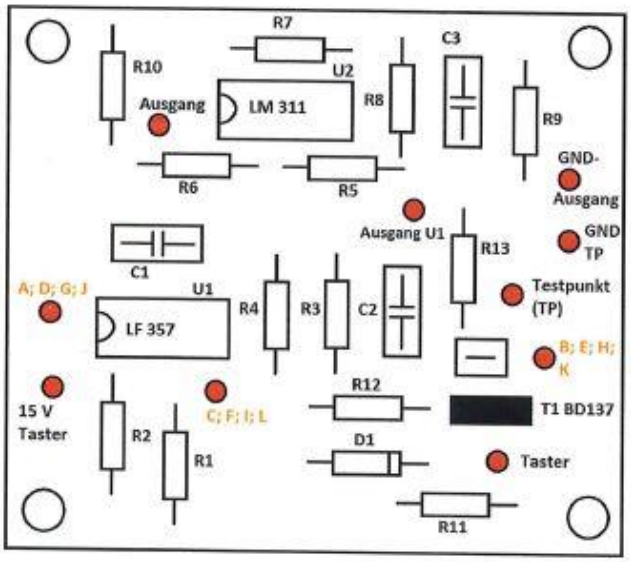

Andi Seiler E1-Elektronik 24.03.2015 Tel. 089/3299-1797 andreas.seiler@ipp.mpg.de

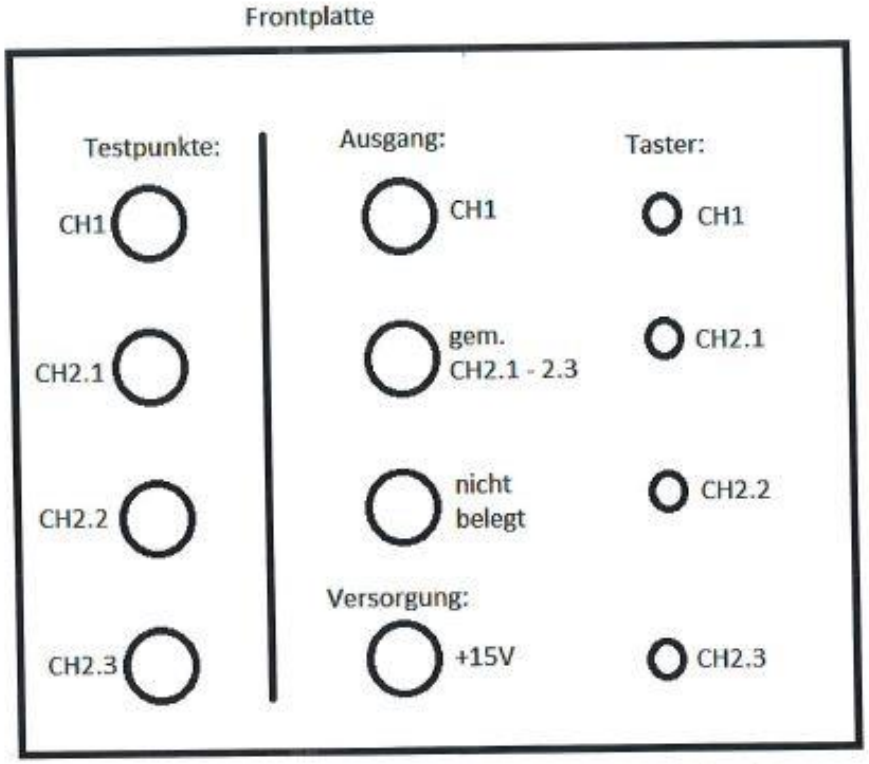

gemeinsamer Ausgang: Channel 2.1 bis Channel 2.3 sind miteinander verodert

Achtung bei LM311:

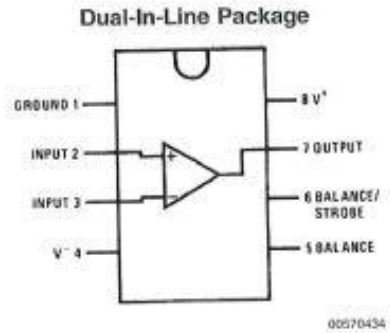

Top View
Order Number LM111J-8, LM111J-8/883(Note 21),
LM311M, LM311MX or LM311N
See NS Package Number J08A, M08A or N08E

=>

Andi Seiler E1-Elektronik 24.03.2015 Tel. 089/3299-1797 andreas.seiler@ipp.mpg.de

Driving Ground-Referred Load

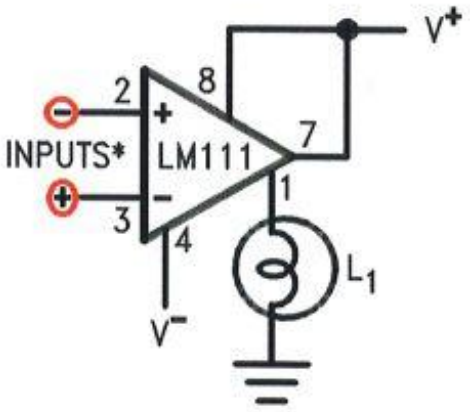

00570416

*Input polarity is reversed when using pin 1 as output.

Voltage comparator LM111/211/311/311B

EQUIVALENT SCHEMATIC

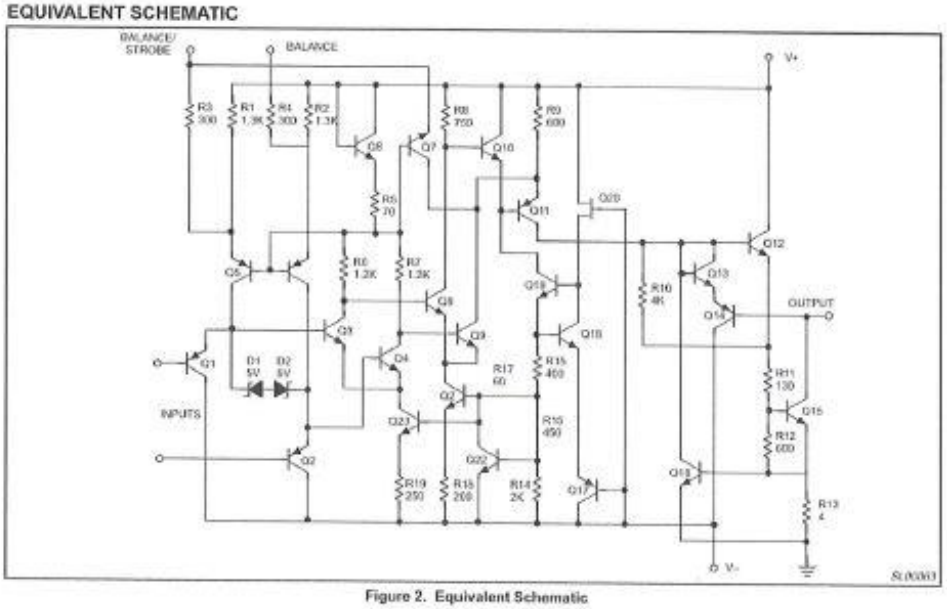

Figure 2. Equivalent Schematic

Andi Seiler E1-Elektronik 24.03.2015 Tel. 089/3299-1797 andreas.seiler@ipp.mpg.de

ASDEX Upgrade

RTSP — Pelletgruppe

IPP Max-Planck-Institut für Plasmaphysik

Lichtschranken

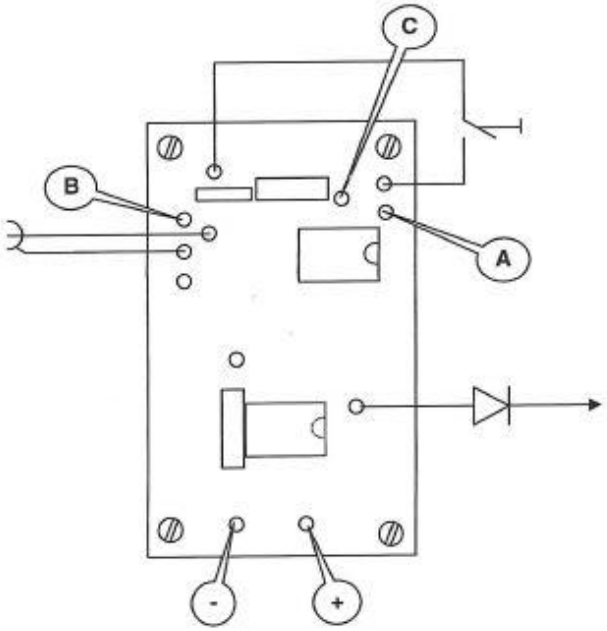

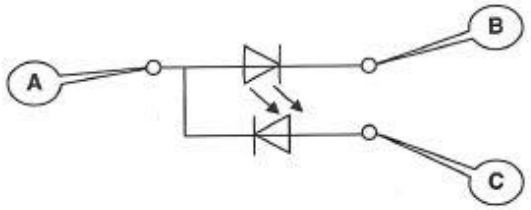

RTSP — Pelletgruppe

ASDEX Upgrade

IPP Max-Planck-Institut für Plasmaphysik

Lichtschranken

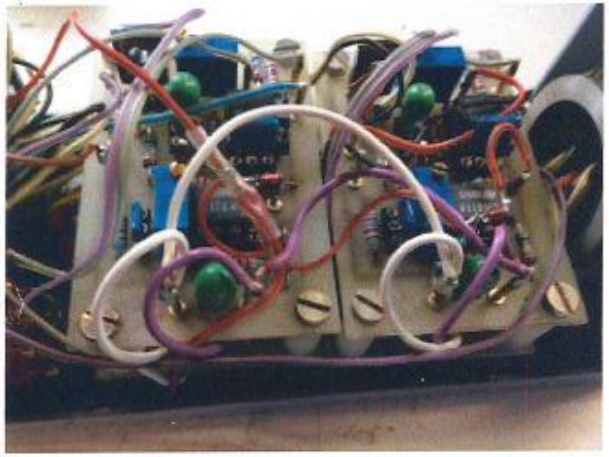

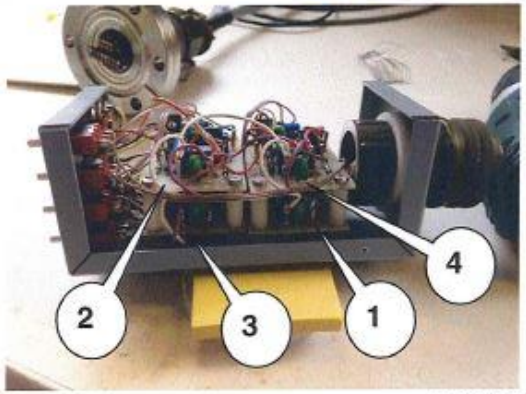

W. Weisbart

RTSP Lichtschranke 2

12.12.2014

E.3 Light barrier: Pin assignment – Amphenol plug

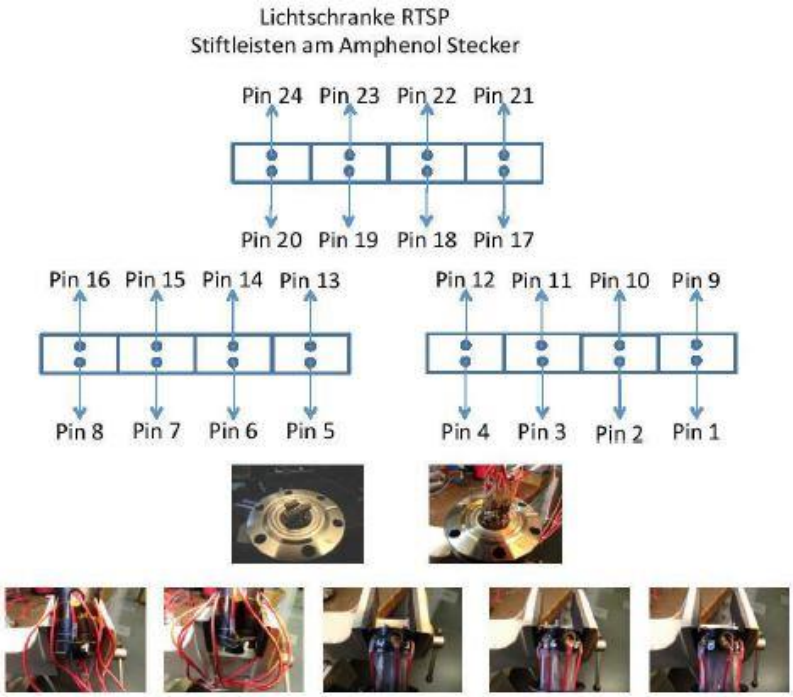

Rev.		Lichtschranke RTSP				Datum:	17.11.2017		Blatt	1
Name Klemmleiste:		Amphenol Stecker				Name:	M. Beck		von	1
Nr.	Amphenol	Stiftleiste		Kabel	Lichtschranke Nr.	Kabel		Diode		
1	A	PIN	1	Phase + Schirm	LB 1	Phase		Anode		
2	A	PIN	1	Phase + Schirm	LB 2	Schirm		Kathode		
3	B	PIN	2	Schirm	LB 1	Schirm		Kathode		
4		PIN	3	NC						
5		PIN	4	NC						
6	K	PIN	5	Schirm	LB 8	Schirm		Kathode		
7		PIN	6	NC						
8	I	PIN	7	Phase	LB 5	Phase		Anode		
9	J	PIN	8	Phase + Schirm	LB 8	Phase		Anode		
10	J	PIN	8	Phase + Schirm	LB 5	Schirm		Kathode		
11		PIN	9	NC						
12	C	PIN	10	Phase	LB 2	Phase		Anode		
13	L	PIN	11	Phase	LB 5	Phase		Anode		
14		PIN	12	NC						
15		PIN	13	NC						
16		PIN	14	NC						
17	H	PIN	15	Schirm	LB 6	Schirm		Kathode		
18		PIN	16	NC						
19	D	PIN	17	Phase + Schirm	LB 4	fase		Anode		
20	D	PIN	17	Phase + Schirm	LB 7	Schirm		Kathode		
21		PIN	18	NC						
22		PIN	19	NC						
23	G	PIN	20	Phase + Schirm	LB 6	Phase		Anode		
24	G	PIN	20	Phase + Schirm	LB 3	Schirm		Kathode		
25	E	PIN	21	Schirm	LB 4	Schirm		Kathode		
26		PIN	22	NC						
27		PIN	23	NC						
28	F	PIN	24	Phase	LB 7	Phase		Anode		

M.Beck 17.11.2017

Anschlußplan Amphenol - Lichtschranke.xls

Kes:	Lichtschranke RTSP		Datum:	07.11.17	Blatt	1
Name Klemmleiste:	Amphenol-Stecker		Name:	M. Beck	von	1

Nr.	Amphenol	Stiftleiste		Kabel	Lichtschranke Nr.	Kabel		Diode			
1	A	PIN	1	Phase + Schirm	LB 1	Phase		Anode			
2	A	PIN	1	Phase + Schirm	LB 2	Schirm		Kathode			
3	B	PIN	2	Schirm	LB 1	Schirm		Kathode			
4		PIN	3	NC							
5		PIN	4	NC							
6	K	PIN	5	Schirm	LB 6	Schirm		Kathode			
7		PIN	6	NC							
8	I	PIN	7	Phase	LB 3	Phase		Anode			
9	J	PIN	8	Phase + Schirm	LB 8	Phase		Anode			
10	J	PIN	8	Phase + Schirm	LB 5	Schirm		Kathode			
11		PIN	9	NC							
12	C	PIN	10	Phase	LB 2	Phase		Anode			
13	L	PIN	11	Phase	LB 5	Phase		Anode			
14		PIN	12	NC							
15		PIN	13	NC							
16		PIN	14	NC							
17	H	PIN	15	Schirm	LB 6	Schirm		Kathode			
18		PIN	16	NC							
19	D	PIN	17	Phase + Schirm	LB 4	Fase		Anode			
20	D	PIN	17	Phase + Schirm	LB 7	Schirm		Kathode			
21		PIN	18	NC							
22		PIN	19	NC							
23	G	PIN	20	Phase + Schirm	LB 6	Phase		Anode			
24	G	PIN	20	Phase + Schirm	LB 3	Schirm		Kathode			
25	E	PIN	21	Schirm	LB 4	Schirm		Kathode			
26		PIN	22	NC							
27		PIN	23	NC							
28	F	PIN	24	Phase	LB 7	Phase		Anode			

M. Beck Amphenol 07.12.17

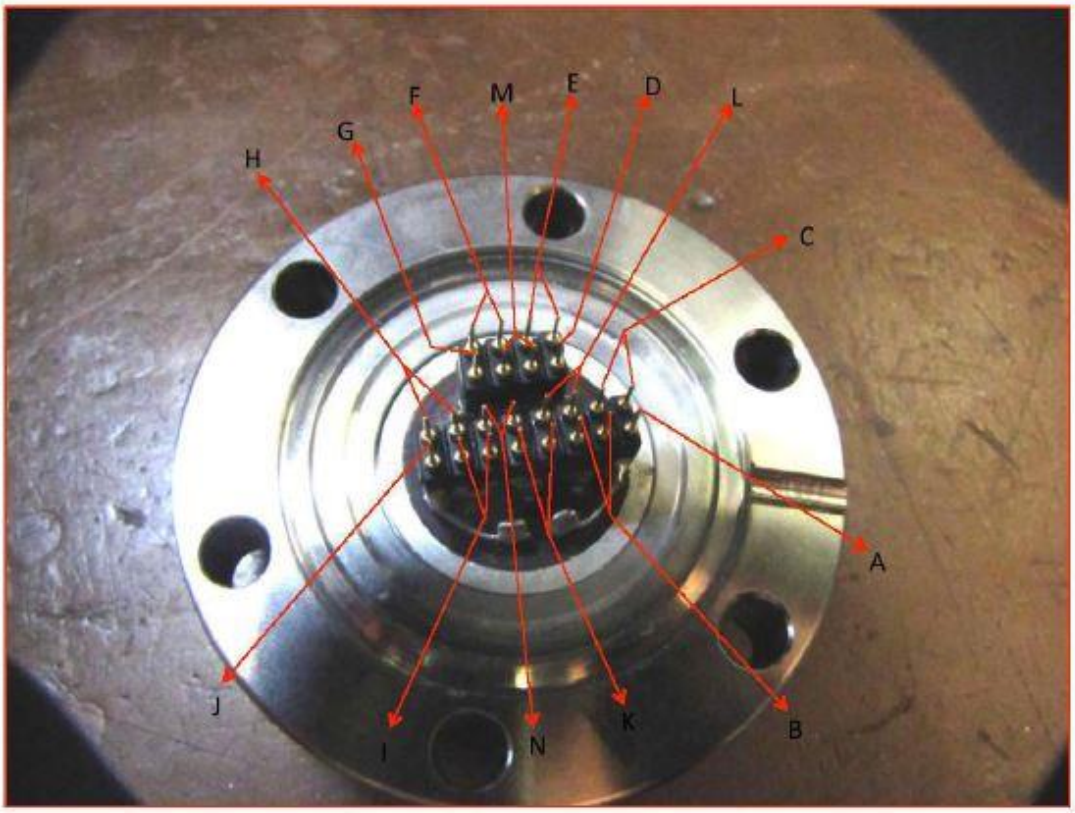

E.4 Simatic control system

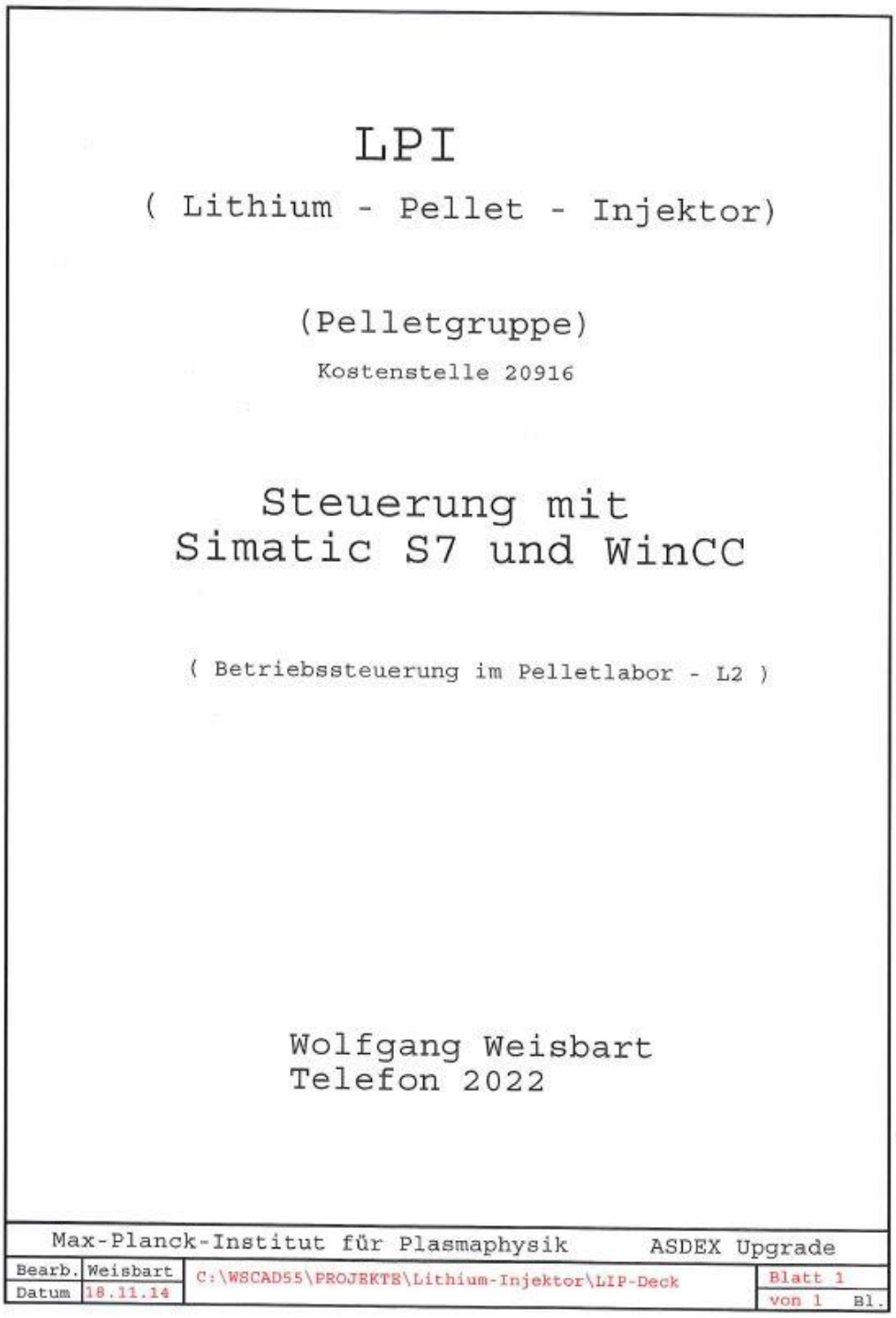

LPI

(Lithium - Pellet - Injektor)

(Pelletgruppe)

Kostenstelle 20916

Steuerung mit
Simatic S7 und WinCC

(Betriebssteuerung im Pelletlabor - L2)

Wolfgang Weisbart
Telefon 2022

Max-Planck-Institut für Plasmaphysik		ASDEX Upgrade	
Bearb.	Weisbart	C:\WSCAD55\PROJEKTE\Lithium-Injektor\LIP-Deck	Blatt 1
Datum	18.11.14		von 1 Bl.

Inhalt von: Lithium - Pellet - Injektor Seite : 1

Nr.	Datei	Projektseite	Kommentar	Datum
1	LPI_I.0001		Inhaltsangabe	12.02.2015
2	LIP.0001		Übersicht Zentralgerät	10.02.2015
3	LIP.0002		Digitalei Engänge EB0	11.02.2015
4	LIP.0003		Digitale Ausgänge AB0	10.02.2015
5	LIP.0004		Anloge Eingänge PEW128-PEW134	11.02.2015
6	LIP.0005		Anloge Eingänge PEW136-PEW142	11.02.2015
7	LIP.0006		Übersicht Erweiterungsgerät	11.02.2015
8	LIP.0007		Digitaleingänge E21-E22	11.02.2015
9	LIP.0008		Digitaleingänge E23	11.02.2015
10	LIP.0009		Digitalausgänge A21-A22	11.02.2015
11	LIP.0010		Anloge Eingänge PEW50-PEW56	12.02.2015
12	LIP.0011		Anloge Ausgänge PAW50-PAW52	11.02.2015
13	LIP.0012		Digitalausgänge Ventilinsel	10.02.2015
14	RTSP_ST.0001		Steckerplan	04.02.2015
15	RTSP_ST.0002		Steckerplan	04.02.2015
16	RTSP_fG.0001		Pneumatic	20.11.2014

Datum
Bearb.

ASDEX Upgrade Pellet | IPP Max-Planck-Institut für Plasmaphysik | Lithium - Pellet - Injektor | Inhaltsangabe

C:\WSCAD55\PROJEKTE\Lithium-Injektor\LPI_I

Blatt 1
von 1

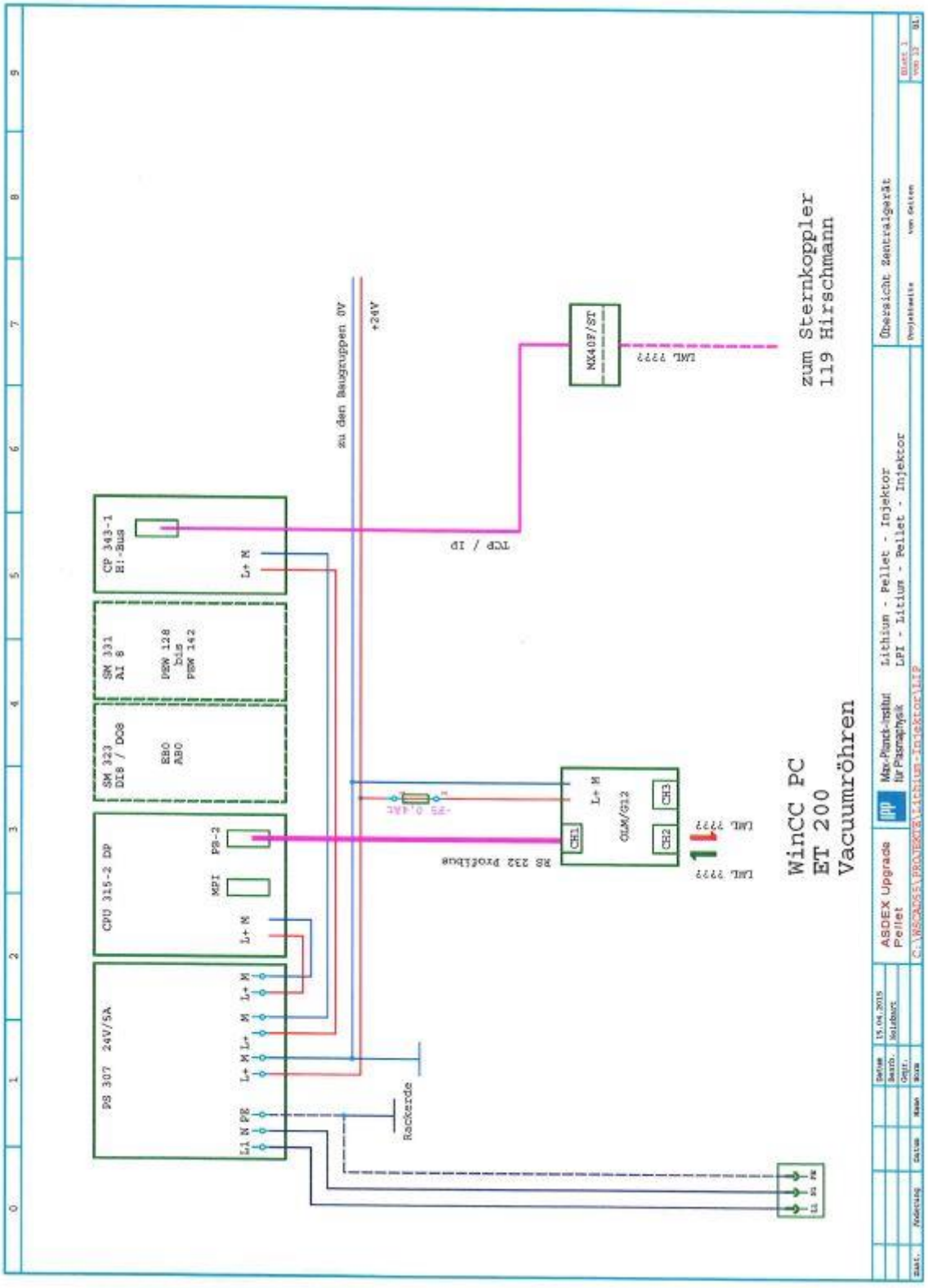
zum Sternkoppler
119 Hirschmann
WinCC PC
ET 200
Vacuumröhren
Lithium - Pellet - Injektor
LPI - Litium - Pellet - Injektor
Max-Planck-Institut für Plasmaphysik
ASDEX Upgrade
Pellet
Übersicht Zentralgerät
zu den Baugruppen 0V
+24V
TCP / IP
RS 232 Profibus
Rackerde
PS 307 24V/5A
CPU 315-2 DP
SM 323 DI8 / DO8
SM 331 AI 8
CP 343-1 El-Bus
NX40F/ST
CUM/CU2

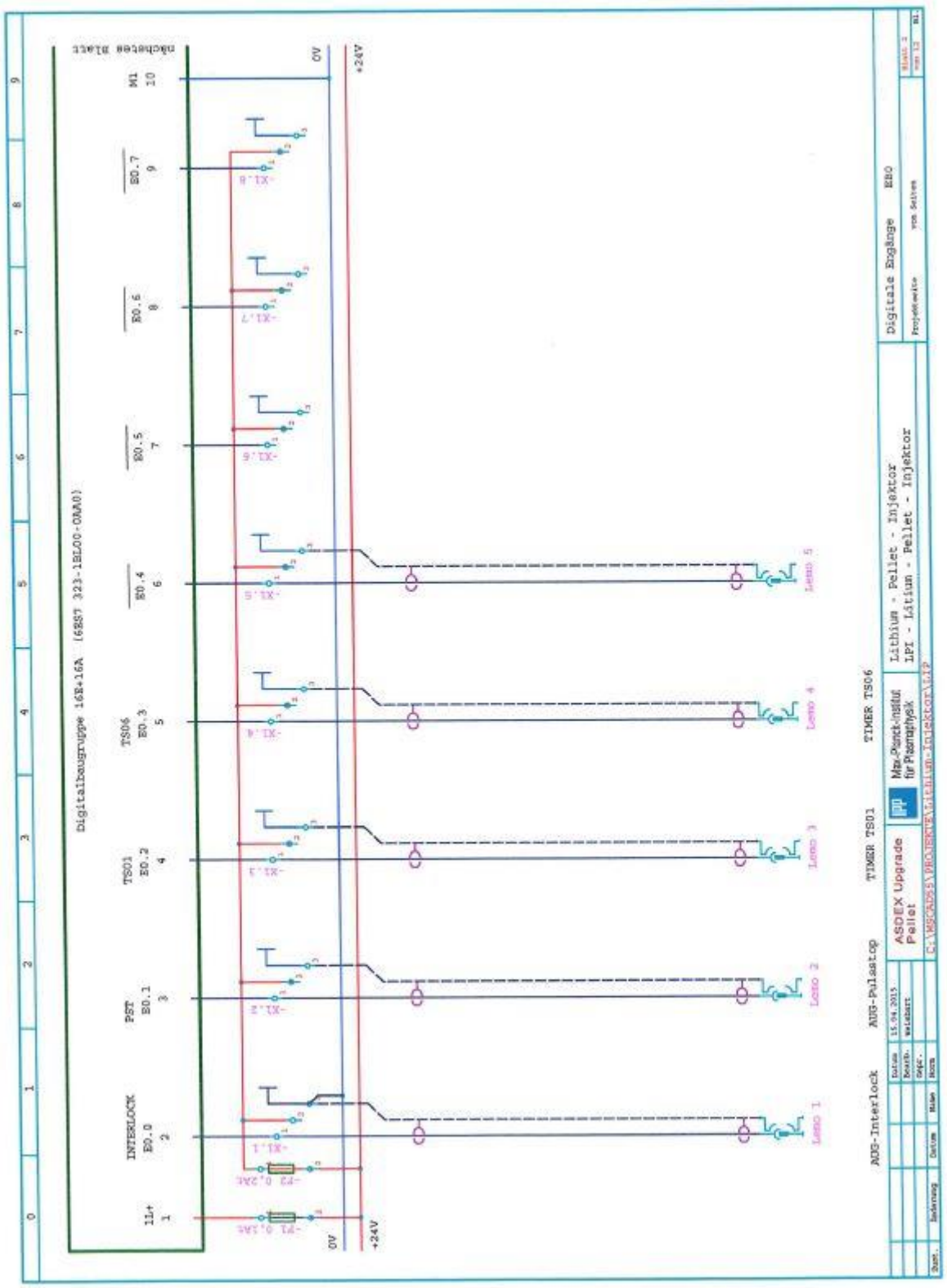
Digitalbaugruppe 16E+16A (6ES7 323-1BL00-0AA0)
INTERLOCK
PST
TS01
TS06
M1
0V
+24V
Lithium - Pellet - Injektor
LPI - Lithium - Pellet - Injektor
Max-Planck-Institut für Plasmaphysik
ASDEX Upgrade Pellet
ADS-Interlock
ADS-Pulsatop
TIMER TS01
TIMER TS06
Digitale Eingänge
EB0

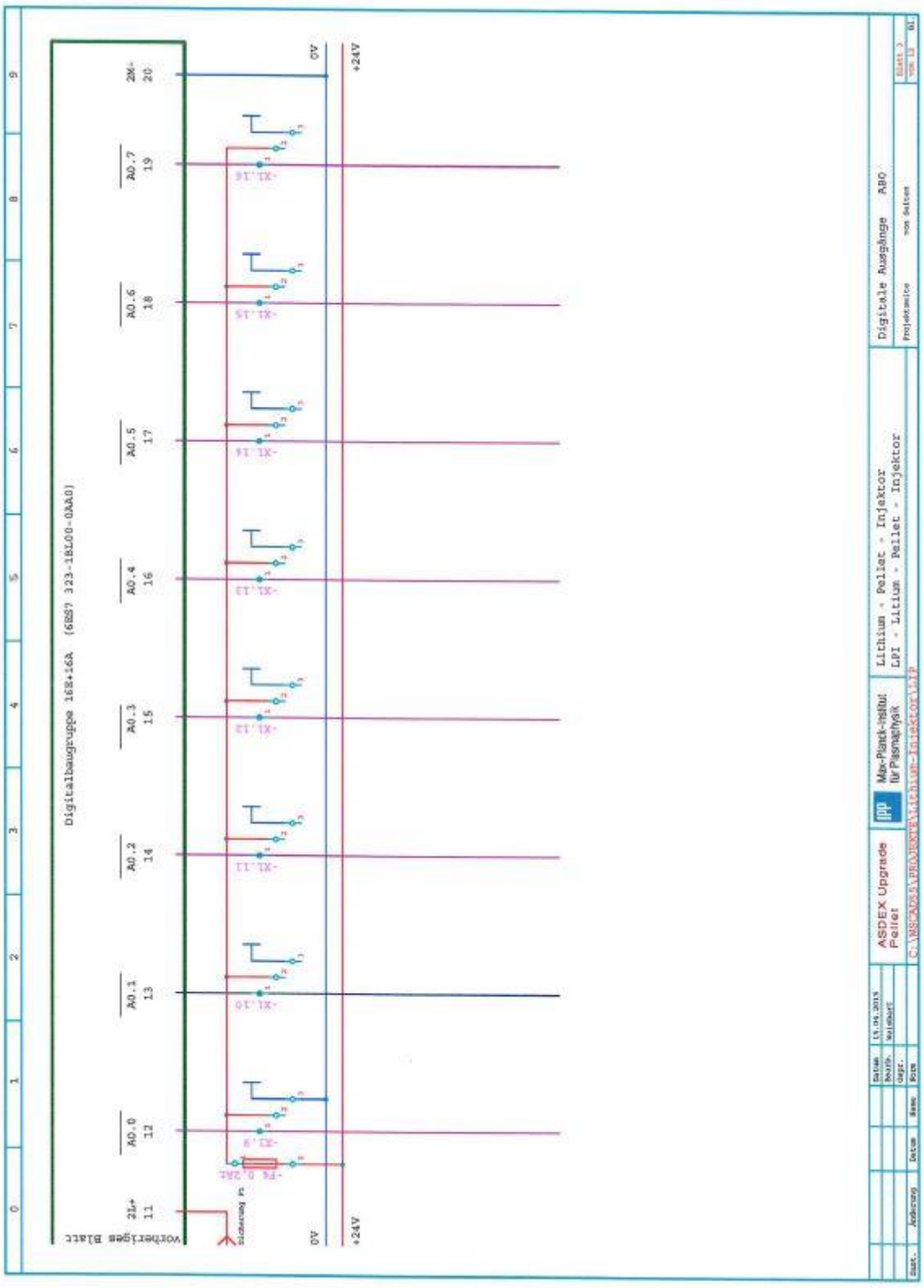
Digitalbaugruppe 168+16A (6ES7 323-1BL00-0AA0)
Vorbelegte Blatt
0V
+24V
ASDEX Upgrade
Pellet
Max-Planck-Institut für Plasmaphysik
Lithium - Pellet - Injektor
LPI - Lithium - Pellet - Injektor
Digitale Ausgänge A80

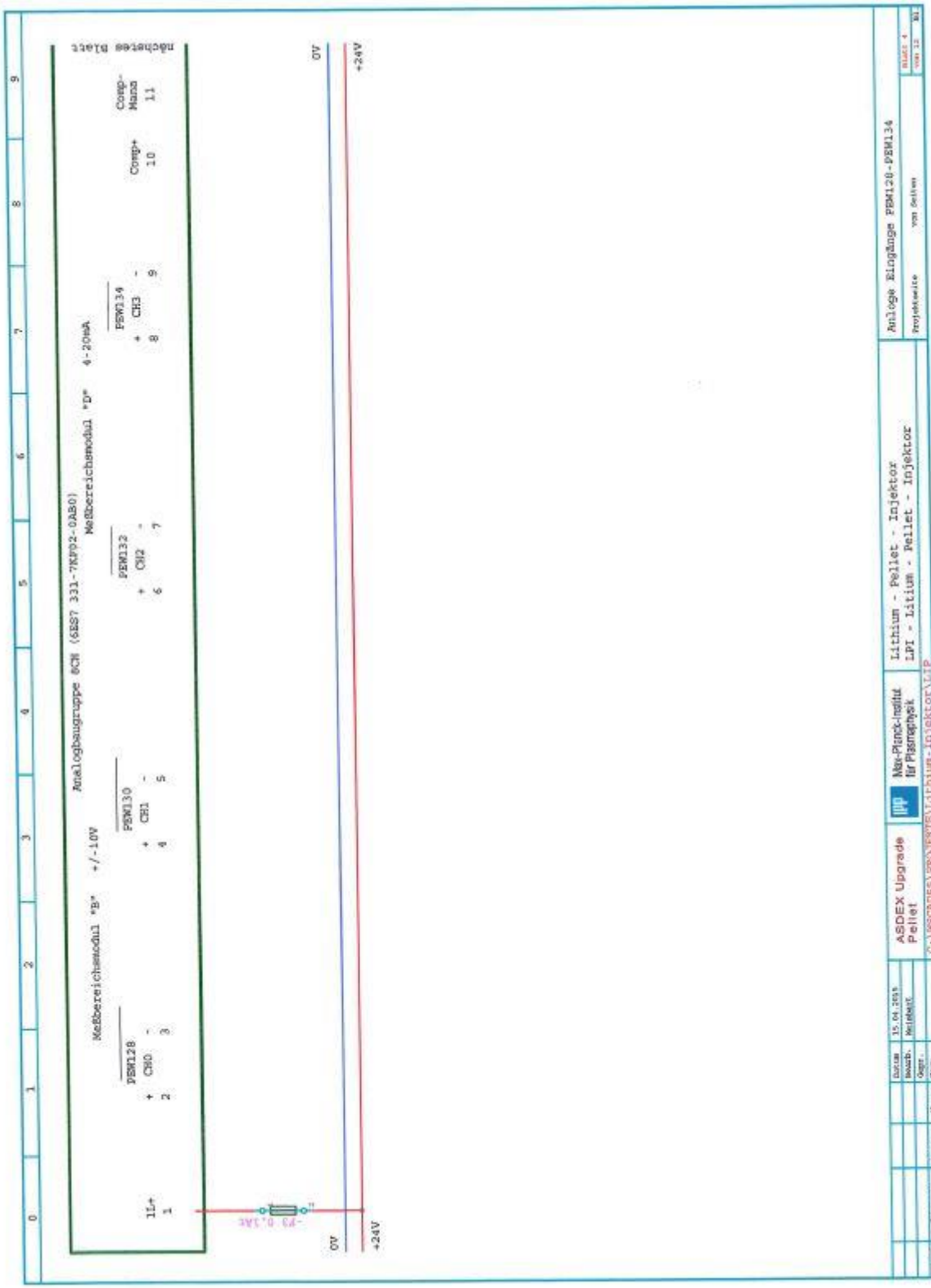
Analogbaugruppe 8CM (6ES7 331-7KF02-0AB0)
Messbereichsmodul "B" +/-10V
Messbereichsmodul "D" 4-20mA
PEM130
PEM132
PEM134
PEM128
CH0
CH1
CH2
CH3
Comp+
Comp-
1L+
0V
+24V
Lithium - Pellet - Injektor
LPI - Lithium - Pellet - Injektor
Analoge Eingänge PEM128-PEM134
ASDEX Upgrade
Pellet
Max-Planck-Institut für Plasmaphysik

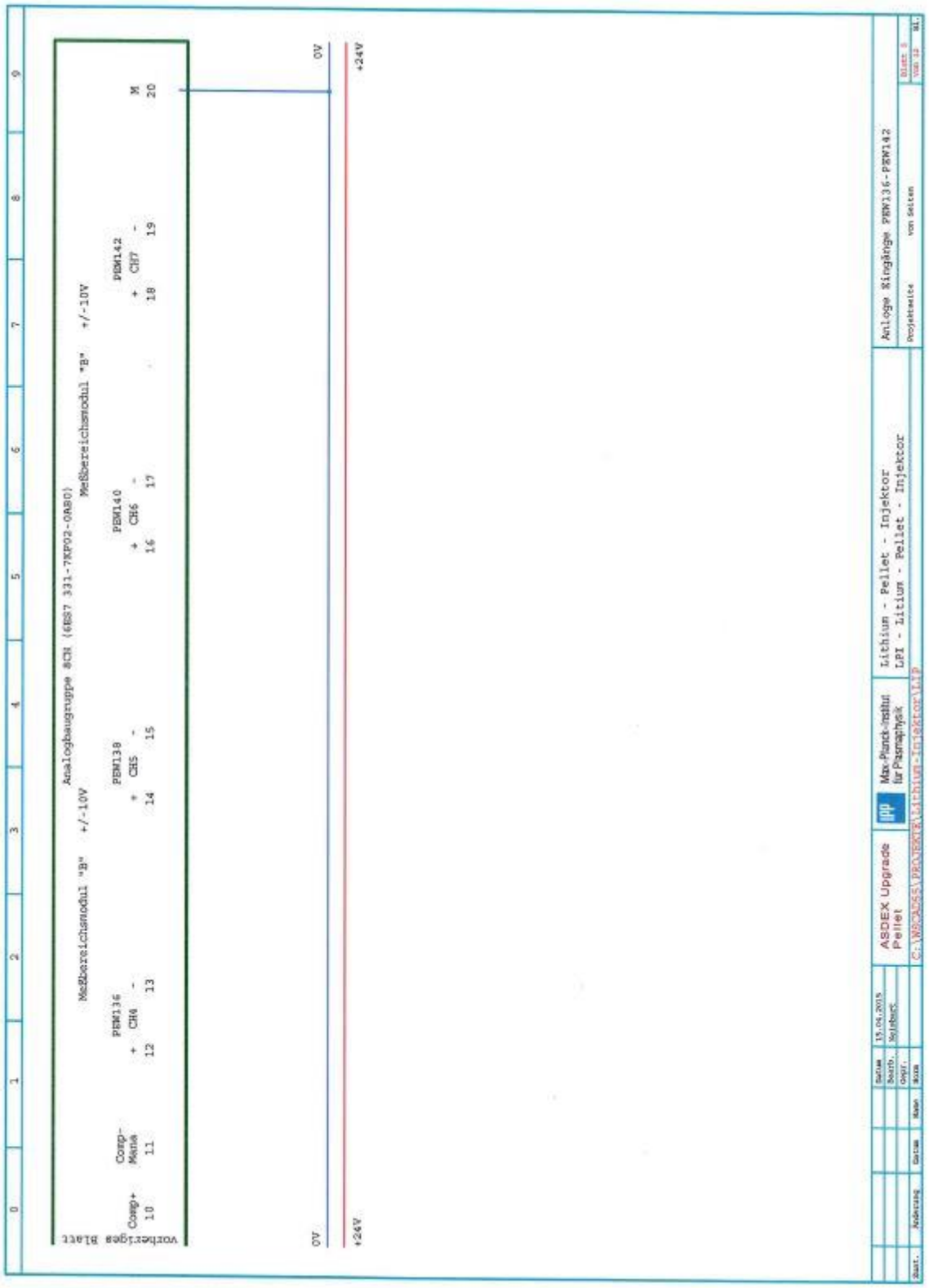
Analogbaugruppe 8CH (6ES7 331-7KF02-0AB0)
Messbereichsmodul "B" +/-10V
Messbereichsmodul "B" +/-10V
Messbereichsmodul "B" +/-10V
PEM136
PEM138
PEM140
PEM142
+ CH4 -
+ CH5 -
+ CH6 -
+ CH7 -
Comp+ 10
Comp- Masse 11
12 13
14 15
16 17
18 19
M 20
Vorbelegte Blatt
0V
+24V
0V
+24V
Lithium - Pellet - Injektor
LPI - Lithium - Pellet - Injektor
Analoge Eingänge PEM136-PEM142
ASDEX Upgrade
Pellet
Max-Planck-Institut für Plasmaphysik
C:\WSCADSS\PROJEKTE\Lithium-Injektor\LPI
15.04.2015
Projektseite
von Seiten

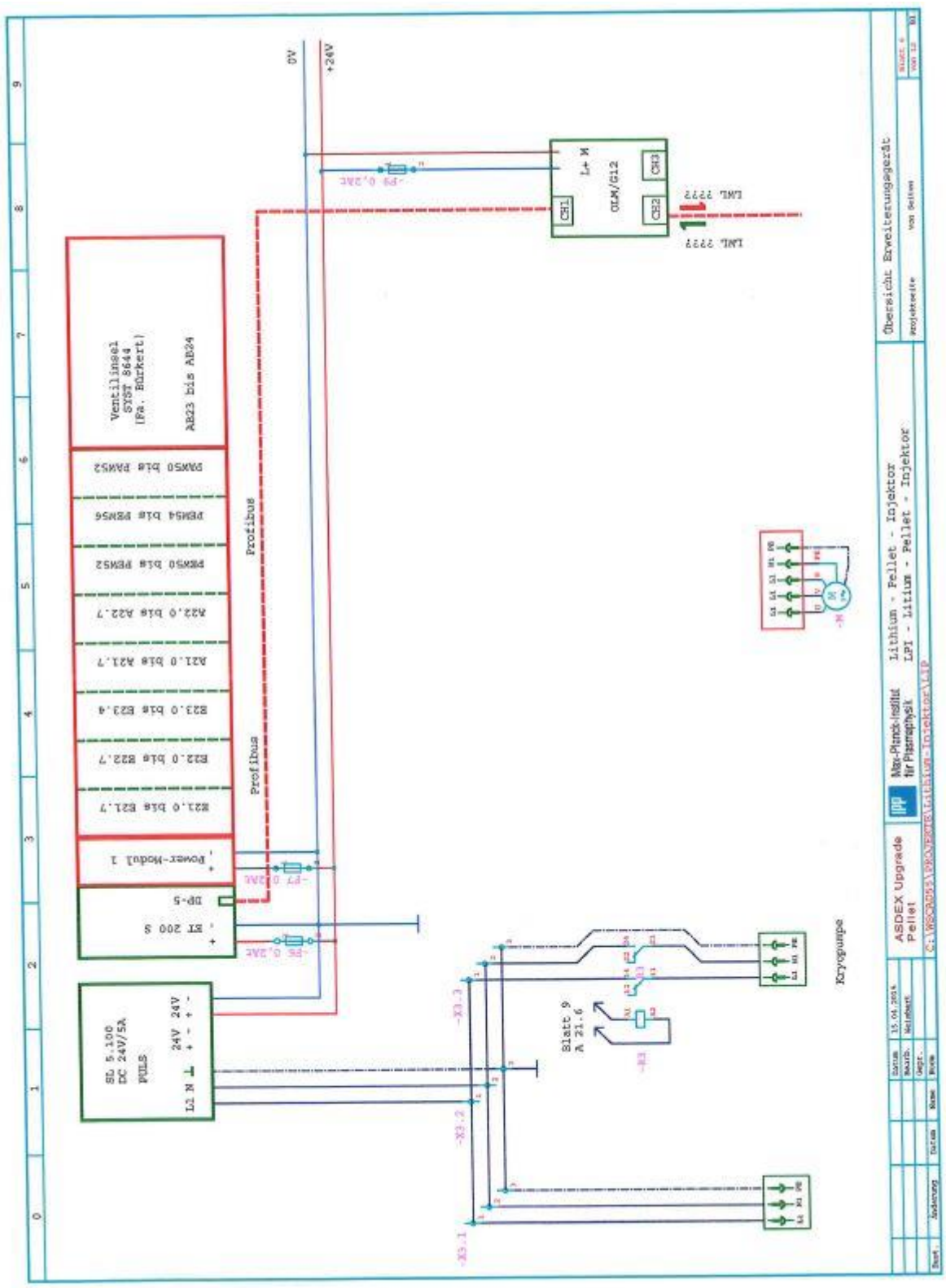
0V
+24V
Profibus
Profibus
Ventilinsel
SYST 8644
(Fa. Bürkert)
AB23 bis AB24
PAM50 bis PAM52
PBM54 bis PBM56
PBM50 bis PBM52
A22.0 bis A22.7
A21.0 bis A21.7
E23.0 bis E23.4
E22.0 bis E22.7
E21.0 bis E21.7
Power-Modul 1
ST 200 S
DP-S
SD 5.100
DC 24V/5A
PULS
L1 N ⊥
24V 24V
+ - + -
CH1
CH2
CH3
L+ M
OEM/G12
LWL 2222
LWL 2222
-PS 0,25AE
-PF 0,25AE
-PE 0,25AE
-X3.3
-X3.2
-X3.1
Blatt 9
A 21.6
-K3
Kryogumpe
-M
Übersicht Erweiterungsgerät:
Lithium - Pellet - Injektor
LPI - Litium - Pellet - Injektor
Max-Planck-Institut für Plasmaphysik
IPP
ASDEX Upgrade
Pellet
C:\WSCAD53\PROJEKTE\Lithium-Injektor\LPIP
Datum
Bearb.
Gepr.
Norm
Änderung
Datum
Name
Blatt

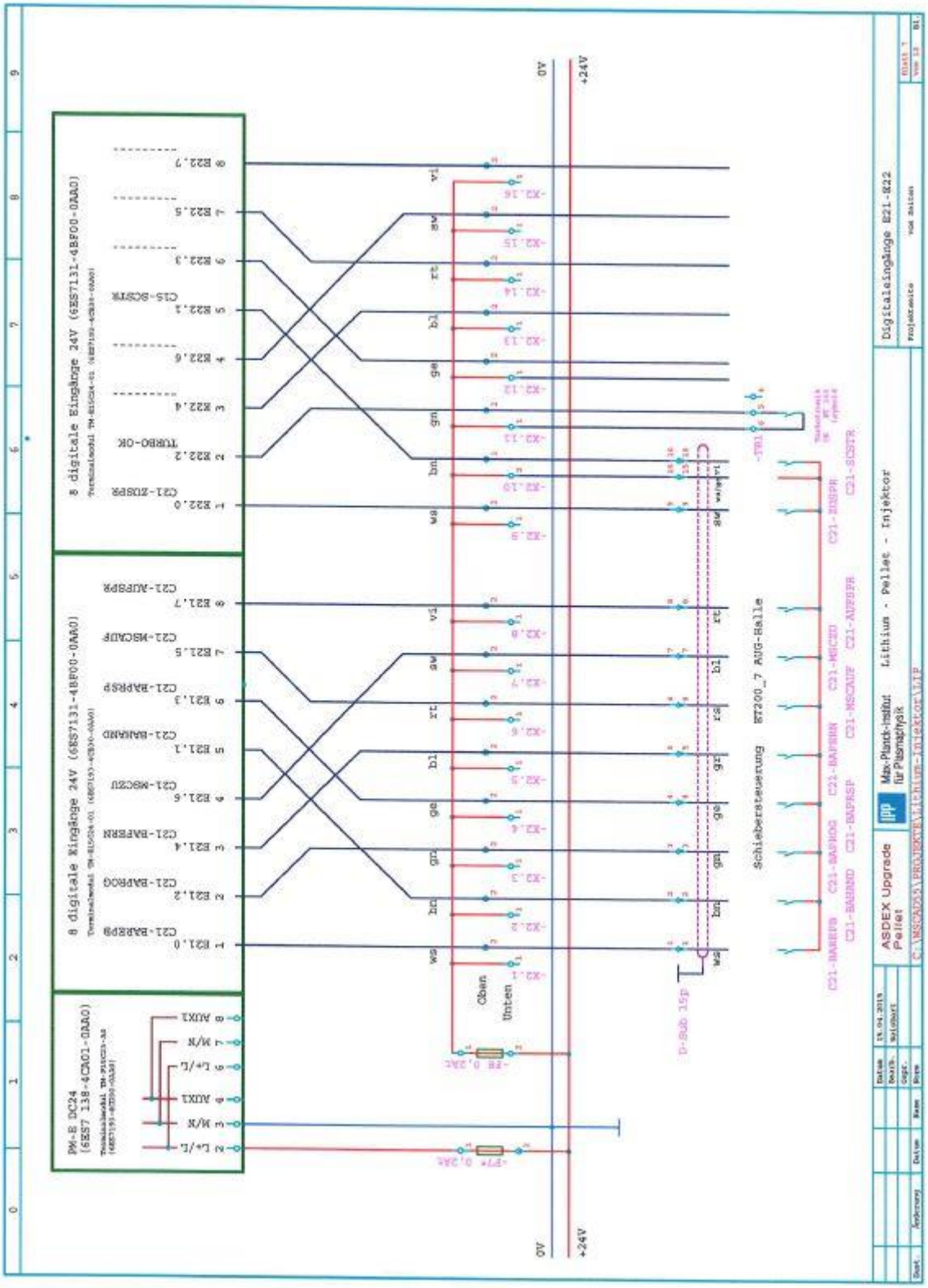
8 digitale Eingänge 24V (6ES7131-4BF00-0AA0)
8 digitale Eingänge 24V (6ES7131-4BF00-0AA0)
PM-E DC24 (6ES7 138-4CA01-0AA0)
0V
+24V
Schieberatesteuerung BT200_7 AUG-Halle
Digitaleingänge B21-B22
ASDEX Upgrade Pellet
Max-Planck-Institut für Plasmaphysik
Lithium - Pellet - Injektor

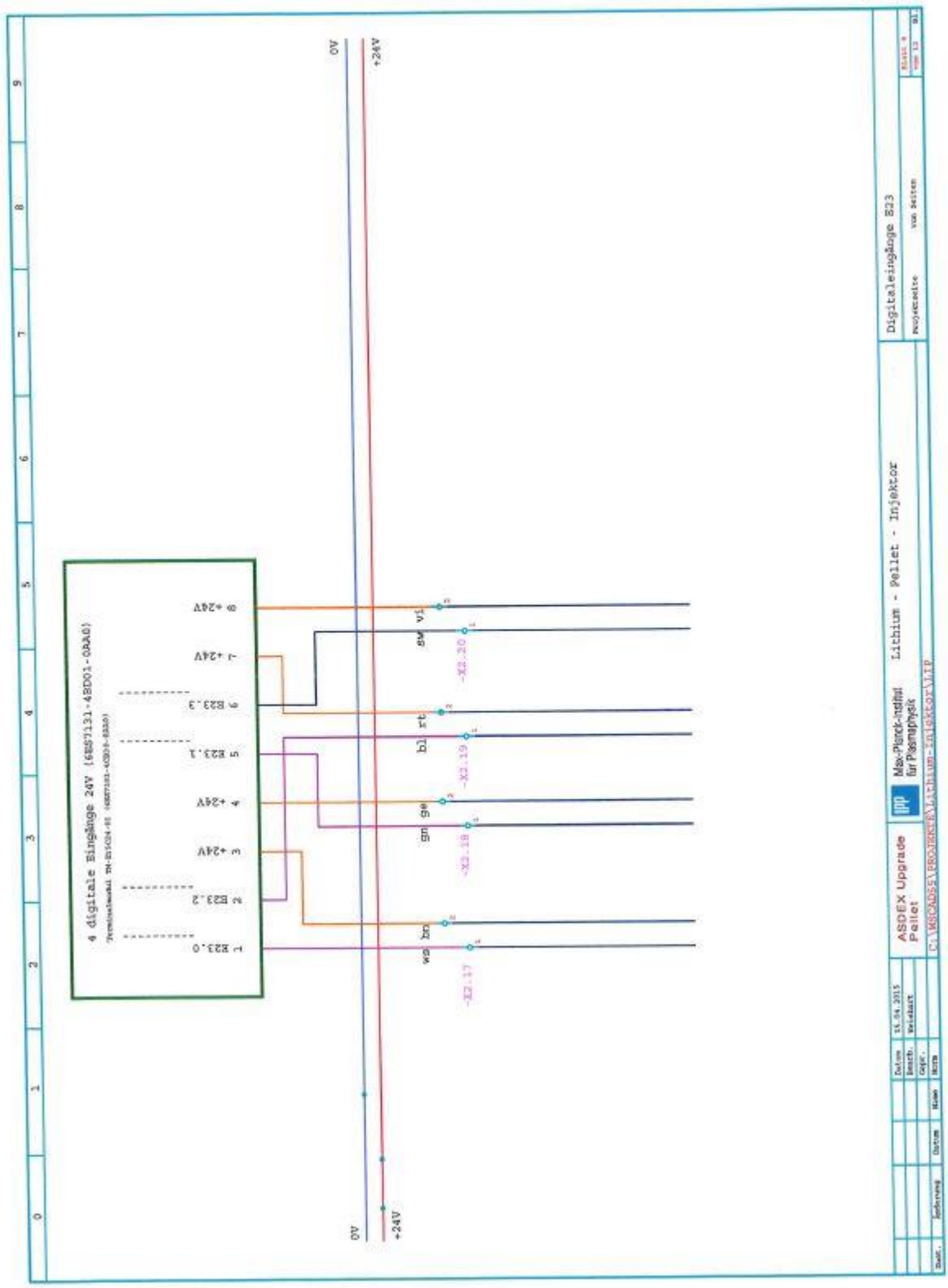
4 digitale Eingänge 24V (6ES7131-4BD01-0AA0)
Digitaleingänge E23
ASDEX Upgrade
Pellet
Max-Planck-Institut für Plasmaphysik
Lichium - Pellet - Injektor
0V
+24V
-X2.20
-X2.19
-X2.18
-X2.17

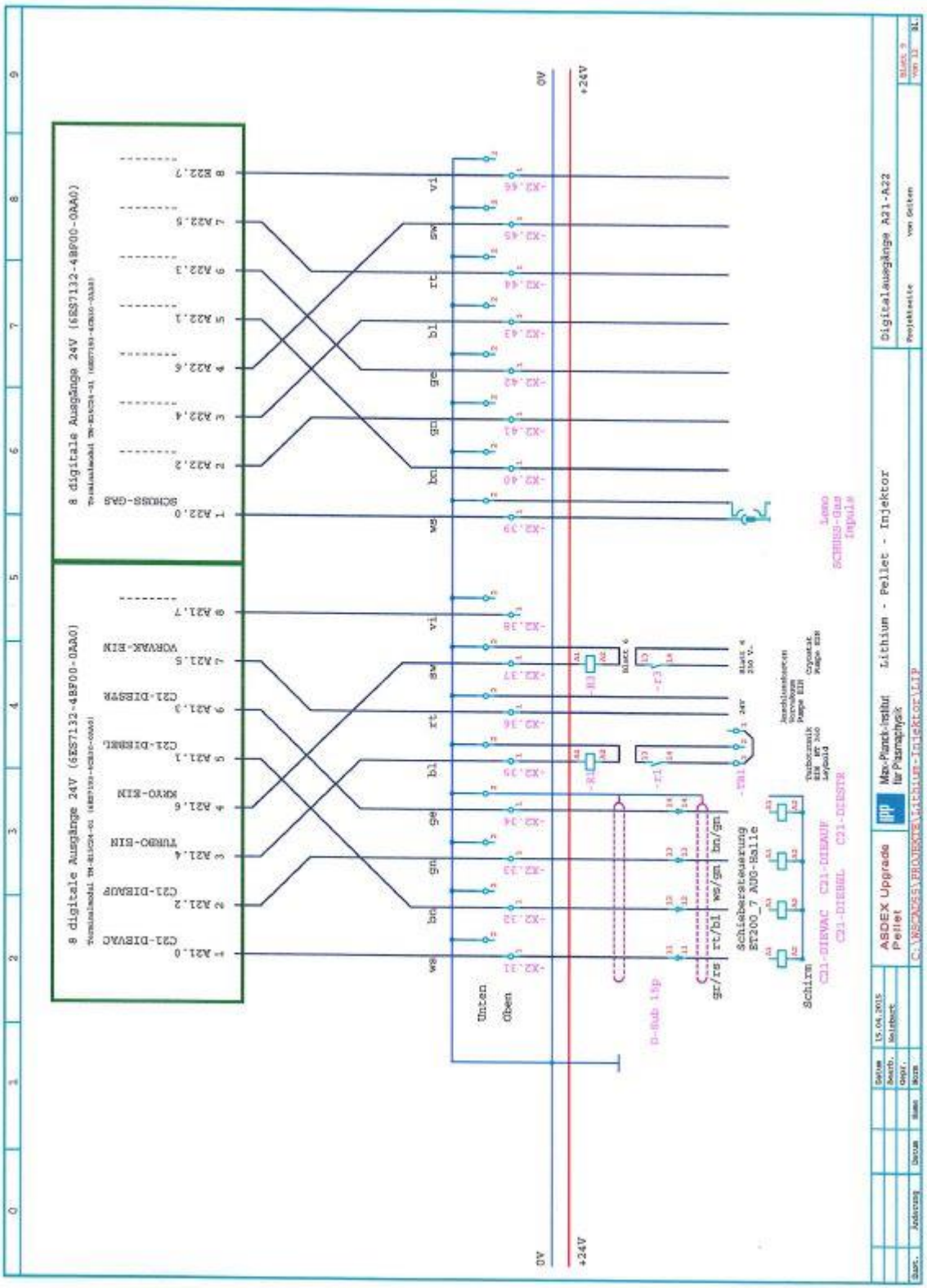
8 digitale Ausgänge 24V (6ES7132-4BF00-0AA0)
8 digitale Ausgänge 24V (6ES7132-4BF00-0AA0)
SCHUSS-GAS
VORVAK-EIN
C21-DIRSVR
C21-DIENBL
KRYO-EIN
TURBO-EIN
C21-DIRAUF
C21-DIVAC
A22.0
A22.2
A22.4
A22.6
A22.1
A22.3
A22.5
A22.7
A21.0
A21.2
A21.4
A21.6
A21.1
A21.3
A21.5
A21.7
0V
+24V
ws
bn
gn
ge
bl
rt
sw
vi
Union
Oben
D-Sub 15p
gr/rs
rt/bl
ws/gn
bn/gn
Schiebesteuerung
ER200_7 AUG-Ballo
Schirm
C21-DIVAC C21-DIRAUF
C21-DIBBL C21-DIESTR
Lemo
SCHUSS-Gas
Impuls
Max-Planck-Institut für Plasmaphysik
Lithium - Pellet - Injektor
ASDEX Upgrade
Pellet
Digitalausgänge A21-A22
Projektseite
von Seiten
C:\MESSES\PROJEKTE\Lithium-Injektor\LIP

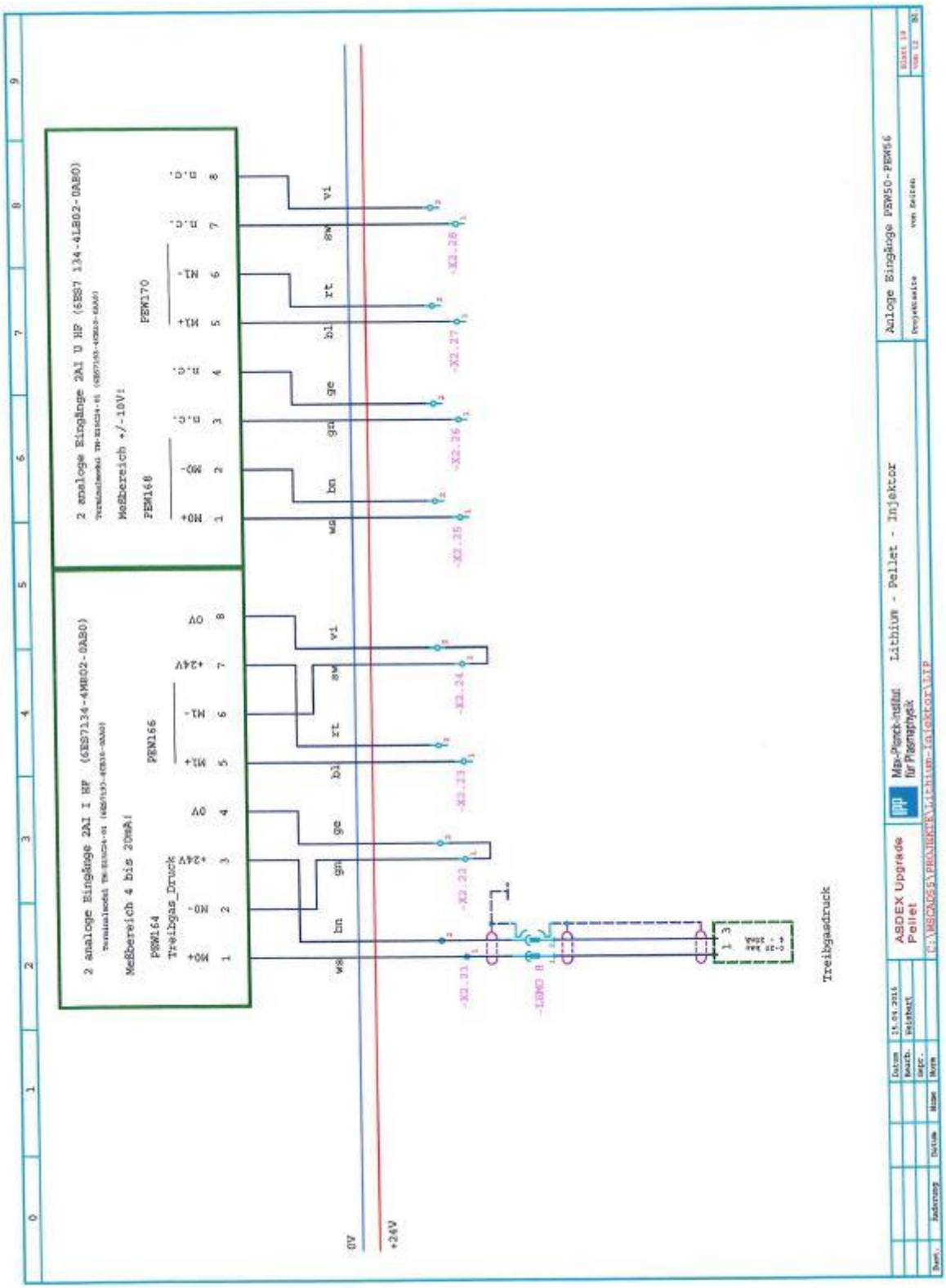
2 analoge Eingänge 2AI U HF (6ES7 134-4LB02-0AB0)
Messbereich +/-10V!
PEM170
PEM168
2 analoge Eingänge 2AI I HF (6ES7134-4MB02-0AB0)
Messbereich 4 bis 20mA!
PEM166
PSM164
Treibgas_Druck
Analoge Eingänge PSM50-PSM56
Max-Planck-Institut für Plasmaphysik
Lithium - Pellet - Injektor
ASDEX Upgrade Pellet
Treibgasdruck
0V
+24V

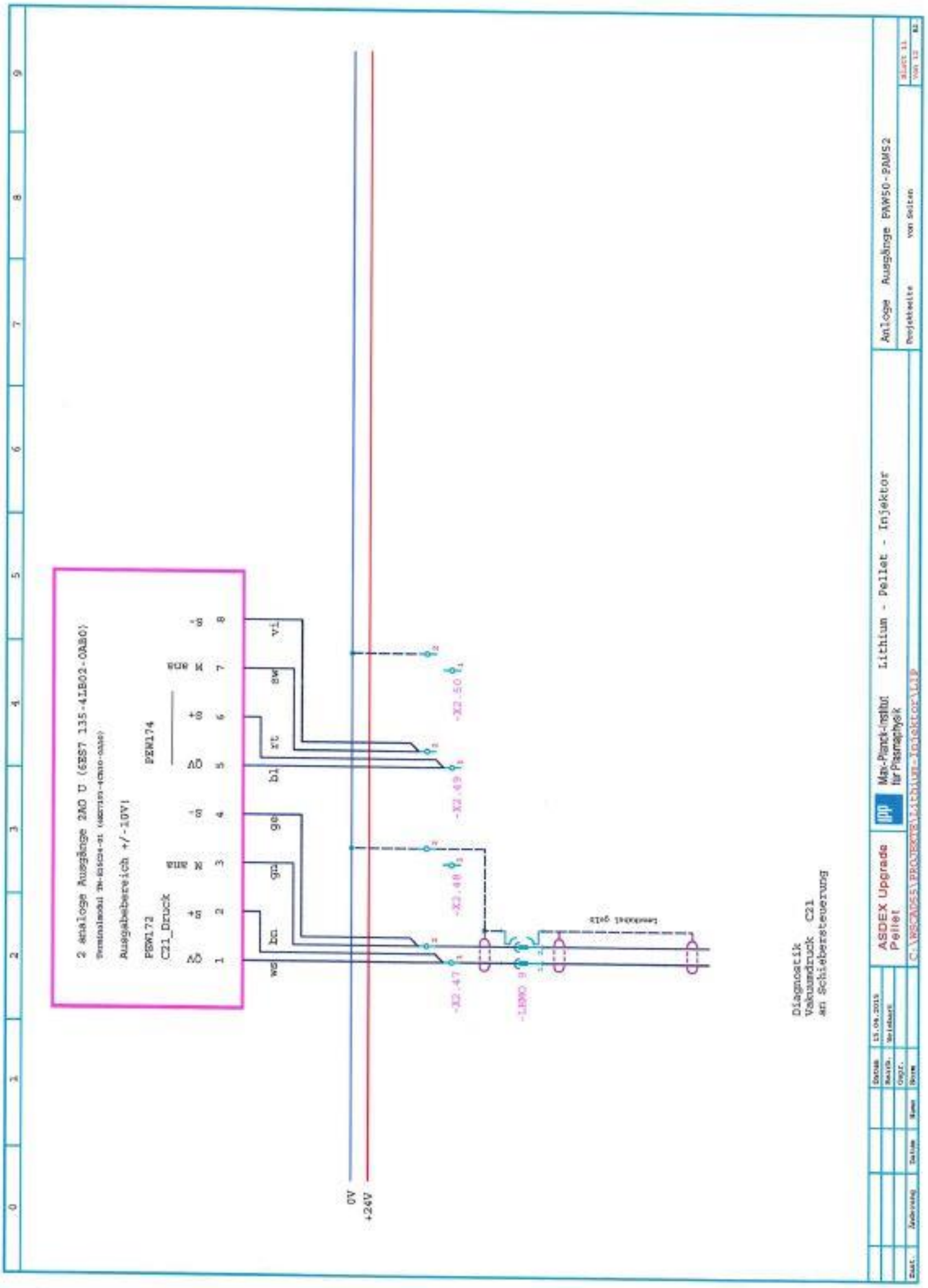
2 analoge Ausgänge 2AO U (6ES7 135-4LB02-0AB0)
Ausgabebereich +/-10V
PEW172
C21_Druck
PEW174
0V
+24V
Diagnostik
Vakuumdruck C21
an Schiebersteuerung
ASDEX Upgrade
Pellet
Max-Planck-Institut für Plasmaphysik
Lithium - Pellet - Injektor
Anloge Ausgänge PAW50-PAW52

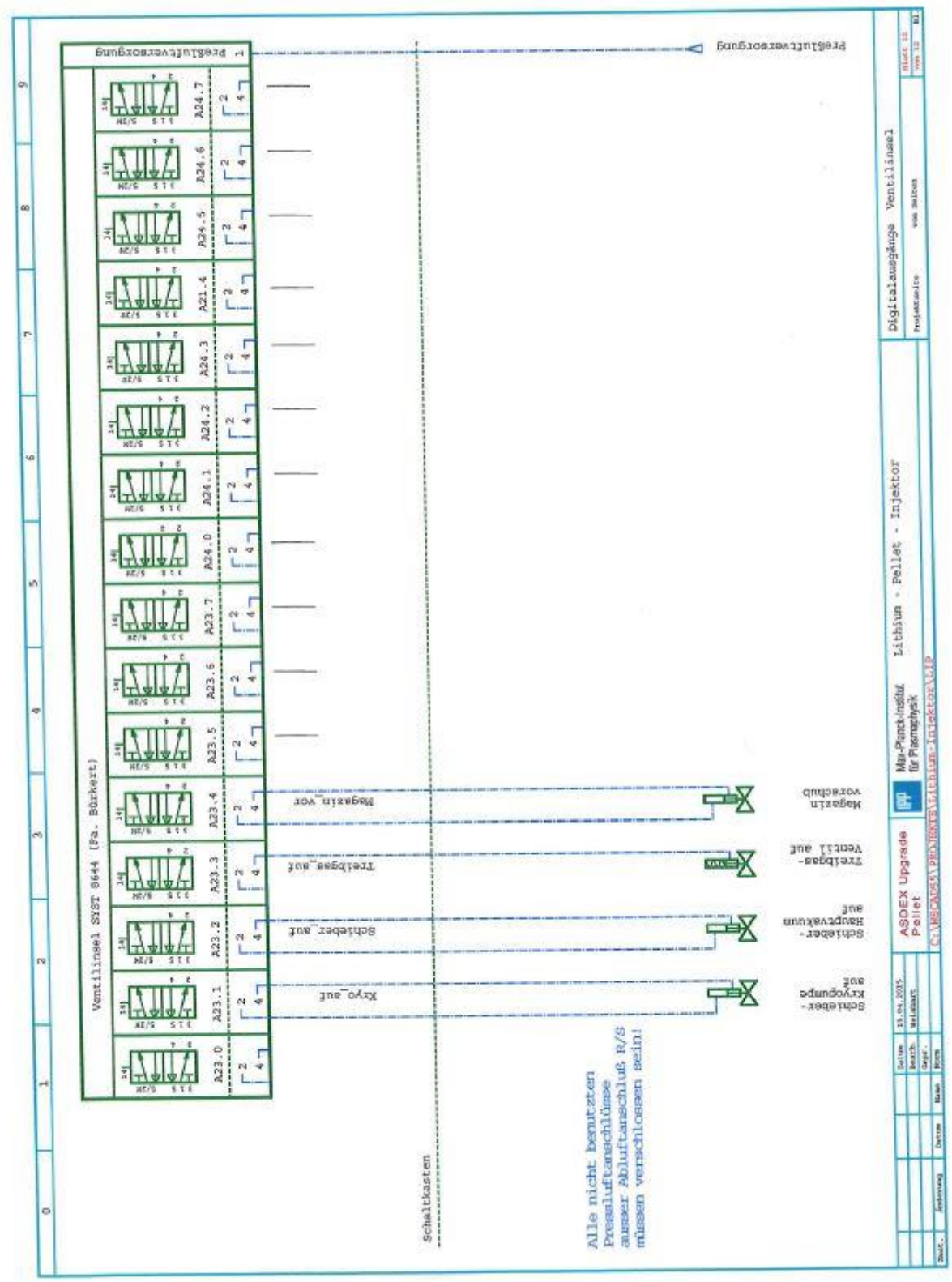
Ventilinsel SYST 8644 (Fa. Bürkert)
Druckluftversorgung
Schaltkasten
Alle nicht benutzten Pressluftanschlüsse ausser Abluftanschluß R/S müssen verschlossen sein!
Kryo_aus
Schieber_aus
Treibgas_aus
Magazin_vor
Schieber-Kryopumpe aus
Schieber-Hauptventil aus
Treibgas-Ventil aus
Magazin vorschub
Digitalausgänge Ventilinsel
Lithium - Pellet - Injektor
Max-Planck-Institut für Plasmaphysik
ASDEX Upgrade Pellet
C:\KRO\DOCS\PROJEKTE\Lithium-Injektor\VLP

E.5 Injector drafts

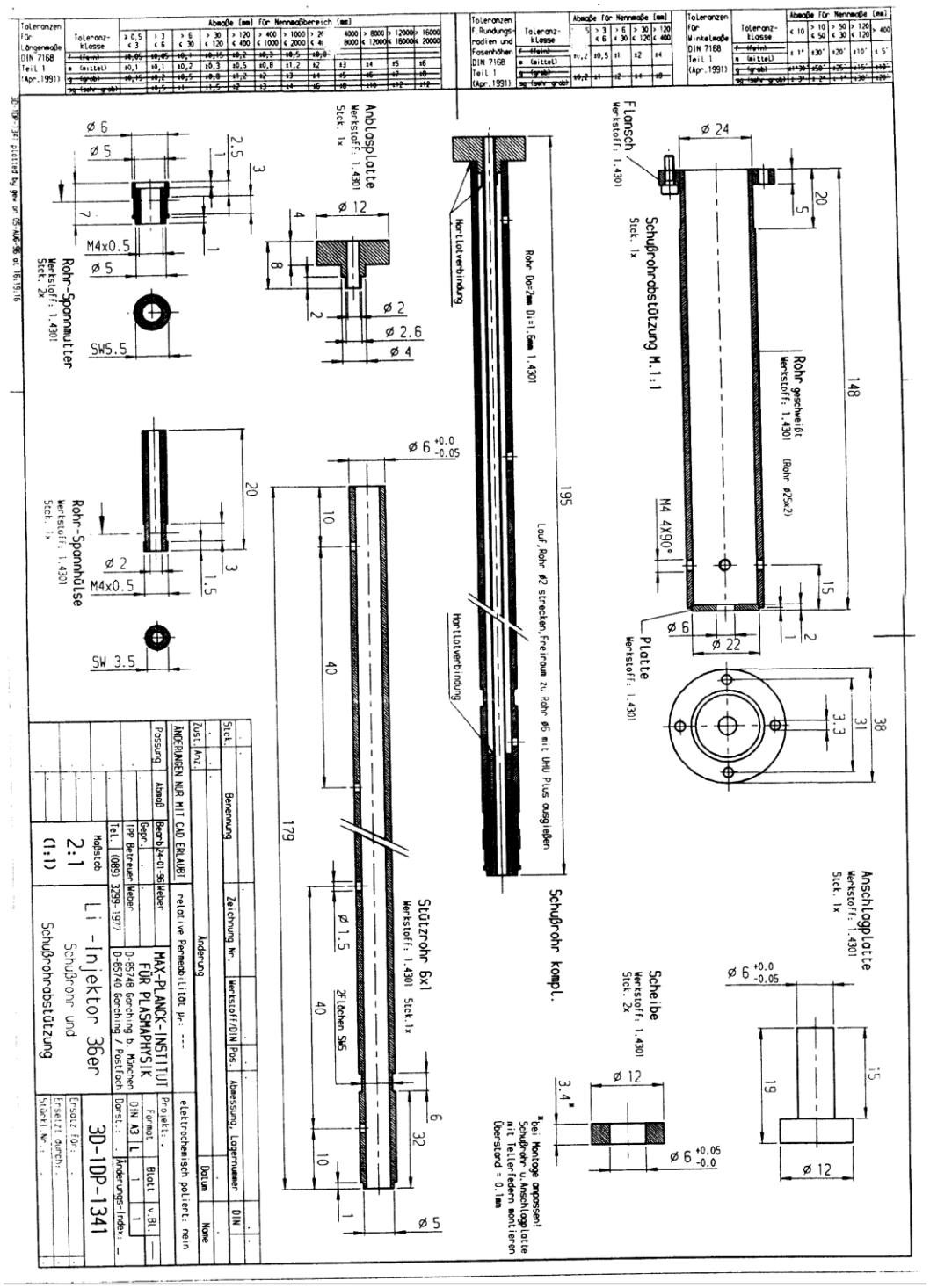

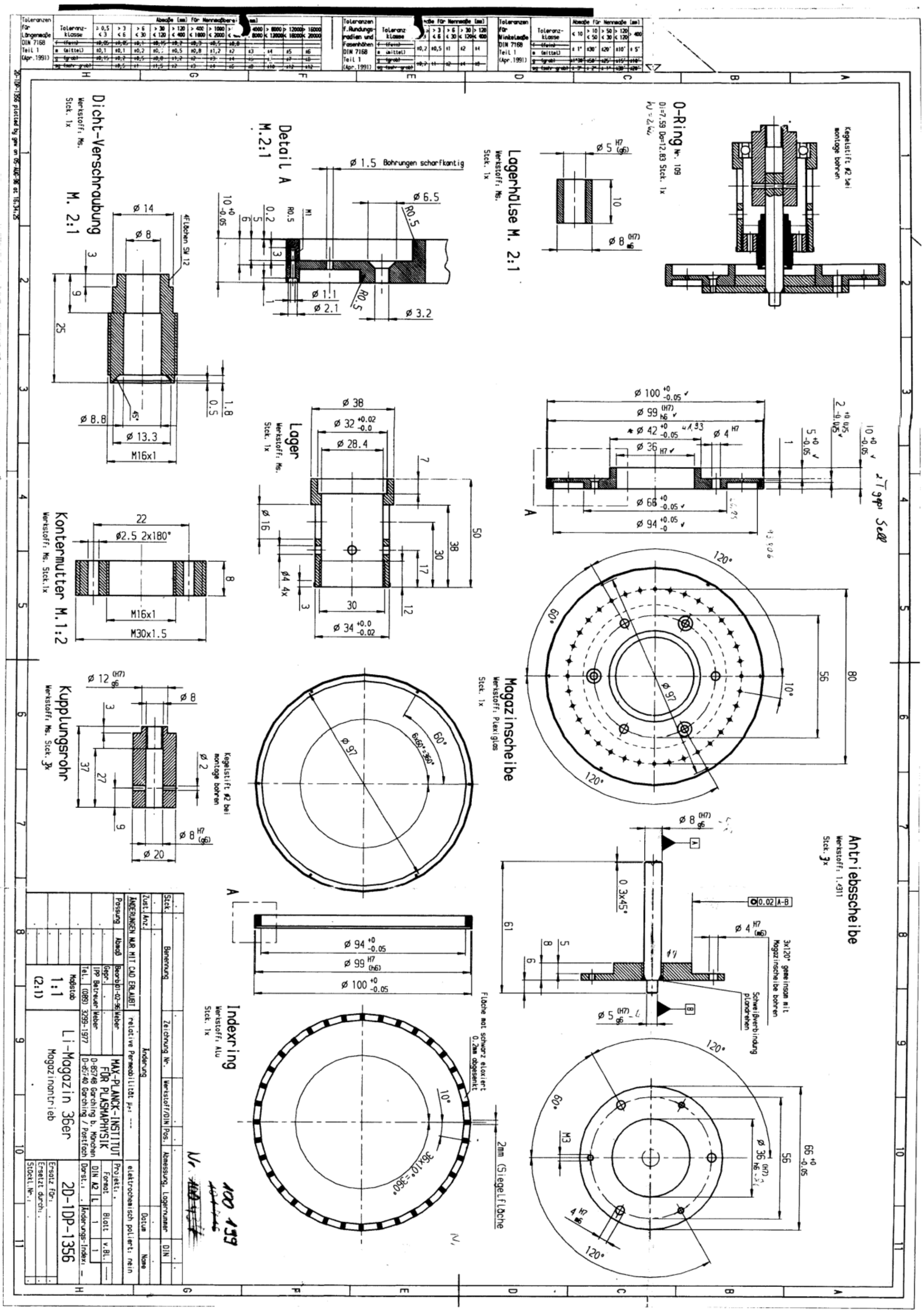
O-Ring
Lagerhülse M. 2:1
Detail A M. 2:1
Dicht-Verschraubung M. 2:1
Lager
Kontermutter M. 1:2
Kupplungsrohr
Magazinscheibe
Antriebsscheibe
Indexring
MAX-PLANCK-INSTITUT FÜR PLASMAPHYSIK
Li-Magazin 36er
Magazinantrieb
2D-IDP-1356

12 References

[1] EIA U.S. Energy Information Administration, "Annual Energy Outlook 2011 with Projections to 2035," 2011. [Online]. Available: https://www.eia.gov/outlooks/aeo/pdf/0383(2011).pdf.

[2] EIA U.S. Energy Information Administration, "International Energy Outlook 2017," 2017. [Online]. Available: https://www.eia.gov/outlooks/ieo/pdf/0484(2017).pdf.

[3] IEA International Energy Agency, "Key world energy statistics," 2016. [Online]. Available: http://large.stanford.edu/courses/2017/ph241/kwan1/docs/KeyWorld2016.pdf.

[4] J.P. Dorian et al., "Global challenges in energy," in *Energy Policy*, vol. 34, 2006, pp. 1984-1991.

[5] S. De et al., "Sustainable Energy Technology and Policies: A Transformational Journey," Singapore, Springer, 2018, pp. 1-9.

[6] U.S. Department of Energy, "The History of Nuclear Energy," [Online]. Available: https://www.energy.gov/sites/prod/files/The%20History%20of%20Nuclear%20Energy_0.pdf. [Accessed 17 01 2019].

[7] World Nuclear Association, "World Nuclear Performance Report 2018," 2018. [Online]. Available: http://www.world-nuclear.org/getmedia/b392d1cd-f7d2-4d54-9355-9a65f71a3419/performance-report.pdf.aspx. [Accessed 12 02 2019].

[8] Iter, "Advantages of fusion," [Online]. Available: https://www.iter.org/sci/Fusion. [Accessed 14 01 2019].

[9] Max-Planck-Institut für Plasmaphysik, "Institut," [Online]. Available: https://www.ipp.mpg.de/17180/institut. [Accessed 18 1 2019].

[10] "Pellets. Max-Planck-Institut für Plasmaphysik," [Online]. Available: https://www.ipp.mpg.de/1124504/pellets. [Accessed 14 01 2019].

[11] I. Langmuir, "Oscillations in Ionized Gases," *Proceedings of the National Academy of Science,*

14(8), pp. 627-637, 1928.

[12] P. A. Sturrock, "Plasma Physics: An Introduction to the Theory of Astrophysical, Geophysical and Laboratory Plasmas," Cambridge, Cambridge University Press, 1994, pp. 1-8.

[13] Max-Planck-Institut für Plasmaphysik, "Plasma," [Online]. Available: https://www.ipp.mpg.de/15096/plasma. [Accessed 19 01 2019].

[14] A. Einstein, "Ist die Trägheit eines Körpers von seinem Energieinhalt abhängig?," in *Annalen der Physik, vol. 323, Issue 13*, 1905, pp. 639-641.

[15] "Speed of light in vacuum. NIST National Institute of Standards and Technology," [Online]. Available: https://physics.nist.gov/cgi-bin/cuu/Value?c%7Csearch_for=universal_in!. [Accessed 22 02 2019].

[16] "Mass Defect. Physics.LibreTexts," [Online]. Available: <https://phys.libretexts.org/Bookshelves/University_Physics/Book%3A_University_Physics_(OpenStax)/Map%3A_University_Physics_III_-_Optics_and_Modern_Physics_(OpenStax)/10%3A__Nuclear_Physics/10.2%3A_Nuclear_Binding_Energy>. [Accessed 22 02 2019].

[17] "What is nuclear fusion?. Max-Planck-Institut für Plasmaphysik," [Online]. Available: https://www.ipp.mpg.de/15047/kernfusion. [Accessed 22 02 2019].

[18] C.M. Braams, P.E. Stott, "Nuclear Fusion: Half a Century of Magnetic Confinement Fusion Research," in *Plasma Physics and Controlled Fusion, vol. 44*, Bristol, CRC Press, 2002, pp. p. 1-7.

[19] W. M. Stacey, "Fusion: An Introduction to the Physics and Technology of Magnetic Confinement Fusion," Darmstadt, Wiley VCH Verlag GmbH, 2010, pp. 8-10.

[20] Max-Planck-Institut für Plasmaphysik, "Ignition conditions," [Online]. Available: https://www.ipp.mpg.de/15144/zuendbedingungen. [Accessed 21 01 2019].

[21] M. Kikuchi, K. Lackner, M. Q. Tran, "Fusion Physics," Vienna, International Atomic Energy Agency, 2012, pp. 27-32.

[22] Max-Planck-Institut für Plasmaphysik, "Kernfusion: Berichte aus der Forschung. Folge 2,"

Garching, Max-Planck-Institut für Plasmaphysik, 2002, pp. 10-12.

[23] Max-Planck-Institut für Plasmaphysik, "Tokamak," [Online]. Available: https://www.ipp.mpg.de/14869/tokamak. [Accessed 21 01 2019].

[24] Wikipedia, "List of fusion experiments," [Online]. Available: https://en.wikipedia.org/wiki/List_of_fusion_experiments. [Accessed 20 02 2019].

[25] "Projects of IPP. Max-Planck-Institut für Plasmaphysik," [Online]. Available: https://www.ipp.mpg.de/16183/projekte. [Accessed 20 01 2019].

[26] Max-Planck-Institut für Plasmaphysik, "Milestones," [Online]. Available: https://www.ipp.mpg.de/3982101/meilensteine. [Accessed 23 02 2019].

[27] ASDEX Upgrade Intranet, "Name: AUG_Torushalle_2008. Picture Gallery," [Online]. Available: https://www.aug.ipp.mpg.de/aug/local/aug_only/AUG_Aufbau/Picture_Gallery/ipage00031.htm. [Accessed 22 02 2019].

[28] Max-Planck-Institut für Plasmaphysik, "Topical research," [Online]. Available: https://www.ipp.mpg.de/16340/stand. [Accessed 23 02 2019].

[29] Max-Planck-Institut für Plasmaphysik, "Introduction: The ASDEX Upgrade tokamak," [Online]. Available: https://www.ipp.mpg.de/16208/einfuehrung. [Accessed 23 01 2019].

[30] Institute of Plasma Physics of the Czech Academy of Sciences, "COMPASS Tokamak," [Online]. Available: http://www.ipp.cas.cz/vedecka_struktura_ufp/tokamak/tokamak_compass/. [Accessed 21 02 2019].

[31] Institute of Plasma Physics of the Czech Academy of Sciences, "COMPASS Upgrade," [Online]. Available: http://www.ipp.cas.cz/vedecka_struktura_ufp/tokamak/compass_u/. [Accessed 23 02 2019].

[32] G. Papp et al., "Runaway electron generation and mitigation on the European medium sized tokamaks ASDEX Upgrade and TCV," in *WPMST1-CP(16)*, Kyoto.

[33] A. Nevil, "Investigations of runaway electron generation, transport, and stability in the DIII-D tokamak," San Diego, UC San Diego Electronic Theses and Dissertations, 2011, pp. 6-10.

[34] M. Kikuchi, K. Lackner, M. Q. Tran, "Fusion Physics," Vienna, IAEA Publications - International Atomic Energy Agency, 2012, pp. 352-353.

[35] R. A. Parra, "Operation, Commissioning and Installation of a High-Speed Lithium Pellet Injector in the ASDEX Upgrade Fusion Reactor," M. Sc. thesis, Technical University Munich, Munich, 2015.

[36] C. Muenther, "Der repetierende Kompaktlithiuminjektor für thermonukleare Fusionsreaktoren," Diploma thesis, Fachhochschule Munich, Munich, 2001.

[37] A. Alexiou, „Konditionierung und Charakterisierung eines modifizierten Raumtemperatur - Festkörper Pellet Injektors," B. Sc. thesis, University of Applied Sciences Munich, Munich, 2011, 2011.

[38] R. A. Parra et al., "A Compact Lithium Pellet Injector fpr Tokamak Pedestal Studies," *Review of Scientific Instruments 87(2),* pp. 1-4, 2016.

[39] P. T. Lang et al., "Impact of lithium pellets on plasma performance in the ASDEX Upgrade all-metal-wall tokamak," *Nucl. Fusion 57,* pp. 9-15, 2017.

[40] R. Hoepfl, "Charakterisierung eines Bornitrid Festkörper-Pelletinjektorsystems zur Wandborierung der Kernforschungsanlage ASDEX Upgrade," B. Sc. thesis, University of Applied Sciences Munich, Munich, 2018, 2018.

[41] A. Alexiou, "Konditionierung und Charakterisierung eines modifizierten Raumtemperatur - Festkörper Pellet Injektors," B. Sc. thesis, University of Applied Sciences Munich, Munich, 2011, 2011, pp. 35-40.

[42] C. Muenther, "Der repetierende Kompaktlithiuminjektor für thermonukleare Fusionsreaktoren," Diploma thesis, Fachhochschule Munich, Munich, 2001, pp. 24-31.

[43] A. Alexiou, *Konditionierung und Charakterisierung eines modifizierten Raumtemperatur - Festkörper Pellet Injektors,* B. Sc. thesis, University of Applied Sciences Munich, Munich, 2011, pp. 26-27.

[44] C. Demirtas, „Modifikation des RTSP-Injektors zur Abschwächung potentiell ELM-triggernder

Gasflüsse in Tokamak H-Mode Plasmen,“ M. Sc. thesis, University of Applied Sciences Munich, Munich, 2012.

[45] R. Hoepfl, "Charakterisierung eines Bornitrid Festkörper-Pelletinjektorsystems zur Wandborierung der Kernforschungsanlage ASDEX Upgrade," B. Sc. thesis, University of Applied Sciences Munich, Munich, 2018, 2018, p. 25.

[46] R. Hoepfl, "Charakterisierung eines Bornitrid Festkörper-Pelletinjektorsystems zur Wandborierung der Kernforschungsanlage ASDEX Upgrade," B. Sc. thesis, University of Applied Sciences Munich, Munich, 2018, 2018, pp. 31-48.

[47] Milos Vlainic, "Post-disruptive runaway electron beams in the COMPASS tokamak," *J. Plasma Phys., vol. 81,* p. 12, 2015.

[48] C. Münther, "Der repetierende Kompaktlithiuminjektor für thermonukleare Fusionsreaktoren," Diploma thesis, Fachhochschule Munich, Munich, 2001, pp. 41-46.

[49] M. M. Dibon, „Entwicklung und Verbesserung eines Blower Gun Pellet Injektors für die Anwendung in thermonuklearen Fusionsanlagen,“ M. Sc. thesis, Technical University Munich, Munich, 2014, p. 16.

[50] P. T. Lang et al., "Compact gas gun injection system for variavle sized solid pellets," in *Review of Scientific Instruments, 65(2316)*, 1994.

[51] H. E. Siekmann, P. U. Thamsen, "Umströmung von Körpern," in *Strömungslehre. Springer Lehrbuch*, Heidelberg, Springer, 2008, pp. 224-226.

[52] R. A. Parra, "Operation, Commissioning and Installation of a High-Speed Lithium Pellet Injector in the ASDEX Upgrade Fusion Reactor," M. Sc. thesis, Technical University Munich, Munich, 2015, pp. 46-51.

[53] R. Zhang, "Design considerations of Plasma Facing Components in Tokamak Fusion Reactors. Stanford University," 2014. [Online]. Available: large.stanford.edu/courses/2014/ph241/zhang1/. [Accessed 2019 03 06].

[54] R. Hoepfl, "Charakterisierung eines Bornitrid Festkörper-Pelletinjektorsystems zur

Wandborierung der Kernforschungsanlage ASDEX Upgrade," B. Sc. thesis, University of Applied Sciences Munich, Munich, 2018, 2018, pp. 98-100.

[55] J. Cerovsky et al., "Upcoming studies of runaway electrons at the COMPASS tokamak," Prague, 2018.

[56] "Data sheet of rotary piston pumps E 250 and DK200. Trilliumus," [Online]. Available: http://trilliumus.com/wp-content/uploads/2017/05/leybold-e-and-dk-rotary-piston-pump-manual.pdf. [Accessed 27 02 2019].

[57] "Leybold Vacuum. Turbovac Operating Instructions, 2004," 2004.

[58] "Idealvac. Leybold Turbotronik NT20 controller manual," [Online]. Available: https://www.idealvac.com/files/ManualsII/turbotronik_nt20_1.pdf. [Accessed 27 02 2019].

[59] "Pfeiffer Vacuum. MPT 200," [Online]. Available: https://vacuum-shop.com/product/pt-r40153/mpt200-dn40iso-kf.html. [Accessed 27 02 2019].

[60] „Safety data sheets. Airliquide," [Online]. Available: https://www.airliquide.com/safety-data-sheets. [Zugriff am 11 03 2019].

[61] ASDEX Upgrade Intranet, "Name:_AUG7a_M_Dibon. Picture Gallery," [Online]. Available: https://www.aug.ipp.mpg.de/aug/local/aug_only/AUG_Aufbau/Picture_Gallery/ipage00009.htm. [Accessed 22 02 2019].

[62] A. Buckmore, The Science of Small Arms Ballistics, CRC Press, 2018.